Searches for supersymmetric particles in e^+e^- collisions up to 208 GeV and interpretation of the results within the MSSM

J.Abdallah[1], T.Alderweireld[2], S.Amato[3], S.Ask[4], M.Berggren[1], M.C.Espirito Santo[5], M.Gandelman[3], C.Garcia[6], K.Hultqvist[7], P.D.Johansson[7], B.T.King[8], A.Lipniacka[7], J.H.Lopes[3], M.Margoni[9], F.Mazzucato[9], S.Paiano[10], A.Perrotta[10] T.Rovelli[10] A.Savoy-Navarro[4] U.Schwickerath[11] P.Verdier[12] A.J.Washbrook[8]

Abstract

DELPHI data collected at centre-of-mass energies up to 208 GeV have been analysed to search for charginos, neutralinos and sfermions in the framework of the Minimal Supersymmetric Standard Model (MSSM) with R-parity conservation. No evidence for a signal was found in any of the channels. The results of each search were used to derive upper limits on production cross-sections and masses. In addition, the combined result of all searches excludes regions in the parameter space of the constrained MSSM, leading to limits on the mass of the Lightest Supersymmetric Particle and other supersymmetric particles. All limits are given at 95% confidence level.

Contributed Paper for EPS 2003 (Aachen) and LP 2003 (FNAL)

[1] LPNHE, IN2P3-CNRS, Univ. Paris VI et VII, Tour 33 (RdC), 4 place Jussieu, FR-75252 Paris Cedex 05, France

[2] Univ. de l'Etat Mons, Av. Maistriau 19, B-7000 Mons, Belgium

[3] Univ. Federal do Rio de Janeiro, C.P. 68528 Cidade Univ., Ilha do Fundão BR-21945-970 Rio de Janeiro, Brazil

[4] Department of Physics, University of Lund, Sölvegatan 14, SE-223 63 Lund, Sweden

[5] LIP, IST, FCUL - Av. Elias Garcia, 14-1°, PT-1000 Lisboa Codex, Portugal

[6] IFIC, Valencia-CSIC, and D.F.A.M.N., U. de Valencia, Avda. Dr. Moliner 50, ES-46100 Burjassot (Valencia), Spain

[7] Fysikum, Stockholm University, Box 6730, SE-113 85 Stockholm, Sweden

[8] Department of Physics, University of Liverpool, P.O. Box 147, Liverpool L69 3BX, UK

[9] Dipartimento di Fisica, Università di Padova and INFN, Via Marzolo 8, IT-35131 Padua, Italy

[10] Dipartimento di Fisica, Università di Bologna and INFN, Via Irnerio 46, IT-40126 Bologna, Italy

[11] CERN, CH-1211 Geneva 23, Switzerland

[12] Université Claude Bernard de Lyon, IPNL, IN2P3-CNRS, FR-69622 Villeurbanne Cedex, France

Searches for supersymmetric particles in e$^+$e$^-$ collisions up to 208 GeV and interpretation of the results within the MSSM

DELPHI Collaboration

Abstract

DELPHI data collected at centre-of-mass energies up to 208 GeV have been analysed to search for charginos, neutralinos and sfermions in the framework of the Minimal Supersymmetric Standard Model (MSSM) with R-parity conservation. No evidence for a signal was found in any of the channels. The results of each search were used to derive upper limits on production cross-sections and masses. In addition, the combined result of all searches excludes regions in the parameter space of the constrained MSSM, leading to limits on the mass of the Lightest Supersymmetric Particle and other supersymmetric particles. All limits are given at 95% confidence level.

J.Abdallah[24], P.Abreu[22], W.Adam[52], P.Adzic[12], T.Albrecht[18], T.Alderweireld[2], R.Alemany-Fernandez[9], T.Allmendinger[18], P.P.Allport[23], S.Almehed[25], U.Amaldi[29], N.Amapane[47], S.Amato[49], E.Anashkin[37], A.Andreazza[28], S.Andringa[22], N.Anjos[22], P.Antilogus[26], W-D.Apel[18], Y.Arnoud[15], S.Ask[25], B.Asman[46], J.E.Augustin[24], A.Augustinus[9], P.Baillon[9], A.Ballestrero[47], P.Bambade[20], R.Barbier[26], D.Bardin[17], G.Barker[18], A.Baroncelli[40], M.Battaglia[9], M.Baubillier[24], K-H.Becks[54], M.Begalli[6], A.Behrmann[54], N.Benekos[33], A.Benvenuti[5], C.Berat[15], M.Berggren[24], L.Berntzon[46], D.Bertrand[2], M.Besancon[41], N.Besson[41], D.Bloch[10], M.Blom[32], M.Bonesini[29], M.Boonekamp[41], P.S.L.Booth[23], G.Borisov[21], O.Botner[50], B.Bouquet[20], T.J.V.Bowcock[23], I.Boyko[17], M.Bracko[45], R.Brenner[50], E.Brodet[36], P.Bruckman[19], J.M.Brunet[8], L.Bugge[34], P.Buschmann[54], M.Calvi[29], T.Camporesi[9], V.Canale[39], F.Carena[9], C.Carimalo[24], N.Castro[22], F.Cavallo[5], M.Chapkin[44], Ph.Charpentier[9], P.Checchia[37], R.Chierici[9], P.Chliapnikov[44], J.Chudoba[9], S.U.Chung[9], K.Cieslik[19], P.Collins[9], R.Contri[14], G.Cosme[20], F.Cossutti[48], M.J.Costa[51], B.Crawley[1], D.Crennell[38], J.Cuevas[35], J.D'Hondt[2], J.Dalmau[46], T.da Silva[49], W.Da Silva[24], G.Della Ricca[48], A.De Angelis[48], W.De Boer[18], C.De Clercq[2], B.De Lotto[48], N.De Maria[47], A.De Min[37], L.de Paula[49], L.Di Ciaccio[39], A.Di Simone[40], K.Doroba[53], J.Drees[54,9], M.Dris[33], G.Eigen[4], T.Ekelof[50], M.Ellert[50], M.Elsing[9], M.C.Espirito Santo[9], G.Fanourakis[12], D.Fassouliotis[12], M.Feindt[18], J.Fernandez[42], A.Ferrer[51], F.Ferro[14], U.Flagmeyer[54], H.Foeth[9], E.Fokitis[33], F.Fulda-Quenzer[20], J.Fuster[51], M.Gandelman[49], C.Garcia[51], Ph.Gavillet[9], E.Gazis[33], T.Geralis[12], R.Gokieli[9,53], B.Golob[45], G.Gomez-Ceballos[42], P.Goncalves[22], E.Graziani[40], G.Grosdidier[20], K.Grzelak[53], J.Guy[38], C.Haag[18], A.Hallgren[50], K.Hamacher[54], K.Hamilton[36], J.Hansen[34], S.Haug[34], F.Hauler[18], V.Hedberg[25], M.Hennecke[18], H.Herr[9], S-O.Holmgren[46], P.J.Holt[9], M.A.Houlden[23], K.Hultqvist[46], J.N.Jackson[23], Ch.Jarlskog[25], G.Jarlskog[25], P.Jarry[41], D.Jeans[36], E.K.Johansson[46], P.D.Johansson[46], P.Jonsson[26], C.Joram[9], L.Jungermann[18], F.Kapusta[24], S.Katsanevas[26], E.Katsoufis[33], G.Kernel[45], B.P.Kersevan[9,45], A.Kiiskinen[16], B.T.King[23], N.J.Kjaer[9], P.Kluit[32], P.Kokkinias[12], C.Kourkoumelis[3], O.Kouznetsov[17], Z.Krumstein[17], M.Kucharczyk[19], J.Kurowska[53], B.Laforge[24], J.Lamsa[1], G.Leder[52], F.Ledroit[15], L.Leinonen[46], R.Leitner[31], J.Lemonne[2], V.Lepeltier[20], T.Lesiak[19], W.Liebig[54], D.Liko[52], A.Lipniacka[46], J.H.Lopes[49], J.M.Lopez[35], D.Loukas[12], P.Lutz[41], L.Lyons[36], J.MacNaughton[52], A.Malek[54], S.Maltezos[33], F.Mandl[52], J.Marco[42], R.Marco[42], B.Marechal[49], M.Margoni[37], J-C.Marin[9], C.Mariotti[9], A.Markou[12], C.Martinez-Rivero[42], J.Masik[13], N.Mastroyiannopoulos[12], F.Matorras[42], C.Matteuzzi[29], F.Mazzucato[37], M.Mazzucato[37], R.Mc Nulty[23], C.Meroni[28], W.T.Meyer[1], E.Migliore[47], W.Mitaroff[52], U.Mjoernmark[25], T.Moa[46], M.Moch[18], K.Moenig[9,11], R.Monge[14], J.Montenegro[32], D.Moraes[49], S.Moreno[22], P.Morettini[14], U.Mueller[54], K.Muenich[54], M.Mulders[32], L.Mundim[6], W.Murray[38], B.Muryn[19], G.Myatt[36,9], T.Myklebust[34], M.Nassiakou[12], F.Navarria[5], K.Nawrocki[53], R.Nicolaidou[41], P.Niezurawski[53], M.Nikolenko[17,10], A.Nygren[25], A.Oblakowska-Mucha[19], V.Obraztsov[44], A.Olshevski[17], A.Onofre[22], R.Orava[16], K.Osterberg[16], A.Ouraou[41], A.Oyanguren[51], M.Paganoni[29], S.Paiano[5], J.P.Palacios[23], H.Palka[19], Th.D.Papadopoulou[33], L.Pape[9], C.Parkes[23], F.Parodi[14], U.Parzefall[9], A.Passeri[40], O.Passon[54], L.Peralta[22], V.Perepelitsa[51], A.Perrotta[5], A.Petrolini[14], J.Piedra[42], L.Pieri[40], F.Pierre[41], M.Pimenta[22], E.Piotto[9], T.Podobnik[45], V.Poireau[41], M.E.Pol[6], G.Polok[19], P.Poropat[48], V.Pozdniakov[17], N.Pukhaeva[2,17], A.Pullia[29], J.Rames[13], L.Ramler[18], A.Read[34], P.Rebecchi[9], J.Rehn[18], D.Reid[32], R.Reinhardt[54], P.Renton[36], F.Richard[20], J.Ridky[13], M.Rivero[42], D.Rodriguez[42], A.Romero[47], P.Ronchese[37], E.Rosenberg[1], P.Roudeau[20], T.Rovelli[5], V.Ruhlmann-Kleider[41], D.Ryabtchikov[44], A.Sadovsky[17], L.Salmi[16], J.Salt[51], A.Savoy-Navarro[24], U.Schwickerath[9], A.Segar[36], R.Sekulin[38], M.Siebel[54], A.Sisakian[17], G.Smadja[26], O.Smirnova[25], A.Sokolov[44], A.Sopczak[21], R.Sosnowski[53], T.Spassov[9], M.Stanitzki[18], A.Stocchi[20,9], J.Strauss[52], B.Stugu[4], M.Szczekowski[53], M.Szeptycka[53], T.Szumlak[19], T.Tabarelli[29], A.C.Taffard[23], F.Tegenfeldt[50], J.Timmermans[32], N.Tinti[5], L.Tkatchev[17], M.Tobin[23], S.Todorovova[13], A.Tomaradze[9], B.Tome[22], A.Tonazzo[29], P.Tortosa[51], P.Travnicek[13], D.Treille[9], G.Tristram[8], M.Trochimczuk[53], C.Troncon[28], M-L.Turluer[41], I.A.Tyapkin[17], P.Tyapkin[17], S.Tzamarias[12], V.Uvarov[44], G.Valenti[5], P.Van Dam[32], J.Van Eldik[9], A.Van Lysebetten[2], N.van Remortel[2], I.Van Vulpen[32], G.Vegni[28], F.Veloso[22], W.Venus[38], F.Verbeure[2], P.Verdier[26], V.Verzi[39], D.Vilanova[41], L.Vitale[48],

V.Vrba[13], H.Wahlen[54], A.J.Washbrook[23], C.Weiser[18], D.Wicke[9], J.Wickens[2], G.Wilkinson[36], M.Winter[10], M.Witek[19], O.Yushchenko[44], A.Zalewska[19], P.Zalewski[53], D.Zavrtanik[45], N.I.Zimin[17], A.Zintchenko[17], M.Zupan[12]

[1]Department of Physics and Astronomy, Iowa State University, Ames IA 50011-3160, USA
[2]Physics Department, Univ. Instelling Antwerpen, Universiteitsplein 1, B-2610 Antwerpen, Belgium
and IIHE, ULB-VUB, Pleinlaan 2, B-1050 Brussels, Belgium
and Faculté des Sciences, Univ. de l'Etat Mons, Av. Maistriau 19, B-7000 Mons, Belgium
[3]Physics Laboratory, University of Athens, Solonos Str. 104, GR-10680 Athens, Greece
[4]Department of Physics, University of Bergen, Allégaten 55, NO-5007 Bergen, Norway
[5]Dipartimento di Fisica, Università di Bologna and INFN, Via Irnerio 46, IT-40126 Bologna, Italy
[6]Centro Brasileiro de Pesquisas Físicas, rua Xavier Sigaud 150, BR-22290 Rio de Janeiro, Brazil
and Depto. de Física, Pont. Univ. Católica, C.P. 38071 BR-22453 Rio de Janeiro, Brazil
and Inst. de Física, Univ. Estadual do Rio de Janeiro, rua São Francisco Xavier 524, Rio de Janeiro, Brazil
[7]Comenius University, Faculty of Mathematics and Physics, Mlynska Dolina, SK-84215 Bratislava, Slovakia
[8]Collège de France, Lab. de Physique Corpusculaire, IN2P3-CNRS, FR-75231 Paris Cedex 05, France
[9]CERN, CH-1211 Geneva 23, Switzerland
[10]Institut de Recherches Subatomiques, IN2P3 - CNRS/ULP - BP20, FR-67037 Strasbourg Cedex, France
[11]Now at DESY-Zeuthen, Platanenallee 6, D-15735 Zeuthen, Germany
[12]Institute of Nuclear Physics, N.C.S.R. Demokritos, P.O. Box 60228, GR-15310 Athens, Greece
[13]FZU, Inst. of Phys. of the C.A.S. High Energy Physics Division, Na Slovance 2, CZ-180 40, Praha 8, Czech Republic
[14]Dipartimento di Fisica, Università di Genova and INFN, Via Dodecaneso 33, IT-16146 Genova, Italy
[15]Institut des Sciences Nucléaires, IN2P3-CNRS, Université de Grenoble 1, FR-38026 Grenoble Cedex, France
[16]Helsinki Institute of Physics, HIP, P.O. Box 9, FI-00014 Helsinki, Finland
[17]Joint Institute for Nuclear Research, Dubna, Head Post Office, P.O. Box 79, RU-101 000 Moscow, Russian Federation
[18]Institut für Experimentelle Kernphysik, Universität Karlsruhe, Postfach 6980, DE-76128 Karlsruhe, Germany
[19]Institute of Nuclear Physics and University of Mining and Metalurgy, Ul. Kawiory 26a, PL-30055 Krakow, Poland
[20]Université de Paris-Sud, Lab. de l'Accélérateur Linéaire, IN2P3-CNRS, Bât. 200, FR-91405 Orsay Cedex, France
[21]School of Physics and Chemistry, University of Lancaster, Lancaster LA1 4YB, UK
[22]LIP, IST, FCUL - Av. Elias Garcia, 14-1º, PT-1000 Lisboa Codex, Portugal
[23]Department of Physics, University of Liverpool, P.O. Box 147, Liverpool L69 3BX, UK
[24]LPNHE, IN2P3-CNRS, Univ. Paris VI et VII, Tour 33 (RdC), 4 place Jussieu, FR-75252 Paris Cedex 05, France
[25]Department of Physics, University of Lund, Sölvegatan 14, SE-223 63 Lund, Sweden
[26]Université Claude Bernard de Lyon, IPNL, IN2P3-CNRS, FR-69622 Villeurbanne Cedex, France
[27]Univ. d'Aix - Marseille II - CPP, IN2P3-CNRS, FR-13288 Marseille Cedex 09, France
[28]Dipartimento di Fisica, Università di Milano and INFN, Via Celoria 16, IT-20133 Milan, Italy
[29]Università degli Studi di Milano - Bicocca, Via Emanuelli 15, IT-20126 Milan, Italy
[30]Niels Bohr Institute, Blegdamsvej 17, DK-2100 Copenhagen Ø, Denmark
[31]IPNP of MFF, Charles Univ., Areal MFF, V Holesovickach 2, CZ-180 00, Praha 8, Czech Republic
[32]NIKHEF, Postbus 41882, NL-1009 DB Amsterdam, The Netherlands
[33]National Technical University, Physics Department, Zografou Campus, GR-15773 Athens, Greece
[34]Physics Department, University of Oslo, Blindern, NO-1000 Oslo 3, Norway
[35]Dpto. Fisica, Univ. Oviedo, Avda. Calvo Sotelo s/n, ES-33007 Oviedo, Spain
[36]Department of Physics, University of Oxford, Keble Road, Oxford OX1 3RH, UK
[37]Dipartimento di Fisica, Università di Padova and INFN, Via Marzolo 8, IT-35131 Padua, Italy
[38]Rutherford Appleton Laboratory, Chilton, Didcot OX11 OQX, UK
[39]Dipartimento di Fisica, Università di Roma II and INFN, Tor Vergata, IT-00173 Rome, Italy
[40]Dipartimento di Fisica, Università di Roma III and INFN, Via della Vasca Navale 84, IT-00146 Rome, Italy
[41]DAPNIA/Service de Physique des Particules, CEA-Saclay, FR-91191 Gif-sur-Yvette Cedex, France
[42]Instituto de Fisica de Cantabria (CSIC-UC), Avda. los Castros s/n, ES-39006 Santander, Spain
[43]Dipartimento di Fisica, Università degli Studi di Roma La Sapienza, Piazzale Aldo Moro 2, IT-00185 Rome, Italy
[44]Inst. for High Energy Physics, Serpukov P.O. Box 35, Protvino, (Moscow Region), Russian Federation
[45]J. Stefan Institute, Jamova 39, SI-1000 Ljubljana, Slovenia and Laboratory for Astroparticle Physics,
Nova Gorica Polytechnic, Kostanjeviska 16a, SI-5000 Nova Gorica, Slovenia,
and Department of Physics, University of Ljubljana, SI-1000 Ljubljana, Slovenia
[46]Fysikum, Stockholm University, Box 6730, SE-113 85 Stockholm, Sweden
[47]Dipartimento di Fisica Sperimentale, Università di Torino and INFN, Via P. Giuria 1, IT-10125 Turin, Italy
[48]Dipartimento di Fisica, Università di Trieste and INFN, Via A. Valerio 2, IT-34127 Trieste, Italy
and Istituto di Fisica, Università di Udine, IT-33100 Udine, Italy
[49]Univ. Federal do Rio de Janeiro, C.P. 68528 Cidade Univ., Ilha do Fundão BR-21945-970 Rio de Janeiro, Brazil
[50]Department of Radiation Sciences, University of Uppsala, P.O. Box 535, SE-751 21 Uppsala, Sweden
[51]IFIC, Valencia-CSIC, and D.F.A.M.N., U. de Valencia, Avda. Dr. Moliner 50, ES-46100 Burjassot (Valencia), Spain
[52]Institut für Hochenergiephysik, Österr. Akad. d. Wissensch., Nikolsdorfergasse 18, AT-1050 Vienna, Austria
[53]Inst. Nuclear Studies and University of Warsaw, Ul. Hoza 69, PL-00681 Warsaw, Poland
[54]Fachbereich Physik, University of Wuppertal, Postfach 100 127, DE-42097 Wuppertal, Germany

1 Introduction

Supersymmetry (SUSY) [1] is at present one of the most attractive possible extensions of the Standard Model (SM) and its signatures could be observed at LEP through a large variety of different channels. This paper presents searches for the pair production of charginos, neutralinos, sleptons and squarks. The searches were performed and interpreted in the most model-independent way possible in terms of production cross-sections and masses. The results were interpreted in the framework of SUSY models, with different search channels complementing each other in constraining the parameter space.

The data collected by the DELPHI experiment in e^+e^- collisions at centre-of-mass energies ($\sqrt{s}$) up to 208 GeV were used. No signal was found in any of the channels.

The paper is organised as follows. In section 2 the basic supersymmetry framework is described: the general phenomenology is discussed in section 2.1, and implications of more constrained models used for interpreting the data are given in section 2.2. The DELPHI detector is described in section 3, and in section 4 the data sets and event generators are reviewed. In section 5 the general analysis framework is described, the analysis methods are briefly mentioned and the specific search strategies for chargino, neutralino, slepton and squark searches are discussed. The results of each search are separately presented and interpreted in section 6. In section 7 the results are combined and interpreted in the framework of constrained SUSY scenarios with supergravity-inspired (SUGRA) breaking of supersymmetry. A brief summary is given in section 8.

Previous results published by DELPHI can be found in references [2] to [9].

2 SUSY framework

The searches presented in this paper were performed in the framework of the Minimal Supersymmetric extension of the Standard Model (MSSM) [1]. R-parity [1] conservation is assumed, implying that the Lightest Supersymmetric Particle (LSP) is stable and SUSY particles ("sparticles") are pair-produced. In addition, they decay directly or indirectly into the LSP. In this paper the lightest neutralino, $\tilde{\chi}_1^0$, is assumed to be the weakly interacting LSP, which escapes detection giving signatures of missing energy and momentum.

The searches for sparticle production were developed with minimal assumptions, and the selections employed depended primarily on the masses of the particles involved. In particular, the sensitivities of the searches depend on the visible energy released in the decay process. In direct decays into the LSP, this visible energy is largely determined by the mass difference (ΔM) between the decaying sparticle and the LSP. In indirect (cascade) decays, other mass differences can also be important.

The MSSM has a large number of free parameters in addition to the SM ones. The most model-independent interpretation of the results is in terms of those masses or cross-sections which explicitly affect each production channel. A common interpretation of the results from the various searches can also be performed in terms of the parameters of the model, but this requires a manageable number of free parameters. For this reason, assumptions must be made and specific scenarios defined for such an interpretation. The

---

[1]R-parity is a multiplicative quantum number defined as $R = (-1)^{3(B-L)+2S}$ where B, L and S are the baryon number, the lepton number and the spin of the particle, respectively. SM particles have R=+1 while their SUSY partners have $R = -1$.

general phenomenology of the searches will be discussed in section 2.1, followed by a description of the implications of more specific scenarios in section 2.2.

2.1 General phenomenology

<u>Squarks and Sleptons</u>

The "sfermions", squarks and sleptons, are the scalar partners of the SM fermions. The left- and right-handed chiral states of each SM fermion, f_L and f_R, have as SUSY partners two scalars, usually labelled $\tilde{f}_L$ and $\tilde{f}_R$.

Sleptons and squarks could be pair-produced at LEP via e^+e^- annihilation into Z/γ, leading to $\tilde{f}_R\overline{\tilde{f}_R}$ or $\tilde{f}_L\overline{\tilde{f}_L}$ final states. Selectrons could also be produced through t-channel neutralino exchange. The selectron cross-section therefore depends critically on the neutralino mass, and destructive interference can make it very small. The t-channel contribution also introduces the possibility of $\tilde{e}_L\tilde{e}_R$ production.

If the unification of sfermion masses at a high mass scale typical of Grand Unified Theories (GUT) is assumed, lower masses and lower cross-sections for a given universal mass parameter are typically expected for the partners of right-handed fermions. Under this assumption, the kinematic accessibility of first and second family sfermions at LEP depends only on their assumed common mass at the unification scale. Squarks are in general expected to be heavier than sleptons. However, for sfermions of the third family the large Yukawa couplings lower the masses and large mixing between left and right states may occur. In this case, the lighter mass states of third family sleptons and squarks, $\tilde{\tau}_1$ (stau), $\tilde{b}_1$ (sbottom) and $\tilde{t}_1$(stop), are candidates for the lightest charged supersymmetric particle.

In large regions of the SUSY parameter space the dominant decay of the sfermions is to the corresponding fermion and the lightest neutralino, $\tilde{f} \to f\tilde{\chi}_1^0$. In the case of the stop, the decay $\tilde{t} \to t\tilde{\chi}_1^0$ is not kinematically allowed at LEP, and the dominant 2-body decay channel is expected to be $\tilde{t} \to c\tilde{\chi}_1^0$ ($\tilde{t} \to b\tilde{\chi}_1^\pm$ being disfavoured by existing limits on the chargino mass). If $m_{\tilde{\nu}} < M_{\tilde{t}_1}$, the three-body decay $\tilde{t}_1 \to b\ell\tilde{\nu}$ may compete with the $c\tilde{\chi}_1^0$ decay.

Thus final state topologies with a pair of leptons or jets and missing energy are the relevant ones in the search for sleptons and squarks, respectively, and the total energy of the detectable final state particles (and thus the sensitivity of the search) depends primarily on the mass difference between the sfermion and the LSP.

<u>Charginos and Neutralinos</u>

In the MSSM there are four neutralinos, $\tilde{\chi}_i^0, i = 1, 4$ (numbered in order of increasing mass) and two charginos $\tilde{\chi}_i^\pm, i = 1, 2$ which are linear combinations of the SUSY partners of neutral and charged gauge and Higgs bosons (gauginos and higgsinos). The lightest states can be mainly gaugino or higgsino, or strongly mixed (for similar gaugino and higgsino mass parameters).

Neutralinos (charginos) could be pair-produced at LEP via s-channel Z (Z/γ) exchange or t-channel exchange of a selectron (sneutrino). The t-channel contribution can be important if the slepton is light. The interference with the s-channel diagram is constructive in the case of neutralinos but destructive in the case of charginos.

Expected decays are $\tilde{\chi}_i^0 \to \tilde{\chi}_1^0 f\bar{f}$ and $\tilde{\chi}_j^\pm \to \tilde{\chi}_1^0 f\bar{f}'$. If the sfermions are heavy, these decays proceed via Z or W emission. However, sfermion emission may also contribute if the sfermions are light, increasing the partial width for decays into the corresponding

fermions, and two-body decays into $\bar{\text{f}}\tilde{\text{f}}$ can dominate if kinematically allowed. The one-loop decay $\tilde{\chi}_2^0 \to \tilde{\chi}_1^0 \gamma$ can be important in specific regions of the parameter space when other decays are suppressed.

Thus the sfermion mass spectrum may significantly affect both the production cross-section and the decay modes of charginos and neutralinos, and many final state topologies are possible.

In the case of chargino pair production, the final state is expected to be four jets if both charginos decay hadronically, two jets and one lepton if one chargino decays into $\ell\nu\tilde{\chi}_1^0$, and leptons only if both charginos decay into leptons. The branching-ratio of $\tilde{\chi}_1^\pm \to \tilde{\chi}_2^0 \, \text{f} \, \bar{\text{f}}'$ can be sizable, in particular in the regions of the parameter space where $\tilde{\chi}_2^0 \to \tilde{\chi}_1^0 \gamma$ is important. In this case, the above topologies are accompanied by photons.

If the mass difference ΔM between the chargino and the LSP is very small the visible energy released in the decay is very small, making the signal hard to detect. The simultaneous production of a photon by initial state radiation (ISR) was used to explore such regions as this allows a very efficient background rejection (at the expense of a low signal cross-section). Still lower mass differences imply a long lifetime of the chargino, which can then be identified as a heavy stable charged particle or one with a displaced decay vertex.

In the case of the detectable $\tilde{\chi}_1^0 \tilde{\chi}_k^0$ neutralino production channels (*i.e.* excluding $\tilde{\chi}_1^0 \tilde{\chi}_1^0$), the most important signatures are expected to be acoplanar pairs of jets or leptons [2] with high missing energy and momentum. Although $\tilde{\chi}_1^0 \tilde{\chi}_2^0$ and $\tilde{\chi}_1^0 \tilde{\chi}_3^0$ are expected to dominate in most of the parameter space, channels like $\tilde{\chi}_2^0 \tilde{\chi}_3^0$ and $\tilde{\chi}_2^0 \tilde{\chi}_4^0$ must also be considered for a complete coverage. These give rise to cascade decays with multiple jets or leptons in the final state, possibly accompanied by photons from $\tilde{\chi}_2^0 \to \tilde{\chi}_1^0 \gamma$.

2.2   Constraining the parameter space

To make the model more predictive the unification of some parameters at a high mass scale typical of Grand Unified Theories (GUT) can be assumed [10]. The MSSM parameters and the assumptions that can be relevant in the interpretation of the results are listed below:

- **tan β**, the ratio of the vacuum expectation values of the two Higgs doublets;
- **μ**, the Higgsino mixing mass parameter;
- **M_1, M_2, M_3**, the $U(1) \times SU(2) \times SU(3)$ gaugino masses at the electroweak (EW) scale: when gaugino mass unification at the GUT scale is assumed, with a common gaugino mass **$m_{1/2}$**, the relation between M_1 and M_2 is $M_1 = \frac{5}{3}M_2\tan^2\theta_W \sim 0.5M_2$;
- **$M_{\tilde{\text{f}}}$**, the sfermion masses: under the assumption of sfermion mass unification, **m_0** is the common sfermion mass at the GUT scale;
- The pseudoscalar Higgs mass, **m_A** on which the masses in the Higgs sector depend: if scalar mass unification is assumed, m_A at the EW scale can be derived from m_0;
- the trilinear couplings **A_{f}** determining the mixing in the sfermion families: the third family trilinear couplings are the most relevant ones, **A_τ, A_b, A_t**, and under the assumption of universal parameters at high mass scale there is a common trilinear coupling **A**.

Mass mixing terms at the EW scale given by $m_\tau(A_\tau - \mu\tan\beta)$, $m_b(A_b - \mu\tan\beta)$ and $m_t(A_t - \mu/\tan\beta)$ are considered for $\tilde{\tau}$, $\tilde{\text{b}}$ and $\tilde{\text{t}}$, respectively. The mass splitting grows

---

[2]In this context, acoplanar means that the direction of one of the leptons/jets is not in the plane formed by the direction of the other lepton/jet and the beam line. Through this paper, the acoplanarity angle between the direction of two particles is defined as the complementary (with respect to $180°$) of the angle between their direction in the plane transverse to the beam direction.

with the mixing terms, and for large $|\mu|$ this can give light $\tilde{\tau}_1$ and $\tilde{b}_1$ states if $\tan\beta$ is large, or a light $\tilde{t}_1$ for small $\tan\beta$.

In the model referred to as the "Constrained MSSM" (CMSSM) in the following, sfermion and gaugino mass unification are assumed. The parameter set is then reduced to $M_2, m_0, \tan\beta, \mu, m_A$ and three A_f couplings. This is the model considered in section 7.

Further tightening the assumptions, the individual A_f couplings can be replaced by a universal coupling A and m_A can be related to the other parameters by assuming scalar (including Higgs bosons) mass unification. Requiring in addition the correct reproduction of the EW symmetry scale, which fixes the absolute value of μ, defines the minimal supergravity-broken MSSM (mSUGRA).

The direct results of the searches are first derived and presented in the most model-independent way possible. Under the assumptions described above, the results are then used to constrain the SUSY parameters. Presently the strongest constraints on SUSY models come from the MSSM Higgs searches [11].

Chargino production is the most important direct SUSY detection channel for large regions of the parameter space. However, if sfermions are light (corresponding to a low m_0 scenario), or if the parameters take particular values, the chargino production cross-section can be greatly suppressed or undetectable final states can dominate (in particular for small mass splittings). The most relevant of these cases are the following:

High m_0

For high m_0, the sfermions are heavy and have little influence on the observable phenomenology. The chargino pair-production cross-section is large and the chargino is excluded nearly up to the kinematic limit. The search for charginos in non-degenerate scenarios has been applied down to $\Delta M = M_{\tilde{\chi}_1^\pm} - M_{\tilde{\chi}_1^0} = 3 \text{ GeV}/c^2$. The region $\Delta M < 3 \text{ GeV}/c^2$ is covered by the search requiring an ISR photon and by the searches for long-lived charginos. Moreover, small values of ΔM occurring in scenarios without gaugino mass unification [12] have also been investigated.

At low $\tan\beta$ ($\tan\beta < 1.2$), neutralino searches can extend the coverage beyond the kinematic limit for chargino production. This concerns the region of (low) negative μ and $M_2 > 60 \text{ GeV}/c^2$. In particular, searches for neutralino cascade decays are crucial for investigating $M_2 < 120 \text{ GeV}/c^2$ where the $\tilde{\chi}_1^0 \tilde{\chi}_2^0$ cross-section is small.

Low m_0

If m_0 is low, light sfermions affect the chargino and neutralino production cross-sections. In particular, the decrease of m_0 causes the chargino production cross-section to drop in the region where the gaugino components dominate (low M_2 and high $|\mu|$). Down to $m_0 \simeq 200 \text{ GeV}/c^2$, the cross-section remains high enough to allow chargino exclusion nearly up to the kinematic limit. For lower m_0 the neutralino production cross-section is very much enhanced, and neutralino searches become sensitive instead.

If m_0 is very low ($m_0 \simeq 100 \text{ GeV}/c^2$), sleptons can be sufficiently light to affect drastically the decay patterns of charginos and neutralinos, and nearly invisible final states can become dominant in some cases. However, for such low m_0 and low M_2 (below $200 \text{ GeV}/c^2$) sleptons can also be searched for in direct pair production.

If $M_{\tilde{\chi}_1^\pm} > m_{\tilde{\nu}}$ and the mass difference $M_{\tilde{\chi}_1^\pm} - m_{\tilde{\nu}}$ is small, the chargino decay chain $\tilde{\chi}_1^\pm \to \tilde{\nu}\ell \to \nu\tilde{\chi}_1^0\ell$ is dominant, and leads to an experimentally undetectable final state (the only visible final state lepton has very low momentum). However, in this case the search for selectrons can be used to constrain the sneutrino mass (under the assumption of unification) and thus the chargino mass.

It can also happen, in scenarios with large mixing among sfermions and high $\tan\beta$ and M_2, that 'blind spots' occur in the chargino detection sensitivity due to $\tilde\chi_1^\pm \to \tilde\tau\nu \to \tau\tilde\chi_1^0\nu$ with a small mass difference $M_{\tilde\tau} - M_{\tilde\chi_1^0}$. In this case $\tilde\chi_1^0\tilde\chi_2^0$ or $\tilde\chi_2^0\tilde\chi_2^0$ production with $\tilde\chi_2^0 \to \tilde\tau\tau$ are the only detectable channels. A specific search was designed for this case.

3 Detector description

The DELPHI detector is described in detail in [13]. The central tracking system consisted of a Time Projection Chamber (TPC), supplemented by a system of silicon tracking detectors and drift chambers. These included the Vertex Detector (VD), closest to the beam pipe, the Inner Detector (ID) and the Outer Detector (OD). These were situated inside a solenoidal magnetic field of 1.2 T, parallel to the beam axis. The average momentum resolution for charged particles in hadronic final states is in the range $\Delta p/p^2 \simeq 0.001 - 0.01~(\mathrm{GeV}/c)^{-1}$.

The electromagnetic (EM) calorimeters were symmetric around the plane perpendicular to the beam ($\theta = 90°$) [3], with the High density Projection Chamber (HPC) extending from 88.7° to 43.1° (barrel region), the Forward Electromagnetic Calorimeter (FEMC) from 36° down to 9°, overlapping with the Small angle Tile Calorimeter (STIC), the DELPHI luminometer, which covered the range $1.7° \le \theta \le 10.6°$. The region of poor electromagnetic calorimetry at a polar angle close to 40° was instrumented by scintillators (hermeticity taggers) [14] to tag photons.

The Hadron Calorimeter (HCAL) covered 98% of the solid angle. Muons with momenta above 2 GeV/c penetrated the HCAL and were recorded in sets of Muon drift chambers located in the barrel (MUB), forward (MUF) and surround [4] (MUS) regions of the detector.

4 Data samples and event generators

During the year 2000 DELPHI collected data in the centre-of-mass energy range from 201.5 to 208.8 GeV. The average centre-of-mass energy was $<\sqrt{s}> \simeq 206$ GeV and the total integrated luminosity amounted to about 224 pb^{-1}. In 1999 (1998) the DELPHI detector collected about 227 pb^{-1} (158 pb^{-1}) at centre-of-mass energies around 192, 196, 200 and 202 GeV (189 GeV).

The data collected in the years 1999-2000 were analysed in the searches presented in this paper. In some cases the 1998 data were re-analysed for consistency with the improved methods presented in this paper. This is clearly stated in the description of the analyses. Combination with earlier results was performed to obtain cross-section limits and excluded regions of model parameters. Details for each channel are given in section 6.

Quality requirements on the status of the subdetectors most relevant for each analysis were also applied, generically based on the status of the main tracking devices. Muon chambers or calorimeters were considered in channels where muon or electromagnetic shower detection was crucial. The luminosity loss was at most of the order of a few percent and was taken into account in the analyses.

---

[3]In DELPHI, a right-handed Cartesian coordinate system is used with the z direction defined by the direction of the electron beam, and the x-axis pointing towards the centre of the LEP ring. The origin is at the centre of the detector. The polar and azimuthal angles θ and ϕ are defined with respect to the z axis and $\phi = 0$ corresponds to the x-direction, and the coordinate r is defined in the usual way as $r = \sqrt{x^2 + y^2 + z^2}$. In this paper, polar angle ranges are always assumed to be symmetric with respect to the $\theta = 90°$ axis.

[4]The region between the barrel and end-caps parts of DELPHI not covered by the MUF and the MUB chambers

On September 1st 2000, sector 6 of the TPC (corresponding to 1/12 of the TPC acceptance) failed beyond repair. This required modifications of the pattern recognition, and affected the quality of charged track reconstruction. Thus special care had to be taken for each search when analysing the data collected without TPC sector 6. The accumulated integrated luminosities with and without a working sector 6 are respectively 164 pb^{-1} and 60 pb^{-1} at average centre-of-mass energies around 206 GeV.

In order to increase the sensitivity for a discovery, the data collected in 2000 (with and without a fully operational detector) were divided into 4 regions of centre-of-mass energy as given in table 1 [5].

		$\sqrt{s}$ region of analysis	$\mathcal{L}$ (pb^{-1})	$< \sqrt{s} >$ (GeV)
1	Sector 6 On	$\sqrt{s} \leq 205.75$ GeV	78.3	204.9
2	Sector 6 On	$205.75 < \sqrt{s} \leq 207.5$ GeV	78.8	206.7
3	Sector 6 On	207.5 GeV$< \sqrt{s}$	7.2	208.0
4	Sector 6 Off	all $\sqrt{s}$	60.0	206.5

Table 1: Definition of the $\sqrt{s}$ regions used to analyse the data collected in 2000.

To evaluate the signal efficiencies and background contaminations, simulated events were generated using several different programs.

The background process $e^+e^- \to q\bar{q}(n\gamma)$ was generated with PYTHIA 6.125 [15]. For $\mu^+\mu^-(\gamma)$ and $\tau^+\tau^-(\gamma)$, DYMU3 [16] and KORALZ 4.2 [17] were used, respectively. The BHWIDE generator [18] was used for Bhabha events. Simulation of four-fermion final states was performed using EXCALIBUR [19] and grc4f [20].

Two-photon interactions giving hadronic final states were generated using TWOGAM [21], PHOJET [22] and PYTHIA 6.143 [15], while leptonic final states were generated using the generator of [23], including radiative corrections for the $e^+e^- \mu^+\mu^-$ and $e^+e^- \tau^+\tau^-$ final states.

SUSYGEN 2.2004 [24] was used to generate chargino, neutralino, slepton, and sbottom signal events and to calculate cross-sections and branching ratios for these channels. For the nearly mass-degenerate case, the chargino decays were modelled with the results of the computations of reference [12]. Stop events were generated according to the expected differential cross-sections using the BASES and SPRING program packages and taking special care in the modelling of the stop hadronisation [25].

In all cases except for stop generation, JETSET 7.4 [15], tuned to LEP1 data [26], was used for quark fragmentation.

The generated signal and background events were passed through the detailed simulation of the DELPHI detector [13] and then processed with the same reconstruction and analysis programs as the real data. The fast DELPHI simulation code SGV [27] was also used for signal efficiency studies in some analyses. The numbers of simulated events from different background processes were several times the numbers in the real data.

5   Descriptions of the analyses

The analyses described below can be divided into two stages. The first stage was very similar for all searches and consisted of the selection of charged and neutral particles fol-

---

[5] The three energy bins shown in the table for the period in which the detector was fully operational will be referred to in the text by their approximate average centre-of-mass energies: 205, 207 and 208 GeV.

lowed by an event preselection. In the subsequent stage, the analyses differed according to the characteristics of the various signals. Each analysis had a set of additional preselection cuts complementing the ones described in section 5.1.2 followed by more restrictive selections.

As discussed above, the sensitivities of the searches depend on the mass difference (ΔM) between the produced sparticles and the LSP, which determines the visible energy released in the process. The coverage of all the relevant ΔM regions often requires the combination of different searches or the optimisation of the selection criteria separately in each ΔM interval. Sparticle searches for very low values of ΔM are particularly challenging and required different preselections. In most searches several different topologies were considered, accounting for the different possible final states; in particular, high and low multiplicity topologies had to be treated separately.

Different analysis techniques were chosen for the various searches: some analyses were based on successive requirements on individual event variables ("sequential cut analyses"), others used multidimensional techniques based on likelihood ratios or neural networks. The preselection and the details of each analysis are described in the following parts of this section.

5.1 Basic selections and techniques

5.1.1 Particle selection

The following quality requirements were applied to the charged and neutral particles observed in the detector.

Charged particles were required to have momentum p above 100 MeV/c and below $0.75\sqrt{s}$, a relative momentum error less than 100%, and to extrapolate back to within 5 cm of the main vertex in the transverse ($r\phi$) plane and 10 cm/$\sin\theta$ in the longitudinal (z) direction. Similar but more stringent criteria were applied to particles whose tracks extrapolated to the TPC, but which gave no signal in the TPC.

In the stau analysis (see section 5.2.3) charged particle tracks were required to have TPC information, or all three of the detectors VD, ID and OD used in the reconstruction of the track [6]. In addition, only tracks with an angle to the beam exceeding 15° were kept.

In the nearly degenerate chargino search (see section 5.4.2) there was no lower bound on the momentum for tracks at polar θ angle above 25°, while $p > 150$ MeV/c was required otherwise. In addition, the impact parameter requirements were less stringent.

Energy clusters in the calorimeters were taken as neutral particles if not associated to a charged particle and if above an energy threshold ranging from 300 to 500 MeV for deposits in the electromagnetic calorimeters (depending on the region of the detector) and 900 MeV for deposits in the hadron calorimeter. Cuts removing clusters created by radioactivity in the lead of the HPC or by particles from cosmic ray showers were also applied.

5.1.2 General event preselection

In the general preselection, events were kept if there were at least two charged particles, at least one of them had a transverse momentum above 1.5 GeV/c, and the transverse

---

[6]In this paper, whenever tracks reconstructed with TPC information are selected, more than 4 of the 16 pad rows are required.

energy of the event [7] exceeded 4 GeV/c. The main background processes rejected by this were two-photon interactions (for which most of the energy is deposited in the forward regions of the detector), neutral or single track final states (like $e^+e^- \to \gamma\gamma$, $e\gamma \to e\gamma$) and beam-related backgrounds (such as beam-gas interactions).

For chargino searches in nearly degenerate scenarios a different preselection was used: at least two charged particles were required, as well as one isolated electromagnetic cluster with transverse energy above a $\sqrt{s}$ dependent threshold close to 5 GeV and a mass recoiling against it above 90 GeV/c^2. Two-photon and beam-gas backgrounds were reduced by rejecting events with a large fraction of their total energy in the forward region of the detector.

5.1.3 Particle identification and reconstruction algorithms

The following criteria for particle and event classification were common to the different searches.

Particle jets were reconstructed using three different approaches:

- The DURHAM [28] algorithm was used to cluster the particles into a fixed number of jets: two or four.
- The LUCLUS [15] algorithm was applied with the critical distance set to $d_{\text{join}} = 10$ GeV/c or $d_{\text{join}} = 2.5$ GeV/c . The final number of jets is, thus, variable (and lower in the first case).
- A specific algorithm optimised for the low multiplicity jets resulting from τ decays was used for $\tilde{\tau}$ pair production searches. This method considered all possible ways of clustering the charged particles in the event into groups, always requiring the invariant mass to be below 2 GeV/c^2. Clearly identified leptons were considered as a single group, except for pairs of oppositely charged, well identified electrons close together which were allowed to be grouped with other particles, since they could be from a converted photon.

  If possible, the event was clustered into two groups with invariant mass below 2 GeV/c^2. If no such combination existed, the one with the smallest number of groups was kept. When more than one way of obtaining two groups both with invariant mass below 2 GeV/c^2 was found, the grouping yielding the lowest sum of masses was retained. Once the best grouping of the charged tracks was found, it was attempted to associate the neutrals in the event to the particle groups. Also in this step, the grouping yielding the lowest sum of masses was chosen. However, as very few long-lived neutral hadrons are expected in τ-decays, neutral hadronic clusters were never included in the clusters, but treated as isolated neutrals. Also electromagnetic clusters which could not be merged into any of the groups without the invariant mass exceeding 2 GeV/c^2, were left as isolated neutrals. In addition, a special procedure was applied to identify and correct for neutral clusters that were likely to be either bremsstrahlung photons or a shower induced by an electron that was not correctly assigned to the track by the reconstruction program.

Isolated leptons or photons in the event are often very important in distinguishing signal and background. In the present searches, two isolation criteria were defined, depending on the multiplicity of the event:

- In low multiplicity searches, charged particles were classified as isolated if the total charged energy, excluding the energy of the particle itself, within 10° of the track

---

[7]The transverse energy is defined as the sum of the absolute values of the transverse momenta of all particles in the event.

direction was below 2 GeV. Slightly tighter cuts in the impact parameters (1 cm and 5 cm in $r\phi$ and z respectively) and in the momentum error were also applied.

- In high multiplicity searches, a photon was considered isolated if its angular separation from any neutral or charged particle was greater than 15°. A lepton was tagged as isolated if its angular separation from all the jets (computed without the lepton using the LUCLUS algorithm with $d_{join} = 40$ GeV/c) was greater than 20°.

The identification of the track made by a muon, electron, or hadron was "tight","loose", or "veto". Tight identification was unambiguous. A particle could simultaneously be loosely identified as several different species. A wrong identification could be vetoed.

The identification of muons was provided primarily by the DELPHI standard algorithm described in [13] which relies on the association of charged particles to signals in the muon chambers and the HCAL.

Electron and photon identification was performed by the algorithm described in [29] which combines deposits in the EM calorimeters with tracking information and takes possible radiation and interaction effects into account by a clustering procedure in an angular region around the main shower. In low multiplicity topologies a very loose electron identification based on the ratio E/p between the energy deposited in the EM calorimeter and the momentum of the associated charged track was also used. In the $\tilde{\tau}$ analysis (see section 5.2.3), the clustering procedure was not used for tracks in the barrel region of the detector, since it tended to treat charged pions from τ decays wrongly, if they were accompanied closely by neutral pions.

Below, whenever the identification level is not specified, it is assumed to be "tight" for electrons and "loose" for muons. In the case of electrons, "tight" identification basically adds some isolation requirements to the identification ones.

e/γ separation inside the acceptance of the STIC luminometer was performed on a statistical basis, by using the veto information of the two planes of the scintillator counters placed in front of it.

In the stau analysis a particle was considered as a tight hadron if it was not classified as a muon or electron and had an associated energy in the hadron calorimeter exceeding 50% of its momentum or else was considered as a loose hadron if it had hadronic energy associated and it was not tightly identified as a muon or electron. If both the electromagnetic and hadronic energies were small (less than 1 and 6 GeV respectively), and the difference between hadronic energy and the track momentum was above 10 GeV, the particle was assigned both the loose muon and loose hadron code.

Decays of b-quarks were tagged using a probabilistic method based on the impact parameter of tracks with respect to the main vertex [30]. $\mathcal{P}_E^+$ stands for the corresponding probability estimator for tracks with positive impact parameter, the sign of the impact parameter being defined by the jet direction. The combined probability $\mathcal{P}_{comb}$ included in addition contributions from properties of reconstructed secondary vertices.

All searches made use of the information from the hermeticity taggers [14] to reject events with photons in the otherwise insensitive region at polar angles around 40° and 140°. If there were active taggers not associated to reconstructed jets, the event was rejected if the tagger was located in the direction of the missing momentum. In the stau analysis, where neutrinos from tau decays made the estimation of the direction of the missing momentum unreliable, events containing active and isolated taggers were rejected irrespective of the direction of the missing momentum.

5.1.4   Analysis techniques

<u>Likelihood ratio method</u>

In the likelihood ratio method used, several discriminating variables are combined into one on the basis of their one-dimensional probability density functions (pdf's). If the variables used are independent, this gives the best possible background suppression for a given signal efficiency [31]. For a set of variables $\{x_i\}$, the pdf's of these variables are estimated by normalised frequency distributions for the signal and the background samples. We denote the pdf's of these variables $f_i^S(x_i)$ for the signal events and $f_i^B(x_i)$ for the background events submitted to the same selection criteria. The likelihood ratio function is defined as $\mathcal{L}_{\mathcal{R}} = \prod_{i=1}^{n} \frac{f_i^S(x_i)}{f_i^B(x_i)}$. Events with $\mathcal{L}_{\mathcal{R}} > \mathcal{L}_{\mathcal{R}_{\mathcal{CUT}}}$ are selected as candidate signal events. The choice of variables and the value of $\mathcal{L}_{\mathcal{R}_{\mathcal{CUT}}}$ were optimised using simulated event samples by minimising the signal cross-section that was expected to be excluded at 95% confidence level in the absence of a signal.

<u>Neural networks</u>

A neural network provides a different way of defining one discriminating variable from multidimensional distributions of event variables given as inputs. In the form used here (see section 5.3) it contains three layers of nodes: the input layer where each neuron corresponds to a discriminating variable, the hidden layer, and the output layer which is the response of the neural network. The program used in the squark analysis was SNNS [32]. A "feed forward" architecture is implemented and the "back-propagation" algorithm is used to train the network with simulated events. An independent validation sample was also used not to overtrain the network. A way of enhancing the efficiency of the network without increasing too much the number of its parameters is to define a separate output node for each type of event that the neural network should separate. More details are given in section 5.3.

5.2   Slepton searches

Supersymmetric partners of electrons, muons and taus were searched for. In this paper, data collected by DELPHI from 1998 to 2000 at centre-of-mass energies between 189 and 208 GeV were analysed, and were combined with the previous results [2].

The track selection and the general event preselection described in sections 5.1.1 and 5.1.2 respectively were used. The analyses were then performed in two stages. Firstly, a loose selection was used to obtain a sample of low multiplicity events. Events with less than ten charged particles and a visible invariant mass above 4.5 GeV/c^2 were retained for further analysis. Different selections were then applied in each of the three channels.

5.2.1   Selectron searches

To search for selectrons, the general topology required was two acoplanar electrons and missing energy. All candidates with exactly two well reconstructed, isolated, oppositely charged particles with momentum above 1 GeV/c according to the definition described in section 5.1.3 were first selected. One of the two charged particles was required to be tightly identified as an electron, rejecting events if the other was identified as a muon.

At this stage of the selection the sample consisted mainly of Bhabha and two-photon events. Satisfactory agreement was observed between the data and simulated background, as shown in figure 1 [8].

A series of tighter cuts reduced the SM background further. As two-photon events are predominantly at low polar angles and with low momentum, the visible energy was required to be greater than 15 GeV, the energy deposited in the low angle STIC calorimeter less than 4 GeV and the total transverse momentum with respect to the beam axis greater than 5 GeV/c. To reduce the number of Bhabha events an upper limit on the visible energy of 100 GeV was imposed, while also requiring that the neutral energy not associated to the charged particle tracks be less than 30 GeV. Events were also rejected if there were more than four neutral clusters in total, each with energy above 500 MeV. Bhabha events are coplanar with a large opening angle, hence it was demanded that the opening angle between the two tracks be lower than 165° and the acoplanarity be greater than 15°. Constraints were also imposed on the momenta of the two particles, requiring that both tracks had momentum greater than 2 GeV/c.

5.2.2 Smuon searches

Smuon pair production with decays to muon plus neutralino is expected to give acoplanar muons and missing energy. To select this topology, exactly two well reconstructed, isolated, oppositely charged particles with momenta above 1 GeV/c were required (according to the criteria defined in section 5.1.3). At least one of the particles had to be loosely identified as a muon. It was further required that neither particle be identified as an electron. The selected sample consisted mainly of two-photon events and fair agreement between real data and simulated background was observed (see figure 2). In figure 2(d), the slight discrepancy between data and MC in the tail of the two-photon background distribution is in a kinematic region rejected by visible and forward energy cuts in the next step of the analysis.

To reduce the SM background further a series of tighter cuts were applied. To remove two-photon events, the visible energy was required to be greater than 10 GeV. Also, the energy in the STIC had to be less than 1 GeV. It was also demanded that the transverse momentum be greater than 5 GeV/c. To remove $e^+e^- \to \mu^+\mu^-$ events, an upper limit of 120 GeV on the visible energy was imposed whilst also requiring the unassociated neutral energy to be less than 10 GeV, with no more than two neutral clusters. This background was further suppressed by accepting only events in which the opening angle between the tracks was less than 165° and the acoplanarity was greater than 15°. To reduce t-channel W pair contamination, events were rejected if the positively charged muon was within 40° of the e^+ beam direction, or the negatively charged muon was within 40° degrees of the e^- beam direction.

5.2.3 Stau searches

The signature of stau-pair production is events with two acoplanar taus and high missing energy. Due to the scalar nature of the stau, the two taus are produced centrally. To select this topology, the particles in the events were grouped into clusters according to the algorithm described in section 5.1.3. Events with exactly two particle clusters (possibly accompanied by isolated neutral particles) were considered further if they contained at least one charged particle with momentum above 1 GeV/c, with a relative error less

---

[8]In order to show the different background contributions, the largely dominant Bhabha background was suppressed in these plots by demanding that the opening angle between the two tracks was below 176°.

than 30%. Its track had to be above 30° in polar angle, or to be isolated (no neutral or charged activity in a cone of 20° half-angle around the track). Its calorimetric energy should not exceed its momentum by more than three times the expected error on the calorimetric measurement. A comparison of data and simulated SM background at this stage [9] is shown in figure 3. It was further required that there were no more than six charged particles in the event and the total charge was 0 or ±1.

Tight and loose electrons, muons and hadrons were defined as described in section 5.1.3. In addition, if a particle had a loose identification for one species, and was vetoed for the other two, it was also considered as tightly identified. If a track pointed to a gap in the electromagnetic calorimetry, it was considered as a loose electron, even if the DELPHI algorithm vetoed the electron hypothesis. Tracks with no identification information were treated as loose electrons. Neutral clusters passing the criteria of section 5.1.1 were used if their angle to the beam was above 15°. Furthermore, no identified hadronic secondary interactions inside the tracking system were allowed.

Beyond this point, the analysis differed depending on whether a stau with mass above or below $m_Z/2$ was searched for.

Search for staus with high mass

To suppress the two-photon background, it was required that the total transverse momentum imbalance exceed 4 GeV/c, the total calorimetric energy below 30° in polar angle did not exceed 20% of the beam momentum and the total momentum of the event was within the region: $\theta(\Sigma \vec{p}) > 30°$.

To reduce the background from radiative return to the Z, none of the clusters were allowed to have a total momentum (p^{JET}) above 70% of the beam momentum, the momentum of isolated photons had to be less than 10% of the beam momentum, and the acoplanarity was required to be above 12°. To reject $e^+e^- \rightarrow Z/\gamma \rightarrow \tau^+\tau^-$ events where the decay of one τ yielded visible products with large momentum, while the other decay yielded soft products, the momentum transverse to the thrust axis was required to exceed 0.7 GeV/c.

This selection was supplemented by cuts that depended on the region of the $(M_{\tilde{\tau}}, M_{\text{LSP}})$ plane considered. At any given point in the plane, it was demanded that the accepted events in that point would be kinematically compatible with the corresponding signal: The maximal momentum the τ can have in the lab frame is $p_{max} = \frac{\sqrt{s}}{2}\left(1 - [M_{\text{LSP}}/M_{\tilde{\tau}}]^2\right)\left(1 + \sqrt{1 - M_{\tilde{\tau}}^2/s}\right)$, which is also the end-point of the spectrum of the visible τ - jet momentum. Hence p_{high}^{JET} (the larger of the two jet momenta) was required to be less than p_{max}. For high $\Delta M = M_{\tilde{\tau}} - M_{\text{LSP}}$, the remaining background from two-photon events can be removed by requiring large transverse momentum imbalance. At lower values of ΔM such a cut would dramatically reduce the signal detection efficiency, and other methods must be employed to reduce this source of background. For the remaining two- and four-fermion backgrounds, the situation was the opposite: the requirement that the events should be kinematically compatible with a low ΔM signal imposes a strong cut on p_{high}^{JET}, while other methods must be used for high ΔM.

Therefore, if ΔM was below (above) 20 GeV/c^2 the total missing transverse momentum ($\not{p}_t$) had to exceed 0.8 (1.2) times the maximum transverse momentum a $\gamma\gamma$ event could have without one of the beam-remnant electrons being deflected into the STIC (ie. by

---

[9] In order to show the contribution of all classes of background, the largely dominant Bhabha background was suppressed in these plots by demanding that the missing transverse momentum was above 4 GeV/c, and that the acoplanarity was above 1°.

an angle greater than $\theta_{min} = 1.82°$). This limit depended on the centre-of-mass energy: $p_T^{\lim} = \sqrt{s}\sin\theta_{min}/(1+\sin\theta_{min}) = 0.031\,\sqrt{s}$ [10]. In addition, in the region with ΔM below 20 GeV/c^2 there should be no calorimetric energy below 30°, and $\theta(\Sigma\vec{p})$ had to exceed 45°.

Electrons and muons in WW events might come either directly from the W-decay, or indirectly from τ-decays. In the former case, the momentum of the detected lepton tends to be higher than in the signal, where all electrons and muons would be indirect. Therefore, in order to reduce the background from WW events, it was demanded that the highest momentum of any tightly or loosely identified lepton in the event was less than $(0.1\Delta M + 0.6)P_{Wmin}^{lept}$, where P_{Wmin}^{lept} is the lowest momentum a lepton in the decay $W \rightarrow \ell\nu$ can obtain in the lab-frame if the W is on-shell. In the region of high ΔM, it was also demanded that there be no more than one tightly identified electron or muon in the event.

To suppress the WW background further, the events were analysed as if they were indeed WW events, and the θ angle of the positive W was estimated (θ_{W+}). Only WW events with both W bosons decaying leptonically were present at this stage of the analysis. If neither W decayed to a tau, θ_{W+} can be calculated exactly (albeit usually with two-fold ambiguity). On the other hand, if either W decays to a τ the solution is approximate, since the momentum of the τ is unknown. The W-decay to a muon or an electron could be distinguished from the τ-mode by the presence of a single track cluster with at least a loose lepton identification and a momentum above the lowest possible momentum for the charged lepton from the decay of an on-shell W. Decays that did not fulfil these requirements were assumed to be decays to τ. In these decays, the momentum of the initial τ was estimated as the average momentum of taus from W decay, calculated for tau momenta above the measured jet momentum. The direction of the momentum of the tau was taken as the measured jet direction.

W pair-production is highly asymmetric, while the signal is symmetric. The W pair-production process tends to have higher p_{high}^{JET} and θ_{W+}. In addition, p_{high}^{JET} and θ_{W+} are correlated in such processes, while they are independent in $\tilde{\tau}$ production. In order to exploit the difference in the distribution and correlation of these observables, it was required that

$$\theta_{W+} < \begin{cases} -3.0(x - 0.325) + A & \text{if } x < 0.325 \\ A & \text{if } 0.325 \leq x < 0.52 \\ -2.1(x - 0.52) + A & \text{if } x \geq 0.52 \end{cases}$$

where θ_{W+} is in radians and $x = p_{high}^{\text{JET}}/p_{beam}$, and A is a constant chosen to be 1.6 (2.1) for ΔM below (above) 20 GeV/c^2. The boundary of the region in the $(\theta_{W+}, p_{high}^{\text{JET}})$-plane thus defined closely follows a curve of constant ratio between the probability density functions for signal and background (the likelihood ratio).

Search for light staus without coupling to the Z

As discussed in section 6.3, to a large extent a light stau can be excluded using LEP1 results. This is however not possible at the stau mixing angle giving the minimum cross-section, when the coupling to the Z vanishes. The high mass analysis described in the previous section looses its efficiency for stau masses below 15 GeV/c^2. This is mainly

---

[10] The missing transverse momentum was estimated in four different ways: from the transverse momentum of the two jets, as that of all particles passing the quality cuts, as that of all reconstructed particles except those identified as bremsstrahlung photons, and as that of all reconstructed particles. The cut was applied on the smallest of these. This gave stability against possible errors in reconstruction and against the presence of noise or cosmics.

due to the fact that the stau-pairs are highly boosted at such a low mass, so that they fail the acoplanarity cut.

Therefore a specific search was required for low $M_{\tilde{\tau}}$ at the minimal cross-section mixing angle. Two search regions were identified: One optimised for very low masses ($M_{\tilde{\tau}}$ below 10 GeV/c^2, referred to as the "very low mass analysis"), and one for higher masses (the "low mass analysis"). As the high mass analysis can exclude ΔM above 4 GeV/c^2 down to $M_{\tilde{\tau}} = 15$ GeV/c^2, this search was optimised for ΔM between m_τ and 4 GeV/c^2. The signal events in this kinematic region are characterised by containing two taus in the barrel, and being softer than two-fermion events but slightly harder than $\gamma\gamma$ events. Due to the sizable boost of the staus, the two jets tend to be rather back-to-back. Two-tau events were selected as described in the previous section, with the additional requirement that the topology was either 1-prong and 3-prong, or two 1-prongs. In the latter case, there should not be two tightly identified leptons of the same flavour in the event. To select central events, the angle of the most energetic particle in each hemisphere of the detector had to be above 50° to the beam, and the sine of the polar angle of each jet had to be above 0.8. The acollinearity was required to be above 0.4°, $p_{max}^{\mathrm{JET}}/p_{beam}$ had to be below 90%, and the observed mass had to be above 4.5 GeV/c^2. There had to be no energy in a 30° cone around the beam-axis.

In the low mass region, $\theta(\Sigma\vec{p})$ had to be above 55° to the beam, the visible mass had to be below $[15(\Delta M - m_\tau) - (M_{\tilde{\tau}} - 25)/3 - (\Delta M - m_\tau)(M_{\tilde{\tau}} - 25)/2 + 15]$ GeV/c^2, and $\displaystyle{\not}p_t$ had to exceed $\max(0.05, (\Delta M - m_\tau)/4)\, p_T^{\mathrm{lim}}$.

In the very low mass region, it was required that $\displaystyle{\not}p_t$ was above $0.01 p_T^{\mathrm{lim}}$, $p_{max}^{\mathrm{JET}}/p_{beam}$ was above 15%, and $\theta(\Sigma\vec{p})$ was above 15° to the beam. The acollinearity had to be below 15°.

5.3 Squark searches

Supersymmetric partners of top and bottom quarks were searched for. The data collected by DELPHI from 1998 to 2000 at centre-of-mass energies from 189 to 208 GeV were analised. The data samples correspond to a total integrated luminosity of about 606 pb^{-1}. The dominant decays of the stop and sbottom squarks are assumed to be $\tilde{t}_1 \rightarrow c\tilde{\chi}_1^0$ and $\tilde{b}_1 \rightarrow b\tilde{\chi}_1^0$, respectively, and the final topology is two acoplanar jets and missing energy. In the non-degenerate scenario ($\Delta M > 10$ GeV/c^2), the neural network analysis has already been presented in [3]. This analysis has been extended down to $\Delta M = 5$ GeV/c^2. In addition, a new analysis based on a sequential cut approach has been developed to search for nearly degenerate stop with the LSP, investigating ΔM values between 2 and 10 GeV/c^2. Moreover, this analysis has been extended to ΔM values up to 20 GeV/c^2 in order to cross-check the non-degenerate analysis.

5.3.1 Non-degenerate scenarios

After the track selection and the event preselection of section 5.1, events were forced into two jets using the Durham algorithm. A common preselection was then applied for both stop and sbottom analyses. To select hadronic events, the number of charged particles reconstructed with TPC information was required to be greater than three, and the energy in the STIC to be less than 70% of the total energy. The polar angle of the thrust axis had to be above 20°. Then the following event quality cuts were applied. The percentage of good tracks, the ratio of the number of charged particle tracks after the particle selection to the number before, had to be greater than 35%. In addition, the scalar sum of charged particle momenta reconstructed with TPC information was

required to be greater than 55% of the total energy in the event, and the total number of charged particles to be greater than six.

To remove radiative return events, the energy of the most energetic neutral particle was required to be less than 40 GeV. Additional cuts were then applied to restrict the selection to events with missing energy. The transverse missing momentum had to be greater than 4 GeV/c, the polar angle of the missing momentum had to be above 20° and the energy in a 40° cone around the z axis was required to be less than 40% of the event energy. Finally, the visible mass of the events was required to be less than 95 GeV/c^2.

The number of events selected by this preselection was 2178 for 2143±8 expected (combined data from $\sqrt{s}$ =189 to 208 GeV). Figure 4 shows the Monte Carlo comparison to the data. At this level for $\Delta M > 10$ GeV/c^2, stop signal efficiencies ranged from 20% to 70% depending on the mass difference between the stop and the neutralino. Sbottom efficiencies were quite similar except at low ΔM where, for example, the efficiency for $M_{\tilde{b}_1}$=90 GeV/c^2 and $M_{\tilde{\chi}_1^0}$=85 GeV/c^2 was close to zero, because the b quarks are produced almost at rest.

The final selection of events was performed using neural network techniques. Separate searches were made for two different ranges of ΔM: $\Delta M > 20$ GeV/c^2 and $5 < \Delta M \leq 20$ GeV/c^2. The neural network structure was the same for the stop and the sbottom searches. There were ten input nodes (variables), ten hidden nodes (in one layer) and 3 output nodes. The ten input variables were: the ratio between the transverse missing momentum and the visible energy, the transverse energy, the visible mass, the softness defined as $M_{\text{jet1}}/E_{\text{jet1}} + M_{\text{jet2}}/E_{\text{jet2}}$, the acollinearity, the quadratic sum of the transverse momenta of the jets $\sqrt{(P_t^{\text{jet1}})^2 + (P_t^{\text{jet2}})^2}$, the acoplanarity, the sum of the first and third Fox-Wolfram moments, the polar angle of the missing momentum and finally the combined b-tagging event probability. For each ΔM window of the stop and sbottom analyses, the neural network was designed with three ouput nodes to discriminate the signal from the combined two-fermion and four-fermion backgrounds, and from the $\gamma\gamma$ interactions leading to hadronic final states.

Although the three output nodes proved useful in training the network, the selection was made according to the output of the signal node only. Figure 5 shows the number of events as a function of the signal efficiency for the two mass analysis windows of the stop and the sbottom searches. The number of events in the data is in agreement with the Standard Model background predictions over the full range of neural network outputs. The optimisation of the final cuts was performed by minimising the expected confidence level of the signal hypothesis, CL_s [33].

5.3.2   Nearly mass degenerate scenarios

The stop ($\tilde{t}_1$) and the sbottom ($\tilde{b}_1$) can be nearly degenerate in mass with the LSP, without requiring special theoretical assumptions.

The width of the decay $\tilde{t} \rightarrow c\tilde{\chi}_1^0$ is proportional to $M_{\tilde{t}}(1 - M_{\tilde{\chi}_1^0}^2/M_{\tilde{t}}^2)^2$, and therefore proportional to ΔM. So if ΔM gets small enough, the stop acquires a sizable lifetime and may form a quasi-stable (decaying inside the tracking volume) or even stable stop hadron (see [34] for this case). The current analysis focusses on a stop decaying promptly into a charm particle and the LSP.

The event preselection required, in addition to the criteria described in section 5.1.2, that not more than 30% of the total visible energy came from particles with tracks seen in the VD and ID only. To eliminate Bhabhas and leptonic $\gamma\gamma$ backgrounds, the charged multiplicity was required to be greater than five. The $\gamma\gamma$ background was further

suppressed by requiring the energy in a forward cone of 30° around the beam direction to be at most 40% of the total visible energy and smaller than 2 GeV and that no energy was deposited in the STIC calorimeter. To avoid the relatively low hadronic energy region, where the $\gamma\gamma$ background is not well reproduced by the MC, the total transverse charged energy had to be greater than 7 GeV, the total transverse energy of tracks reconstructed with TPC information and the total transverse momentum had to be greater than 4 GeV and 3.5 GeV/c, respectively, and the number of tracks with TPC information had to be at least 4.

The agreement between data and MC after this preselection is shown in figure 6(a) to 6(d).

Figure 6 also demonstrates that the two-fermion and four-fermion backgrounds dominate at this stage of the selection, and that the small contribution from two-photon interactions may be easily identified in the data.

A further selection was performed in order to reduce the remaining backgrounds. Firstly, events having mainly barrel activity were selected. This was achieved by requiring that the energy within a cone of 60° around the beam direction was less than 10 GeV and that the polar angle of the missing momentum was between 45° and 135°. Secondly by demanding that the transverse momentum of the leading particle was less than 10 GeV/c and that the total transverse energy was less than 40 GeV, most of the remaining two- and four-fermion background was rejected. Finally, the total transverse momentum was required to be greater than 5 GeV/c and the scaled acoplanarity [11] greater than 20°. This cut removes most of the remaining background from two-photon processes. The agreement between data and MC after this selection is shown in figure 6(e,f).

5.4 Chargino searches

5.4.1 Non-degenerate scenarios

The visible energy in the event and thus the properties of the chargino decay products are mainly governed by the value of the mass difference (ΔM) between the chargino and the lightest neutralino. This search covers scenarios in which the mass difference ΔM is above 3 GeV/c^2.

For low ΔM the signal events are similar to $\gamma\gamma$ events. For high ΔM they resemble four-fermion final states such as W$^+$W$^-$and ZZ. For intermediate ΔM values, the background is composed of many SM processes in comparable proportions.

In order to allow for all the possible signatures of chargino decays, the signal and background events were divided into four mutually exclusive topologies:

- the $\ell\ell$ topology with no more than five charged particles and no isolated photons;
- the $jj\ell$ topology with more than five charged particles and at least one isolated lepton and no isolated photons;
- the *jets* topology with more than five charged particles and no isolated photons or leptons;
- the *rad* topology with at least one isolated photon.

The signal events selected in a given topology are mostly events of the corresponding decay channel, but events from other channels may also contribute. For instance, for low ΔM (and thus low visible energy) some events with hadronic decays are selected in the $\ell\ell$ topology, and some mixed decay events with the isolated lepton unidentified enter into

---

[11]The scaled acoplanarity is the acoplanarity of the two jets multiplied by the sine of the minimum angle between a jet and the beam axis.

the *jets* topology. This migration effect tends to disappear as ΔM increases. This effect was taken into account in the final efficiency and limit computations.

The signal events were simulated using 132 combinations of $\tilde{\chi}_1^\pm$ and $\tilde{\chi}_1^0$ masses for nine chargino mass values ($M_{\tilde{\chi}_1^\pm} \approx 103, 102, 100, 98, 94, 85, 70, 50$ and 45 GeV/c^2) and with ΔM ranging from 3 GeV/c^2 to 80 GeV/c^2. A total of 264000 chargino events (2000 per mass combination) was generated. The kinematic properties (acoplanarity[12], E_{vis}, $\not{P}_t$,..) of the signal events were studied in terms of their mean value and standard deviation, and six ΔM regions were defined, each containing signal events with similar properties (table 2).

In each of these 24 windows (four topologies, six ΔM regions), a likelihood ratio function ($\mathcal{L}_\mathcal{R}$) was defined. The variables $\{x_i\}$ used to build the $\mathcal{L}_\mathcal{R}$ functions in the present analysis were [4]: the visible energy (E_{vis}), visible mass (M_{vis}), missing transverse momentum ($\not{P}_t$), polar angle of the missing momentum, number of charged particles, total number of particles, acoplanarity, acollinearity, ratio of electromagnetic energy to total energy, percentage of total energy within $30°$ of the beam axis, kinematic information concerning the isolated photons and leptons and two most energetic charged particles, and finally the jet characteristics.

The generation of these 24 likelihood ratio functions was performed in five steps:

- The signal distributions of all the variables $\{x_i\}$ were built with signal events generated with parameter sets giving rise to charginos and neutralinos with masses in the corresponding ΔM region. For each ΔM region the events were classified according to the above topological cuts. The background distributions were built with background events passing the same topological cuts.
- Preselection cuts, different for each ΔM region, were applied in order to reduce the high cross-section backgrounds (two-photon interactions and Bhabha events) and to generate the pdf's. The pdf's were then generated as mentioned in section 5.1.4. Figure 7(8) shows the distributions of some event variables for the *jets*, $\ell\ell$ and *rad* topologies for the 2000 data and simulation with the TPC sector 6 ON (OFF).
- To reduce statistical fluctuations a smoothing was performed by passing the 24 sets of pdf's for signal and background through a triangular filter [35].
- In each window all the combinations of the pdf's were tested, starting from a minimal set of four variables. Every combination defined a $\mathcal{L}_\mathcal{R}$ function (see section 5.1.4) and a $\mathcal{L}_{\mathcal{R}_{\mathcal{CUT}}}$ that minimised the expected excluded cross-section at 95% CL using the monochannel formula [36]. The parameters entering this computation were the number of expected background events and the window efficiency of the chargino selection, defined as the mean efficiency of the chargino-neutralino mass sets belonging to the investigated window [13]. Figure 7(d) (8(d)) shows the good agreement obtained between real and simulated events as a function of the likelihood ratio cut, for $25 \leq \Delta M < 35$ GeV/c^2 in the $jj\ell$ topology for the 2000 data and simulation with the TPC sector 6 ON (OFF).
- The combination of variables corresponding to the lowest excluded cross-section defined the $\mathcal{L}_\mathcal{R}$ function and the $\mathcal{L}_{\mathcal{R}_{\mathcal{CUT}}}$ of this window.

---

[12]To compute the acoplanarity and acollinearity the particles were forced into two jets by the DURHAM algorithm.

[13]The efficiency of one chargino-neutralino mass set is defined as the number of events satisfying $\mathcal{L}_\mathcal{R} > \mathcal{L}_{\mathcal{R}_{\mathcal{CUT}}}$ divided by the total number of chargino events satisfying the topological cuts.

	ΔM regions
1	3≤ΔM< 5 GeV/c^2
2	5≤ΔM< 10 GeV/c^2
3	10≤ΔM< 25 GeV/c^2
4	25≤ΔM< 35 GeV/c^2
5	35≤ΔM< 50 GeV/c^2
6	50 GeV/c^2≤ΔM

Table 2: Definition of the ΔM (mass difference between the chargino and lightest neutralino) regions for the chargino search in non-degenerate scenarios.

5.4.2   Nearly mass-degenerate scenarios

The search for charginos in the nearly mass-degenerate scenarios uses several different techniques, depending on the lifetime of the chargino, which in turn depends on the mass difference ΔM between the chargino and the lightest neutralino (this is the only relevant dependence, at least in the heavy slepton hypothesis).

When ΔM is below the mass of the pion, the chargino lifetime is usually long enough to let it pass through the entire detector before decaying. This range of ΔM can be covered by the search for long-lived heavy charged particles. For ΔM of a few hundred MeV/c^2 the chargino can decay inside the main tracking devices of DELPHI. Therefore, a search for secondary vertices or kinks can be used to cover this region. As the mass difference increases, the mean lifetime shortens until the position of the $\tilde{\chi}_1^\pm$ decay can hardly be distinguished from the main event vertex. In this case, the tagging of an energetic ISR photon can help in exploring the ΔM region between a few hundred MeV/c^2 and 3 GeV/c^2.

The selection criteria described below are similar to the ones used in the analysis of previous data, which have been described in [6].

Search for quasi-stable charginos

The search for heavy stable charged particles is described in [5], and it will only be briefly recalled here. The method used to identify heavy stable particles relied on the ionisation loss measurements in the TPC and on the absence of signal in the DELPHI Cherenkov radiation detectors (RICH). The RICH detectors have two radiators (gas and liquid) with different refractive index ($n = 1.28$ in the liquid, $n = 1.0015$ in the gas radiator of the barrel RICH and $n = 1.0017$ in the gas radiator of the forward RICH). Particles below the Cherenkov threshold ($\beta < 1/n$, that is all particles with mass larger than $\sqrt{n^2 - 1} \cdot |\vec{p}|$) do not emit light ("veto identification"). Heavy stable charged particles crossing the detector would be seen in the tracking system and have as distinctive signature the absence of Cherenkov radiation and an anomalous energy loss in the TPC. Three different search windows were used in the search for heavy stable charginos:

- the charged particle had momentum above 15 GeV/c, and no photons in both the liquid and the gas radiator of the RICH were associated to the track;
- the charged particle had momentum above 5 GeV/c, high ionisation loss in the TPC, and no signal in the gas RICH;

- the charged particle had momentum above 15 GeV/c, a TPC ionisation loss not exceeding 70% of the expectation for a proton, and no signal in the gas RICH.

A fourth search window was considered in [5]. It is however not applicable to the present search as it establishes a correlation between the two hemispheres of the event.

Search for charginos decaying visibly

If a heavy charged particle decays inside the central tracking devices of DELPHI (at a radius between 10 cm and 1 m) then both the incoming and the outgoing track can be reconstructed, and the angle between the tracks can be calculated. Such a search for kinks was originally designed to search for long-lived staus in the Gauge Mediated SUSY Breaking scenario [5]. A similar technique was applied to search for mass-degenerate charginos, with some specific features needed because the visible decay products carry very little momentum in the nearly mass-degenerate case. Details of the selection criteria can be found in [6]. Here only a brief and qualitative summary of the most important selection cuts is given.

A set of rather loose general requirements was applied in order to suppress the low energy background (beam-gas, beam-wall, etc), two-photon, e$^+$e$^-$ and hadronic events. For each event passing the preselection cuts, all the charged particles were grouped in clusters according to their measured point closest to the interaction vertex. A cluster with only one track with momentum above 20 GeV/c was considered as a possible chargino candidate if it was compatible with a particle coming from the interaction point. For each single track cluster fulfilling the above conditions, a search was made for a second cluster possibly formed by the decay products of the $\tilde{\chi}_1^+$ and defining a secondary vertex or kink with the chargino candidate.

Reconstructed secondary vertices could also be the result of particles interacting in the detector material, or having a particle trajectory reconstructed in two separate track segments. Additional requirements rejected these backgrounds in the events with an acceptable secondary vertex [5]. Finally, for an event to be accepted, at least one charged particle had to be found in each hemisphere (defined by the plane containing the beam spot and perpendicular to the line connecting the beam spot to the kink).

The search for events with tracks at large impact parameter described in [5] was not possible in this case: events with only two extremely soft charged particles with large impact parameter are difficult both to trigger on and to discriminate from machine related noise. Such events were however considered if a high p_{t} ISR photon was present, as explained in the next section.

Search for charginos with ISR photons

The visible particles resulting from a chargino decay when it is nearly mass-degenerate with the LSP have typically little energy and momentum. They are hard to trigger on in the experiment, and in addition they are overwhelmed by the background from two-photon events. The ISR photon tag improves detectability and, if the transverse energy of the photon is above some threshold which depends on the minimal polar angle acceptance of the experiment, it rejects most of the two-photon background.

After the preselection, which was summarised in 5.1.2, the following requirements were applied to the data and simulation samples.

- There had to be at least two and at most six good charged particles passing the quality criteria (see section 5.1.1), and no more than ten tracks in total.

- The transverse energy of the ISR photon candidate was required to be greater than $(E_T^\gamma)^{\min} \simeq 0.03 \cdot \sqrt{s}$.
- The mass recoiling against the photon had to be above $2M_{\tilde{\chi}_1^\pm} - \delta M$, where the term δM takes into account the energy resolution in the electromagnetic calorimeters.
- The photon had to be isolated by at least $30°$ with respect to any other charged or neutral particle in the event.
- The sum of the energies of the particles with polar angles within $30°$ of the beam axis (E_{30}) was required to be less than 25% of the total visible energy. If the photon itself was below $30°$, it was the ratio $(E_{30} - E_\gamma)/(E_{\mathrm{vis}} - E_\gamma)$ that was required to be below 0.25.
- If the ISR photon candidate was detected in the very forward DELPHI calorimeter (STIC), it had not to be correlated with a signal in the scintillators placed in front of the STIC.
- $(E_{\mathrm{vis}} - E_\gamma)/\sqrt{s}$ had to be below a kinematic threshold which depended on ΔM and on $M_{\tilde{\chi}_1^\pm}$ (and in any case below 6%).
- The ratio of the absolute value of the missing transverse momentum over the total transverse energy had to be above $0.40/c$ if $\Delta M > 300$ MeV/c^2, and above $0.75/c$ for smaller ΔM.
- If $\Delta M > 1$ GeV/c^2, at least two charged particles in the event had to be consistent with coming from the beam interaction region.

Distributions of some of the variables used in the final selection are shown in figure 9 for data, simulated SM background, and simulated signal events. Although there is a certain overall qualitative agreement of the various distributions, there is already an excess of data. On the other hand, the two-photon generators used in the simulation lack the events which have small $\gamma\gamma$ invariant mass, and in some cases (namely, $\gamma\gamma \to e^+e^-$) no ISR generation is implemented at all. Moreover, background processes such as beam-gas interactions are not included in the simulation. As in previous publications [6], the most likely explanation of such disagreement is therefore a deficit of simulated background events rather than an excess of data from possible new physics. As no attempt will be made in the following to account for the backgrounds missing in the simulation, the exclusion limits that will be obtained are conservative.

5.5 Neutralino searches

The neutralino searches were designed to cover both $\tilde{\chi}_k^0\tilde{\chi}_1^0$ production with $\tilde{\chi}_k^0 \to \tilde{\chi}_1^0 + \mathrm{f}\bar{\mathrm{f}}$, with a signature of acoplanar jets or leptons, and channels of the type $\tilde{\chi}_k^0\tilde{\chi}_j^0$ with k or $j > 2$, which can lead to neutralino cascade decays. To maximise the sensitivity several searches were used for different topologies, namely:

- a search for acoplanar jet events, as from $\tilde{\chi}_1^0\tilde{\chi}_2^0$ with $\tilde{\chi}_2^0 \to \tilde{\chi}_1^0 \mathrm{q}\bar{\mathrm{q}}$;
- a search for acoplanar lepton events, as from $\tilde{\chi}_1^0\tilde{\chi}_2^0$ with $\tilde{\chi}_2^0 \to \tilde{\chi}_1^0 \mathrm{e}^+\mathrm{e}^-$ or $\tilde{\chi}_2^0 \to \tilde{\chi}_1^0 \mu^+\mu^-$;
- a search for multijet events, as from $\tilde{\chi}_i^0\tilde{\chi}_j^0, i = 1, 2, j = 3, 4$ with $\tilde{\chi}_j^0 \to \tilde{\chi}_2^0 \mathrm{q}\bar{\mathrm{q}}$ and $\tilde{\chi}_2^0$ decaying to $\tilde{\chi}_1^0 \mathrm{q}\bar{\mathrm{q}}$ or $\tilde{\chi}_1^0\gamma$;
- a search for multilepton events for the corresponding decays to lepton pairs;
- a search for cascade decays with tau leptons, e.g. $\tilde{\chi}_2^0\tilde{\chi}_1^0$ production with $\tilde{\chi}_2^0 \to \tilde{\tau}\tau$ and $\tilde{\tau} \to \tilde{\chi}_1^0\tau$;
- a search for double cascade decays with tau leptons, e.g. $\tilde{\chi}_2^0\tilde{\chi}_2^0$ production with the same $\tilde{\chi}_2^0$ decay chain as above.

The different searches, briefly described below, were designed to be mutually exclusive in order to allow easy combination of the results. Thus events selected in the likelihood-based searches for acoplanar leptons or jets of section 5.5.1 were explicitly rejected in the searches described in the subsequent sections. The LUCLUS algorithm with $d_{\text{join}} = 10$ GeV/c was used for jet clustering in the analyses described below, with the exceptions of the likelihood ratio acoplanar jets/leptons and double tau cascade searches, as explicitly mentioned in the corresponding sections (see section 5.1.3 for details on the jet clustering algorithms).

5.5.1 Acoplanar jets and acoplanar leptons searches

As mentioned above, the acoplanar jets and acoplanar leptons topologies are dominant in most of the parameter space. For these cases, a search based on the likelihood ratio method was performed and the sequential cut analyses described in [7] were used as a cross-check.

The characteristics of the neutralino decays are mainly determined by the value of ΔM, here defined as the mass difference between the heavier of the produced neutralinos and the LSP ($\tilde{\chi}_1^0$). For low ΔM the signal events are similar to $\gamma\gamma$ events, for high ΔM they resemble four-fermion final states, such as W^+W^- and ZZ. While for intermediate ΔM values the background is composed mainly of two-fermion processes. The total energy of the visible final state particles, E_{vis}, was used to distinguish between regions of different signal and background characteristics in the optimisation of the selections.

Likelihood Ratio analysis

The first step of the analysis was to preselect the events dividing them into three mutually exclusive topologies: ee, $\mu\mu$, and q$\bar{\text{q}}$. The ee topology was defined as events having exactly two isolated lepton candidates (see section 5.1.3). At least one of these had to be a tightly identified electron, and neither identified as a muon. Similarly, the events of the $\mu\mu$ topology were required to contain at least one isolated loose muon candidate and no isolated electron. The q$\bar{\text{q}}$ topology was defined as events with more than five charged particles and no isolated photons or leptons.

In the second step, aimed at removing the dominant SM background processes, events which fulfilled all of the following criteria were selected:

- the polar angles of the most energetic neutral and charged particles were required to be greater than $10°$;
- the missing transverse momentum had to exceed 2 GeV/c, or 4 GeV/c if the visible energy was less than 30 GeV;
- both the acoplanarity and acollinearity had to be greater than $3°$;
- the total visible energy had to be less than $0.75\sqrt{s}$.

The first two requirements remove the bulk of the $\gamma\gamma$ events and off-momentum electrons. The third and fourth reject two-fermion processes. The last requirement removes mainly four-fermion events.

In the q$\bar{\text{q}}$ topology an additional selection was applied to suppress further the large q$\bar{\text{q}}(\gamma)$ background. This was based on the jets reconstructed using the Durham algorithm when forcing the number of jets to two. If the invariant mass of the event was within 40 GeV/c^2 of the Z mass, the acoplanarity of the two jets was required to be at least $10°$.

For different values of visible energy E_{vis} (typical of different values of ΔM), the kinematic properties of the signal were studied in terms of the mean value and standard deviation of several event variables. Five E_{vis} regions were defined, each containing signal

events with similar properties and SM background composition. These regions are given in table 3, together with the corresponding dominant SM background.

	E_{vis} regions	main SM bkg
1	$5 \leq E_{\mathrm{vis}} < 20$ GeV/c^2	$\gamma\gamma$
2	$20 \leq E_{\mathrm{vis}} < 50$ GeV/c^2	$\gamma\gamma$, 2-fermions
3	$50 \leq E_{\mathrm{vis}} < 70$ GeV/c^2	2-fermions
4	$70 \leq E_{\mathrm{vis}} < 110$ GeV/c^2	2- and 4-fermions
5	110 GeV/$c^2 \leq E_{\mathrm{vis}}$	4-fermions

Table 3: Definitions of the visible energy regions of the neutralino search in the acoplanar leptons and jets topologies and the corresponding dominant SM backgrounds.

In the last step of the analysis, for each of the 15 windows (three topologies, five E_{vis} regions) thus defined, a likelihood ratio function was computed. The variables used in the likelihood definition are listed below:

- global variables (all topologies): visible energy, transverse energy, missing momentum, energy and direction of the most energetic charged and neutral particles, transverse momentum with respect to the thrust axis, polar angle of the missing momentum, thrust value, thrust direction and acoplanarity;
- variables specific to the q q̄ topology (calculated forcing the event into two jets): jet directions, energies, widths, invariant mass and y_{cut} value;
- variable specific to the ee and $\mu\mu$ topologies, namely the invariant mass of the two charged particles.

For each variable used in the likelihood, the one-dimensional probability density function (pdf) was defined according to the procedure described in sections 5.1.4 and 5.4.1, and events with $\mathcal{L}_{\mathcal{R}} > \mathcal{L}_{\mathcal{R}_{\mathcal{CUT}}}$ were selected as candidate signal events.

Some event variable distributions for real and simulated data before the likelihood selection are illustrated in figure 10. The signal distribution is shown for illustration purposes, as it contains the contribution of all the generated mass combinations and is arbitrarily normalised. The exact neutralino cross-section values and mass differences depend on the point of the parameter space. A fair agreement between data and the SM expectation is found. A low visible energy event is present in the ee topology (see figure 10(d)), in a region where low but non-zero background was expected from the SM (four-fermion processes). No significant disagreement between data and MC is found in any of the topologies.

Sequential analysis

The detailed selection criteria for the selection based on sequential cuts are given in reference [7] and have not been changed. This analysis was used as a cross-check of the likelihood ratio results. At the final selection level, criteria optimised for different $\Delta M = M_{\tilde{\chi}_2^0} - M_{\tilde{\chi}_1^0}$ regions were designed. They were used as independent selections in the derivation of the results.

5.5.2 Multijet search

The multijet search was optimised for cascade decays of neutralinos with large mass splittings, giving high energy jets. Events with energetic photons, characteristic of the

decay $\tilde{\chi}_2^0 \to \tilde{\chi}_1^0 \gamma$, were treated separately. Events with a photon signature were selected on the basis of reconstructed photons with a polar angle above 20°, isolated by more than 20° from the nearest charged particle. If there was only one such photon its energy was required to be between 10 GeV and 40 GeV; if more than one photon was present, at least two had to have energy greater than 10 GeV.

This selection was similar to the acoplanar jet selection but required a rather large transverse energy and allowed any number of reconstructed jets. Events selected by the searches for acoplanar leptons or acoplanar jets were explicitly rejected.

The detailed selection criteria are similar to the ones described in [7]. Background studies based on earlier data and an improved energy reconstruction motivated several changes in the selection procedure. Three selection stages (preselection, intermediate selection and final selection) are defined and used in the figures and tables. As compared to [7] the preselection, aimed at selecting well reconstructed hadronic events with significant jet activity, was more selective. In the following, the most important steps of the new search are summarised.

At preselection level, at least five charged particles (passing the track selection described in section 5.1.1) were required, at least one of them with a transverse momentum exceeding 2.5 GeV/c. The transverse energy of the event had to be greater than 25 GeV, the visible energy of the event was required to be less than $0.65\sqrt{s}$, and the missing momentum had to be less than $0.4\sqrt{s}/c$. There were several requirements aimed at selecting events with clear jets which were not dominated by single particles with large reconstructed energy. Figures 11(a,b) and 12(a,b) show the distributions of the visible mass divided by the centre-of-mass energy for real data and simulated background events passing the above selection.

At the intermediate selection level, radiative return to the Z, two-photon, and Bhabha background was reduced by excluding events with a neutral particle whose energy exceeded 60 GeV or large amounts of energy in the forward region of the detector (more than 40% of the visible energy within 30° of the beam). Also, the transverse momentum had to exceed 6 GeV/c. The total momentum and the most energetic shower in the event were both required not to be close to the beam direction. A comparison of the $c p_{\mathrm{T}}/\sqrt{s}$ distributions for real data and simulated background following the above selection is shown in figures 11(c,d) and 12(c,d). The excess in data visible in 11(c) and 12(c) was found to be consistent with (low acoplanarity) radiative return to the Z events with misreconstructed missing momentum. In 12(c) the excess is larger and this is due to the data with TPC sector 6 off.

At the final level of the selection the acollinearity and scaled acoplanarity (in a forced 2-jet configuration) had to be greater than 30° and 10°, respectively. To reject WW background it was required that there be no charged particle with a momentum above 30 GeV/c, and no isolated lepton above 10 GeV/c or above 4 GeV/c with an isolation angle greater than 20°.

For events with a photon signature, the mass recoiling against the visible system was required to exceed 20% of the centre-of-mass energy and the scalar sum of momenta reconstructed with TPC information had to be less than 60% of the visible energy.

For the complementary sample, without a photon signature, several of the criteria above were made stricter in order to reject Zγ events. The recoil mass was required to exceed 40% of $\sqrt{s}$ and the energy deposited in electromagnetic calorimeters had to be less than 40 GeV. No isolated neutrals with energy greater than 20 GeV were allowed and the average momentum of particles with tracks reconstructed in the TPC had to be less than 4 GeV/c.

Figures 11(e,f) and 12(e,f) show the distribution of the scaled acoplanarity for real and simulated data after final selections, while figures 12(g,h) show $cp_{\mathrm{T}}/\sqrt{s}$ for data with TPC sector 6 on. A satisfactory agreement between data and SM simulation is found. Four events are observed while three were expected from SM simulation.

5.5.3 Multilepton search

The multilepton search is sensitive to cascade decays involving leptons, which can dominate if there are light sleptons. The selection of [7] was basically left unchanged.

At the preselection level, well reconstructed low multiplicity events with missing energy and missing mass were selected. In particular, the total visible energy including badly reconstructed tracks (not passing the track selection described in section 5.1.1) was required to be less than 140 GeV, the number of charged particles was required to be at least two and at most eight, and events with more than four neutral particles were rejected. Figures 13(a) and 14(a) show a comparison between the visible mass divided by the centre-of-mass energy for real and simulated events passing the preselection.

The selection at the intermediate level served mainly to reject $Z\gamma$, two-photon, and Bhabha events by requiring significant transverse momentum and transverse energy ($p_{\mathrm{T}} >$ 8 GeV/c, $E_{\mathrm{vis}}^T >$ 25 GeV). The distributions of $cp_{\mathrm{T}}/\sqrt{s}$ for real and simulated data, following the intermediate selection are compared in Figures 13(c) and 14(c).

At the final selection level events with two or more charged particles were subjected to criteria designed to reject Bhabha events. In addition, the charge asymmetry for the two most energetic such particles was used to reject W pairs decaying leptonically. Events with four or more tracks were clustered into jets, and those with exactly two jets were rejected if their scaled acoplanarity was less than $15°$. Figures 13.e and 14.e show the acoplanarity distribution for real and simulated data at this level.

5.5.4 Asymmetric tau cascade search

The tau cascade search is sensitive to $\tilde{\chi}_1^0 \tilde{\chi}_2^0$ production with $\tilde{\chi}_2^0 \to \tilde{\tau}\tau$ and $\tilde{\tau} \to \tilde{\chi}_1^0 \tau$, where the second τ produced has very low energy. This search was described in [7] and is briefly summarised here.

At the preselection level, well reconstructed low multiplicity events with missing energy and missing mass were selected. The selection was the same as for the multilepton search (section 5.5.3), with the additional requirement of no more than two reconstructed jets. At least two of the charged particles had also to satisfy stricter criteria on reconstruction and impact parameters. The distributions of the visible mass divided by the centre-of-mass energy for real and simulated data at this level are shown in Figures 13(b) and 14(b).

At the intermediate selection level, the highest and second highest momenta of charged particles were required to be below 40 GeV/c and 25 GeV/c, respectively, and at least one charged particle had to have a transverse momentum above 2.5 GeV/c. The criteria to reject $Z\gamma$, two-photon, and Bhabha events were similar to those used in the multilepton search, except for the removal of the requirement on the transverse energy. Figures 13(d) and 14(d) show the distributions of $cp_{\mathrm{T}}/\sqrt{s}$ for real and simulated data at the intermediate selection level.

At the final selection level, events with two or more isolated charged particles were required to have acollinearity and acoplanarity above $60°$. The smaller of the two momenta had to be below 70% of the greater one, and below 10 GeV/c. For events with two reconstructed jets the scaled acoplanarity was required to be greater than $20°$, and

the acoplanarity and the acollinearity greater than 60°. The acoplanarity distributions for the resulting samples of real and simulated data events are shown in figures 13(f) and 14(f).

5.5.5   Double tau cascade search

The final state of $\tilde{\chi}_2^0 \tilde{\chi}_2^0 \to \tilde{\tau}\tau\tilde{\tau}\tau$ differs from that of stau pair production only in the presence of two soft taus from the stau decays. The search criteria for stau pairs (see section 5.2.3) could therefore be applied with slight modifications, as follows. Instead of exactly two τ-candidates, at least three were required, but the momentum of the third most energetic one had to be less than 4% of the beam momentum. The maximum number of tracks in the event was increased from seven to eight, and as the W^+W^- background is negligible the requirement on $p_{high}^{\rm JET}$ versus θ_{W^+} was removed. Since the only SM processes yielding final states with four taus are ZZ, ZZ* or Zγ^*, the invariant mass of the two most energetic τ-candidates was required to be below 40 GeV/c^2, i.e. well below $m_{\rm Z}$. Variables specific to the two-jet topology, e.g. acoplanarity, were evaluated using the two most energetic τ candidates only, and the remaining requirements of the stau pair search were left unchanged. In the cases were these requirements differed for high and low ΔM, the less stringent selection was applied here. The results of this search are shown in table 22.

6   Results and limits

In this section the number of events selected and expected at the final event selections and the expected signal efficiencies are presented for each channel. No evidence of a significant excess with respect to the SM expectation was found in any of the channels. Thus, exclusion limits at 95% CL can be set. In a relatively model-independent approach, cross-section limits are derived. Sparticle mass limits are then obtained, with assumptions that depend on the channel and will be specified case by case.

6.1   Limit computation

Depending on the searches, limits were derived using the multichannel Bayesian method [37] or the modified frequentist likelihood ratio method [33]. Multichannel approaches allow different search channels to be combined taking into account the information about efficiency, expected background, number of candidates and centre-of-mass energy in each of them.

The two methods typically give similar results. Both methods take a posteriori knowledge about the background into account, and thus give physically reasonable and conservative results in the case of downward fluctuations of the background. Background fluctuations could nevertheless significantly affect the range of exclusion, and for this reason limits expected in the absence of a signal are also given below.

Expected exclusion limits were calculated using exactly the same algorithms and assuming an observed number of events equal to the expectation in the absence of signal.

6.2   Systematic uncertainties

The excluded cross-sections and masses can be affected by the systematic uncertainties related to the SM background rate and signal efficiency determinations. These are mainly due to imperfections in

- the description of the differential cross-sections;
- the modelling of the fragmentation and hard gluon radiation;
- the modelling of the detector response.

The inaccuracy of the differential cross-section description for the various SM processes was studied extensively in the context of their measurements at LEP and is typically small, except for the hadronic $\gamma\gamma$ background. Modelling of fragmentation and hard gluon radiation was studied both in the context of background and efficiency. It mainly affects searches for the stop quark, due to the uncertainties on the modelling of the stop fragmentation. However, the largest contribution to the systematics on both background rate and efficiency determination arises from the modelling of the detector response. This was addressed in several ways, depending on the type of the final state searched for. Below, a review of all of these systematic effects is given, together with the methods used to address them. Then each of the methods used to estimate the systematics is discussed in more detail. Finally, the methods used to propagate those uncertainties in the limit computation are briefly presented.

6.2.1   Review of the main systematic sources

Description of the differential cross-sections:

The uncertainty on the differential cross-sections within the acceptance region of the most important SM processes is [25,38] less than 1% for W^+W^- production, around 0.5% for $Z\gamma$, 2% for ZZ and about 5% [14] for $We\,\nu_e$ and $Z^0e^+e^-$. The uncertainty of the description of the $Z\gamma^*$ process is typically 5%, reaching 20% in the region of very small masses of γ^*. While the uncertainties are small for two-photon interactions giving leptons (less than 5%), the description of the hadronic $\gamma\gamma$ processes is subject to large uncertainties in some regions of the parameter space. The effect was studied comparing various two-photon generators [38]. In the squark analysis at the preselection level `PYTHIA` results were cross-checked with `TWOGAM` and differences up to 15% were observed, with `PYTHIA` giving the higher background. It has been shown [39] that the `PYTHIA` generator represents a more correct background estimation. A systematic uncertainty of 15% on the hadronic $\gamma\gamma$ background was assumed. The impact of these uncertainties on the final background rate determination will depend on the importance of the two-photon background in the different cases. In most of the analyses presented in this paper the contribution of the hadronic $\gamma\gamma$ process at the final selection level is negligible. The search for multi-jet final states without isolated photons from heavier neutralino decay (see section 6.7.1) may serve as an example. In this case 40% of the background originates from the W^+W^- process, 40% from $We\,\nu_e$ and ZZ processes, and 15% from $Z\gamma$. If the presence of photon(s) is required, 80% of the background originates from the $Z\gamma$ process. In summary, the net uncertainties arising from the description of the above processes are of the order of a few percent at most.

Fragmentation and hard gluon radiation modelling:

---

[14]This number is valid in the phase-space regions where these processes are not $\gamma\gamma$-like.

The description of hard gluon radiation leads to uncertainties of at most 10% in the allowed parameter space, in particular for the rate of b-tagged four-jet events from the $Z\gamma$ process. This is not important for most of analyses presented here. Fragmentation uncertainty related effects are typically of the order of 1%. However in the searches for the stop (see section 6.5.1), the stop hadronisation scheme is important and a dedicated generator STOPGEN was used for these studies. In STOPGEN the stop hadronisation is performed non-perturbatively and the ϵ parameter of the Peterson function which regulates the stop fragmentation and hadronisation can be varied. The analyses were applied to the different signal samples and the results were compared. In the stop analysis, the relative systematic error on the efficiency as a consequence of imperfect signal simulation was taken to be 7% for $\Delta M > 10$ GeV/c^2 and 10% for $\Delta M \leq 10$ GeV/c^2. For the sbottom analysis, 7% was used as a conservative number for all ΔM.

Modelling of the detector response:

The modelling of the detector response is the main source of systematics in the searches for new particles. The next section gives a review of the methods which were developed to address primarily the influence of this uncertainty on the SM background rate and efficiency determinations.

6.2.2 Methods to evaluate detector response systematics

The "re-weighting" method

This method estimates the systematic error on the number of selected background events from imperfect simulation of the detector response, as well as from possible large uncertainties in the modelling of the differential cross-section for two-photon processes. It propagates the difference between the data and the simulated background at preselection level to the final selection level for the variables relevant for the analysis.

The propagation is performed as follows. Each discriminating variable used in the event selection is histogrammed both for data and simulated background events at the preselection and final selection levels. From the preselection histograms a weight factor, $N_{\text{Data}}/N_{\text{Back}}$, is calculated for each bin containing at least 1 % of the total number of background events and a non-zero number of data events. These weight factors are then applied, bin by bin, to the background histograms at the final selection level. The contribution to the systematic error of each variable is then determined by subtracting the total number of selected background events from the total number of re-weighted background events at the final selection level.

The total positive (negative) systematic error of the number of background events is then computed as a quadratic sum over positive (negative) error contributions from the different variables:

$$\epsilon^{\pm} = \sqrt{\sum_{N_{\text{Back}}^{\text{RW}}(i) \gtrless N_{\text{Back}}} (N_{\text{Back}}^{\text{RW}}(i) - N_{\text{Back}})^2} \tag{1}$$

where $N_{\text{Back}}^{\text{RW}}(i)$ is the total number of re-weighted background events from variable i and N_{Back} is the number of selected background events without re-weighting.

In this method the correlations between different variables are not taken into account, but as the quadratic sum is performed over all error contributions, the total systematic

error is overestimated [15]. Moreover the statistical fluctuation in the bins of the histograms used to calculate the weight factors lead to an additional overestimation of the error. Another drawback of this method is that the total systematic error obtained grows with the number of studied variables.

The main advantages of this method are the simplicity and conservative error estimation. Because of its conservative nature, it was used in searches where the expected background is small, and background fluctuations have bigger effect on the expected limit than the systematic error. For example, in the squark analysis the systematic error on the background estimated with the method above was 15-60 % (see section 6.5.1). This had only a small effect on the final mass/cross-section limits.

The "shaking" method

The "shaking" method [40] attempts to correct at particle level the simulation description of the detector response and residual effects in the fragmentation.

Changes in the particle multiplicity (by adding or removing some particles) are made in the MC, in such a way that the multiplicities of neutral and charged particles in bins of momentum and polar angle are well described for the hadronic data collected at the Z peak. The momentum and the polar angle of the added particles are randomly changed with respect to the parent particle, while staying in the same phase space region.

The method was tested in the study of systematics of the ZZ cross-section measurement [40]. The multiplicity adjustment is of the order of 1%-2%. It leads to a better agreement between the data taken at energies above Z peak and the SM background, typically predicting slightly higher observed missing energy and momentum.

The method can be used to study the uncertainty on the background and efficiency in hadronic high multiplicity topologies, with or without isolated leptons (or photons). In these topologies, the method gives an estimation of the systematic uncertainty including both the effect of "shaking" the variables and the consequences of additional reconstructed tracks which lie inside the cone for the isolated lepton or photon.

This method was used to study the systematic error of background and efficiency in hadronic neutralino topologies, and the systematic error on the chargino detection efficiency in hadronic, semileptonic and radiative topologies.

Tables 4 and 5 show the relative variation of the efficiency of the chargino (non-degenerate scenarios) and neutralino searches, respectively (see sections 6.6.1 and 6.7) obtained with and without "shaking". The values in table 4 correspond to high multiplicity hadronic and semi-leptonic final states and are averaged over several points with model parameters corresponding to the specific ΔM region (see section 5.4.1 for the ΔM region definition). The values shown in table 5 correspond to the different high multiplicity topologies in the neutralino search and they are averaged over the interesting range of masses.

Except for the lowest ΔM regions in the chargino analysis, where systematic uncertainties due to tracking and neutral energy reconstruction have the biggest effect, the variation in the detection efficiency is very small. The efficiencies for the "shaken" signal are typically larger than for the "unshaken" signal.

In hadronic neutralino topologies the background estimated with the shaking method was typically 10% higher than the "unshaken" background. The variation of both background and efficiency is consistent with "shaking" predicting slightly higher observed missing energy.

---

[15]It was checked by the means of the Kolmogorov test that rescaling the distribution of any of the variables improves the agreement between the data and SM background for the other variables as well.

ΔM	1	2	3	4	5	6
jets	6.8 %	8.8 %	3.1 %	0.5 %	1.0 %	3.4 %
jjℓ	12.9 %	4.1 %	0.5 %	0.4 %	0.0 %	0.9 %

Table 4: The relative difference in the chargino detection efficiency obtained with and without "shaking" in the year 2000 simulation with the DELPHI detector fully operational. The values shown correspond to the different ΔM regions of the hadronic (*jets*) and semi-leptonic (*jjℓ*) topologies in the chargino production (see section 6.6.1).

topology	efficiency change
multijets without γ	2.9 %
multijets with γ	1.3 %
acoplanar jets	1.3 %

Table 5: The relative difference in the neutralino detection efficiency obtained with and without "shaking" in the year 2000 simulation with the DELPHI detector fully operational. The values shown correspond to the different high multiplicity topologies in the neutralino production (see section 6.7) and they are averaged over the interesting range of masses.

Methods dedicated to low multiplicity topologies ("smearing" technique)

The uncertainty on the efficiency of the muon, electron and photon identifications is expected to be a dominant effect in the low multiplicity topologies requiring identified particles. Studies on back-to-back di-muon events and back-to-back di-electron events and photons from radiative return to the Z point to differences between the data and the simulation of at most 5% for electrons and photons, and at most 3% for muons, if the polar angle of these particles is in the range 20-160°, as in all analyses presented here.

The uncertainty on the track momentum reconstruction arising from the modelling of the detector response was also studied and a small effect was found, both on efficiency and background estimates. The estimated background error is of the order of 3% and the estimated systematic error on the efficiency of the order of 3%. These estimates are relevant for neutralino and chargino leptonic topologies, and for all slepton searches.

6.2.3 Methods to propagate statistical and systematic uncertainties in the mass/cross-section limits

Systematic and statistical uncertainties on the parameters involved in the calculation of the limits (mainly, the uncertainties related to the SM background rate and signal efficiency determinations) were propagated into the final results using two methods. The analyses that rely on the modified likelihood ratio method adopted the procedure explained in [33].

For the analyses that use the multichannel method of [37], a different procedure based on the same Bayesian approach was chosen [41]. A probability distribution function (pdf) was assumed for the efficiency and the background in any single channel. A channel may correspond to a single $\sqrt{s}$ and to a single decay type. Such a pdf was assumed to be either Gaussian or binomial, depending on the size of the sample used to estimate the signal or the background, and on the method used to evaluate the uncertainty on the parameter (statistics of the simulation and other systematic uncertainties). Once all the

pdf's are known, they can be convoluted in the formula giving the overall number N_{exp} of signal events expected, according to the theory

$$N_{\text{exp}} = \sum_{i=1}^{\#_{\text{ecm}}} \sum_{j=1}^{\#_{\text{decay}}} \sigma_i \, \mathcal{L}_i \, \varepsilon_{i,j} \, BR_{i,j} \tag{2}$$

and in the number N_{up} of events compatible with the observation (number of candidates in each channel) and with the expected non-signal contribution (number of background events in each channel) at the CL wanted (the formula used is the one described in [37]).

Usually, N_{exp} (which is a constant, if there are no uncertainties associated to the factors that compose it) is compared with N_{up}: if N_{up}, computed at a given CL, remains below N_{exp}, then this point can be excluded at the same CL. However, if N_{exp} itself is not constant, because any of the terms that compose it has a pdf with non zero width, then both the quantities N_{exp} and N_{up} that must be compared may vary. The best way to take the correlation between the two terms into account is to consider the difference $N_{\text{exp}} - N_{\text{up}}$: then, a point is discarded (i.e. incompatible with the experimental outcomes) at a given CL, if

$$N_{\text{exp}} - N_{\text{up}} > 0 \tag{3}$$

at the same CL.

The difference in (3) was computed through a MC integration which takes into account all the pdf's of the variables entering in the calculation. To obtain the usual plots with the upper limits on the signal cross sections, the number $N_{\text{up}}^{(\text{equiv})}$ was computed so that:

$$N_{\text{up}}^{(\text{equiv})} = -(N_{\text{exp}} - N_{\text{up}}) + N_{\text{exp}}^{(0)} \tag{4}$$

where $N_{\text{exp}}^{(0)}$ is the number of signal events expected when no error is considered and the term within parenthesis is the limit on the difference as obtained with the MC integration. $N_{\text{up}}^{(\text{equiv})}$ can therefore be plotted together with $N_{\text{exp}}^{(0)}$ and compared. A given point can be discarded, at the chosen CL, if $N_{\text{exp}}^{(0)} > N_{\text{up}}^{(\text{equiv})}$.

The effect of including systematics in the computation of the limits can become relevant whenever there are large (order 10% or more) relative errors on the efficiency and, in particular, on the expected background. The worsening of the limit as obtained with the exact calculation is however much less significant than the over-conservative approach that would lead to reduce all efficiencies and all backgrounds by one standard deviation, and then computing the limit as if there was no error on the modified parameters.

6.3   LEP1 limits

In this section limits on the masses of SUSY particles from LEP1 data [42] are briefly discussed. In most cases the LEP1 limits have been superseded by LEP2 results, such as those presented in the present paper. However, for certain situations they are still relevant. This is particularly true for limits deriving from comparisons of the measured Z decay widths to SM expectations. Such limits are relatively insensitive to the details of the decays of SUSY particles, although they depend on the coupling of the sparticles to the Z (which is affected by the sparticle field composition).

From 1990 to 1995 LEP was run at centre-of-mass energies near the Z resonance. Model independent fits to all the lineshape and asymmetry data have been carried out, giving accurate values of the resonance parameters [43]. The total decay width of the

Z boson was measured with a precision of about 2.5 MeV/c^2. Decay channels of the Z opened by new physics would increase the Z width. Thus the difference between the measured width and the SM value may be used to constrain SUSY models. If the new particles decay invisibly, limits can be derived in a straightforward manner from the comparison of the measured invisible width to the SM prediction. The combined LEP result gives $\Gamma_{\mathrm{inv}}^{\mathrm{new}} < 2.0$ MeV/c^2 at 95% confidence level [44]. Whether the new particles are visible or invisible, they will contribute to the measured values of the total width Γ_Z. Confronting the measured Z width with the SM expectation an upper limit on the extra partial width $\Gamma^{\mathrm{new}} < 3.2$ MeV/c^2 was obtained [44] [16].

From the limit on $\Gamma_{\mathrm{inv}}^{\mathrm{new}}$, a limit on the sneutrino mass of 43.7 GeV/c^2 may be obtained [44]. A lower mass limit for the lightest chargino of approximately 45 GeV/c^2, independent of the field composition and of the decay modes, has been derived from the analysis of the Z width and decays. Limits for other sparticles depend both on masses and couplings. To a large extent left-handed sleptons below 40 GeV/c^2 can also be excluded using the agreement of the Z decay width with the SM prediction [44].

The composition of the neutralinos affects their production cross-sections and the light states may decouple from the Z. The production then proceeds through t-channel selectron exchange, giving a small cross-section if the selectrons are heavy. Hence no general limit on the LSP mass can be derived from LEP1.

For the third family, the production rates may be affected by potential large mixing of the weak eigenstates. For the stau mixing angle giving the minimal cross-section the coupling to the Z vanishes and no exclusion is possible using this method [17]. Also for squarks, the LEP1 limits depend on the mixing angle. Left squarks below 45 GeV/c^2 are excluded by the Z invisible width if they are nearly mass degenerate with the LSP, decaying invisibly. If the decay is visible, the limit from the total width should be applied instead. Squarks with non-zero mixing cannot be excluded by this method, as the coupling to the Z varies and can vanish [18].

Direct searches at LEP1 set mass limits above 40 GeV/c^2 for sfermions in the case of a decay into a fermion and a neutralino, with $\Delta M > 5$ GeV/c^2 and provided the production cross-section is not supressed due to t-channel contributions (in the case of selectrons) or to Z decoupling (in the case of third family sleptons and squarks).

6.4 Slepton searches

6.4.1 Smuon and selectron searches

<u>Efficiencies and selected events</u>

The efficiency for the signal detection depends on the masses of the slepton and neutralino. The cuts used to reject the backgrounds resulted in typical signal efficiencies of 50% both for the selectron and the smuon channels.

The number of events selected at each energy in the data, together with the estimate of the background is shown in tables 6 and 7 for the selectron and smuon analyses. It can be seen that the principal background arises from leptonic decays of W pairs. No significant evidence of a selectron or smuon signal is apparent in the data.

---

[16] In [45] a method designed to be more model-independent gives $\Gamma^{\mathrm{new}} < 6.3$ MeV/c^2 using older data.

[17] Selectron mass limits of the order of 50 GeV/c^2 have been derived from single photon searches at early colliders, for a nearly massless photino LSP [46].

[18] A sufficiently light stop would contribute through loop corrections to the partial width Γ_{bb}.

The effect of systematic uncertainties on background and efficiency evaluation was studied with the "smearing" method (see section 6.2). The variations both in the detection efficiency and in the background were found to be of the order of 3% on average.

	Selectrons			Smuons		
year	1998	1999	2000	1998	1999	2000
2-fermion events	5.6	8.4	4.2	0.1	2.2	1.4
4-fermion events	29.7	40.9	34.4	18.8	25.5	20.9
$\gamma\gamma$ events	1.7	2.5	2.2	0.5	1.1	2.6
Total	37.0	51.8	40.8	21.4	28.3	23.9
data	40	52	49	19	23	28

Table 6: Selectron and smuon candidates in the different data sets, together with the number of background events expected. The systematic uncertainties on the background were estimated to be of the order of 3% (see section 6.2).

$\sqrt{s}$ (GeV)	Selectron search					
	Preselection		Intermediate		Final	
	Data	MC	Data	MC	Data	MC
189	29460	28558 ± 7	1925	1937.0 ± 2.1	40	37.0 ± 0.4
192	4797	4649 ± 7	315	319.7 ± 2.1	6	7.0 ± 0.4
196	13705	14046 ± 9	812	847.2 ± 2.8	21	17.8 ± 0.6
200	14709	14653 ± 8	993	1001.0 ± 2.5	14	18.5 ± 0.6
202	7125	7154 ± 4	474	491.5 ± 1.4	11	8.6 ± 0.3
205	13229	12687 ± 15	832	774.8 ± 4.7	22	14.7 ± 0.3
207	12735	13315 ± 6	810	813.2 ± 2.0	13	15.4 ± 0.4
208	1202	1231 ± 1	78	75.2 ± 0.2	3	1.4 ± 0.04
206.5(*)	8963	9655 ± 6	524	495.6 ± 1.8	11	9.4 ± 0.5
All	105295	105948 ± 23	6763	6755.2 ± 7	141	129.8 ± 1.3
$\sqrt{s}$ (GeV)	Smuon search					
	Preselection		Intermediate		Final	
	Data	MC	Data	MC	Data	MC
189	18759	18591 ± 7	5378	5501.2 ± 2.1	19	21.4 ± 0.4
192	2985	3058 ± 7	854	860.2 ± 2.1	3	3.4 ± 0.4
196	8908	8874 ± 9	2659	2617.3 ± 2.8	8	10.4 ± 0.6
200	9974	10253 ± 8	2883	3017.8 ± 2.5	6	9.9 ± 0.6
202	4768	4676 ± 4	1439	1377.8 ± 1.4	6	4.6 ± 0.3
205	8773	8695 ± 15	2659	2609.5 ± 4.7	7	8.5 ± 0.3
207	9084	9024 ± 6	2805	2854.7 ± 2.0	11	8.9 ± 0.4
208	820	835 ± 1	253	247.4 ± 0.2	0	0.8 ± 0.04
206.5(*)	6411	6549 ± 6	1696	1621.6 ± 1.8	10	5.6 ± 0.5
All	70482	70555 ± 2	20626	20707.5 ± 2	70	73.4 ± 0.4

Table 7: Results of the selectron and smuon searches at the different selection levels and centre-of-mass energies. The number of events selected in data and expected from the SM simulation are given. Simulation errors are statistical. (*) indicates the 2000 data taken with the sector 6 of the TPC off.

Limits

The results are presented in terms of exclusion regions in the slepton-neutralino mass plane.

Limits on slepton masses can be derived using several assumptions. In the MSSM model, right handed sleptons are expected to have lower masses and lower cross-sections for a given mass. Hence we have assumed that only right handed selectrons and smuons

are sufficiently low in mass to be pair produced at LEP. This leads to conservative mass limits.

Exclusion limits for slepton pair production were obtained taking into account the signal efficiencies for each slepton-neutralino mass point, the cross-section for right-handed slepton production and the branching ratios squared for the direct decay $\tilde{\ell} \to \ell \chi_1^0$, together with the number of data and background events kinematically compatible with the mass combination under test. The estimate of the SUSY cross-section and branching ratios for each mass point were determined with the SUSY parameters $\tan \beta = 1.5$ and $\mu = -200 \, \mathrm{GeV}/c^2$. In addition, for the smuons the exclusion limit was obtained setting the branching ratio of $\tilde{\mu} \to \mu \chi_1^0$ to 1.

Figure 15 shows the 95% CL exclusion region for $\tilde{e}_R \tilde{e}_R$ production, obtained using all the analysed data sets, combined with data taken previously at lower energies. For a mass difference between the selectron and the neutralino above 5 GeV/c^2 right-handed selectrons are excluded up to masses of 98 GeV/c^2, for a neutralino mass up to 60 GeV/c^2, beyond which the limit is weaker. For $\Delta M \geq 15$ GeV/c^2, the excluded mass range is up to 94 GeV/c^2.

Figure 16 shows the 95% CL exclusion regions for $\tilde{\mu}_R \tilde{\mu}_R$ obtained by combining all the analysed data. The obtained exclusion is shown both taking the branching ratios for each mass point with the SUSY parameters $\tan \beta = 1.5$ and $\mu = -200 \, \mathrm{GeV}/c^2$ (lighter shaded region) and setting the branching ratio of $\tilde{\mu} \to \mu \chi_1^0$ to 1 (darker shaded region). For the smuons the limit is determined at small neutralino masses. Masses up to 88 GeV/c^2 are excluded, provided the mass difference between the smuon and the neutralino is above 5 GeV/c^2.

The effect of the systematic and statistical errors of background and efficiency on the mass limits was evaluated in a conservative way by changing the background and the efficiency by $\pm$ 3%. The resulting change in the limit was less than 1 GeV/c^2.

6.4.2 Stau search

Efficiencies and selected events

For the high mass stau-pair search, table 8 summarises the number of accepted events in the data together with the expected number of events from the different background channels. The systematic errors on the background estimates were obtained using the re-weighting method, as described in section 6.2.2. The systematic error on the efficiencies in the high ΔM region was obtained by reversing the cuts designed to remove the τ-pair and WW backgrounds, and comparing the number of selected events with the SM expectation. This method selected a sample which contained 97.6% WW and τ-pair events, while a possible signal would not exceed 1%. In terms of the most important kinematic distributions, the events selected were nevertheless quite similar to a high ΔM signal. The difference between data and the simulated SM processes was 5$\pm$5%, and was taken as the estimate of the systematic uncertainty. For low ΔM, the uncertainty was estimated by the maximal scatter of the efficiency obtained by the fast simulation with respect to the values obtained by the full simulation, and amounted to 15%.

In all ΔM regions, good agreement with the SM expectation was observed. Most of the selected SM events in the simulation contained either one or two τ's (17% and 67%, respectively). In two thirds of the events with less than two τ's, the lepton mistakenly taken as coming from a τ-decay had low momentum, i.e. was indistinguishable from a secondary lepton from a τ-decay.

$\sqrt{s}$ (GeV)	Preselection		Intermediate	
	Data	MC	Data	MC
189	2949	2916 ± 29	80	82 ± 2
192	473	444 ± 4	14	14 ± 0
196	1265	1333 ± 12	36	40 ± 1
200	1351	1264 ± 11	41	39 ± 1
202	716	652 ± 6	12	20 ± 1
205	1284	1228 ± 11	38	34 ± 1
207	1214	1230 ± 11	33	36 ± 1
208	132	116 ± 3	3	3 ± 0
206.5(*)	842	857 ± 8	28	26 ± 1
Total	10226	10040 ± 38	285	294 ± 3
Channel	Background composition			
WW	8 %		85 %	
4-fermion	0 %		2 %	
2-fermion	16 %		1 %	
bhabha	42 %		0 %	
$\gamma\gamma$	34 %		12 %	

$\sqrt{s}$ (GeV)	Final					
	High ΔM		Medium ΔM		Low ΔM	
	Data	MC	Data	MC	Data	MC
189	16	$17.8 \pm 0.4 \,^{+1.7}_{-2.8}$	10	$10.4 \pm 0.4 \,^{+1.0}_{-1.6}$	0	$1.6 \pm 0.5 \,^{+0.2}_{-0.1}$
192	5	$2.8 \pm 0.0 \,^{+0.3}_{-0.5}$	2	$1.6 \pm 0.0 \,^{+0.1}_{-0.3}$	0	$0.1 \pm 0.0 \,^{+0.0}_{-0.0}$
196	7	$7.5 \pm 0.1 \,^{+0.7}_{-1.2}$	3	$4.2 \pm 0.1 \,^{+0.4}_{-0.7}$	0	$0.3 \pm 0.0 \,^{+0.0}_{-0.0}$
200	11	$7.4 \pm 0.1 \,^{+0.7}_{-1.2}$	9	$4.5 \pm 0.1 \,^{+0.4}_{-0.7}$	0	$0.6 \pm 0.1 \,^{+0.1}_{-0.0}$
202	1	$4.1 \pm 0.1 \,^{+0.4}_{-0.7}$	1	$2.6 \pm 0.0 \,^{+0.2}_{-0.4}$	0	$0.3 \pm 0.0 \,^{+0.0}_{-0.0}$
205	6	$7.2 \pm 0.1 \,^{+0.7}_{-1.1}$	4	$4.7 \pm 0.1 \,^{+0.4}_{-0.7}$	1	$0.4 \pm 0.0 \,^{+0.1}_{-0.0}$
207	9	$6.2 \pm 0.1 \,^{+0.6}_{-1.0}$	5	$3.9 \pm 0.1 \,^{+0.3}_{-0.7}$	2	$0.5 \pm 0.1 \,^{+0.1}_{-0.1}$
208	0	$0.7 \pm 0.0 \,^{+0.1}_{-0.1}$	0	$0.4 \pm 0.0 \,^{+0.0}_{-0.1}$	0	$0.2 \pm 0.0 \,^{+0.0}_{-0.0}$
206.5(*)	5	$4.8 \pm 0.1 \,^{+0.5}_{-0.7}$	2	$3.0 \pm 0.1 \,^{+0.3}_{-0.5}$	0	$0.5 \pm 0.0 \,^{+0.0}_{-0.0}$
Total	60	$58.4 \pm 0.5 \,^{+2.3}_{-3.8}$	36	$35.3 \pm 0.5 \,^{+1.3}_{-2.3}$	3	$4.5 \pm 0.5 \,^{+0.2}_{-0.2}$
Channel	Background composition					
WW	82 %		77 %		54 %	
4-fermion	3 %		4 %		2 %	
2-fermion	3 %		4 %		0 %	
bhabha	0 %		0 %		0 %	
$\gamma\gamma$	12 %		15 %		44 %	

Table 8: Stau candidates, together with the number of background events expected, at the different selection levels and centre-of-mass energies. The column labelled "High ΔM" corresponds to the point with $M_{\tilde{\tau}}$=80 GeV/c^2 and M_{LSP}=0 GeV/c^2, the one labelled "Medium ΔM" to $M_{\tilde{\tau}}$=80 GeV/c^2 and M_{LSP}=40 GeV/c^2, and the one labelled "Low ΔM" to $M_{\tilde{\tau}}$=65 GeV/c^2 and M_{LSP}=60 GeV/c^2. The composition of the SM background for all centre-of-mass energies summed is also given. (*) indicates the 2000 data taken with the sector 6 of the TPC off.

The efficiencies have been determined using 5000 events for each point of a 1 GeV/c^2 × 1 GeV/c^2 grid in the ($M_{\tilde{\tau}}$,M_{LSP}) plane, using the fast detector simulation, and range from 20% to 30% for ΔM> 20 GeV/c^2. The results have been verified with the full detector simulation and analysis chain (figure 17(a)).

In the low mass analysis, a total of 196 events kinematically compatible with $M_{\tilde{\tau}}$ = 25 GeV/c^2 and ΔM = m_τ were selected, and the SM background was estimated to be $196.1^{+10.1}_{-4.1}$. The contribution from $\gamma\gamma \rightarrow \tau\tau$ to the background was 91%, and the remainder was other $\gamma\gamma$ processes (8%) and τ-pairs (1%). In the very low mass analysis, 59 events compatible with $M_{\tilde{\tau}}$ = 5.5 GeV/c^2 and ΔM = m_τ were selected, while the SM background was estimated to be 69.7 ± 1.8 events. The background was dominated by τ-pairs (89%) and $\gamma\gamma$ processes (7%). The remaining 4% came from four-fermion processes.

In the low mass search, the efficiency only needed to be evaluated at a limited number of points, and in particular at $\Delta M = m_\tau$. Therefore, the full detector simulation could be used at $\Delta M = m_\tau$ for $M_{\tilde{\tau}}$ between 2 and 45 GeV/c^2 (figure 17(b)). It was verified with the fast simulation and, for a smaller number of $M_{\tilde{\tau}}$ values, with the full simulation that the efficiencies were higher for higher ΔM. To determine its systematic error, the evaluation of the efficiency was repeated using the fast simulation. The error was taken as the difference between the full and fast simulation results and amounted to 15%.

Limits

Limits on sfermion masses can be derived using several different assumptions. Scalar mass unification suggests lower masses and cross-sections for the partners of right handed fermions. For third generation sfermions, Yukawa couplings can be large, leading to an appreciable mixing between the pure weak hypercharge states. The production cross-section depends on the mixing angle, due to the variation in strength of the coupling to the Z component of the weak current, and has a minimum at $52°$ at LEP2 energies [47]. For the staus, results are therefore presented also for this case. For completeness, the results for the partner of the left-handed τ are also given.

For each $M_{\tilde{\tau}} - M_{LSP}$ mass combination, the predicted number of observed SUSY events was compared with the observed number of kinematically compatible events in data and simulated background. The likelihood ratio based method presented in [33] was used to combine samples at different energies, in order to derive the confidence level of the signal hypothesis, CL_s. Systematic errors were taken into account when calculating CL_s [19]. All points where CL_s is less than 5% are excluded by the observations.

From the low mass search, at the minimum cross-section, the 95% CL limit on the stau mass was 26.3 GeV/c^2 for $\Delta M = m_\tau$, 30.2 GeV/c^2 for $\Delta M = 3$ GeV/c^2, and 40.5 GeV/c^2 for $\Delta M = 4$ GeV/c^2. The corresponding expected limits were 26.3 GeV/c^2, 32.3 GeV/c^2, and 42.1 GeV/c^2, respectively. For $\Delta M = m_\tau$, the limit improves to 29.6 (31.1) GeV/c^2 for $\tilde{\tau}_R$ ($\tilde{\tau}_L$), with an expected limit of 30.0 (31.9) GeV/c^2.

The low mass search does not exclude $M_{\tilde{\tau}}$ below 6.3 GeV/c^2 for ΔM below 3 GeV/c^2. However, since figure 18 shows that the special search for very low $M_{\tilde{\tau}}$ excludes $\Delta M = m_\tau$ if $M_{\tilde{\tau}} < 10$ GeV/c^2, and since the efficiency is increasing with ΔM, all mass-combinations below $M_{\tilde{\tau}} = 10$ GeV/c^2 are nevertheless excluded.

Figure 19 shows the 95% CL $\tilde{\tau}_R$ exclusion region obtained by combining the previous data at 130 to 184 GeV with the data taken in 1998 to 2000 up to 208 GeV. Figure 20 shows the exclusion regions in the case of the mixing corresponding to the minimal production cross-section. In addition, the limit for $\tilde{\tau}_L$ was also evaluated, and was found to be 84.7 GeV/c^2 (expected limit 84.9 GeV/c^2) for $M_{LSP} = 0$ GeV/c^2. The excess of candidates at low ΔM for high stau-mass seen in both figures is compatible with a statistical fluctuation: The observed limit was everywhere contained inside the 90% confidence band for the expected limit, calculated from the Poisson distributed background.

In summary, a stau mass limit can be set at 81.9 to 84.7 GeV/c^2 (depending on mixing) for mass differences between the stau and the LSP above 15 GeV/c^2. The same limits hold for LSP masses below 68 GeV/c^2 and mass differences between the stau and the LSP above 6 GeV/c^2. The expected limit in the same region ranges from 82.1 to 84.9 GeV/c^2. The lowest stau mass allowed by the DELPHI data is 26.3 GeV/c^2 (any mixing-angle and any $\Delta M \geq m_\tau$).

---

[19]The largest effect of the systematic uncertainty on the limit was observed at high ΔM, but nowhere exceeded 800 MeV/c^2.

6.5 Squark searches

6.5.1 Efficiencies and selected events

In the non-degenerate scenario, the efficiencies of the stop and sbottom signal selection are summarised in figure 21. For the part of the 2000 data taking in which the TPC was no longer fully operational, signal samples were simulated with the modified version of the reconstruction program used for real data and SM processes. Systematic uncertainties on the efficiency determination have been estimated as explained in section 6.2.1.

The number of events selected and the expected background at the final selection level are shown in table 9. The systematic uncertainties shown in the table have been estimated using the "re-weighting" method described in section 6.2.2. Moreover, in the mass limit computation an additional relative uncertainty of 15% related to the determination of the hadronic $\gamma\gamma$ contribution (see section 6.2.1) has been added.

Sbottom Analysis				
	$\Delta M \geq 20$ GeV/c^2		$5 < \Delta M < 20$ GeV/c^2	
$\sqrt{s}$	data	MC	data	MC
189	2	$0.43 \pm 0.08^{+0.12}_{-0.03}$	1	$0.47 \pm 0.20^{+0.19}_{-0.05}$
192	0	$0.05 \pm 0.009^{+0.02}_{-0.02}$	0	$0.06 \pm 0.024^{+0.01}_{-0.03}$
196	0	$0.17 \pm 0.04^{+0.03}_{-0.03}$	1	$0.22 \pm 0.08^{+0.02}_{-0.07}$
200	0	$0.14 \pm 0.03^{+0.02}_{-0.03}$	0	$0.27 \pm 0.08^{+0.05}_{-0.3}$
202	0	$0.07 \pm 0.02^{+0.03}_{-0.01}$	1	$0.13 \pm 0.04^{+0.04}_{-0.03}$
205	0	$0.49 \pm 0.05^{+0.05}_{-0.06}$	0	$0.43 \pm 0.17^{+0.05}_{-0.23}$
207	0	$0.36 \pm 0.04^{+0.07}_{-0.03}$	0	$0.38 \pm 0.17^{+0.13}_{-0.16}$
208	0	$0.05 \pm 0.007^{+0.073}_{-0.001}$	0	$0.04 \pm 0.017^{+0.063}_{-0.008}$
206.5(*)	0	$0.33 \pm 0.04^{+0.01}_{-0.10}$	0	$0.12 \pm 0.03^{+0.02}_{-0.05}$
Total	2	$2.10 \pm 0.12^{+0.17}_{-0.13}$	3	$2.12 \pm 0.34^{+0.25}_{-0.42}$

Stop Analysis				
	$\Delta M \geq 20$ GeV/c^2		$10 < \Delta M < 20$ GeV/c^2	
$\sqrt{s}$	data	MC	data	MC
189	3	$2.28 \pm 0.22^{+0.78}_{-0.01}$	3	$0.87 \pm 0.21^{+0.28}_{-0.02}$
192	2	$0.92 \pm 0.11^{+0.17}_{-0.40}$	0	$0.27 \pm 0.07^{+0.01}_{-0.10}$
196	0	$2.35 \pm 0.22^{+0.34}_{-0.24}$	3	$0.78 \pm 0.15^{+0.08}_{-0.20}$
200	1	$2.14 \pm 0.13^{+0.07}_{-0.39}$	0	$0.91 \pm 0.16^{+0.13}_{-0.11}$
202	1	$1.16 \pm 0.07^{+0.49}_{-0.12}$	0	$0.49 \pm 0.08^{+0.18}_{-0.12}$
205	5	$2.00 \pm 0.11^{+0.34}_{-0.28}$	0	$0.75 \pm 0.18^{+0.07}_{-0.42}$
207	1	$2.32 \pm 0.11^{+0.43}_{-0.10}$	1	$0.78 \pm 0.18^{+0.16}_{-0.27}$
208	0	$0.19 \pm 0.01^{+0.26}_{-0.01}$	0	$0.08 \pm 0.018^{+0.14}_{-0.003}$
206.5(*)	1	$2.67 \pm 0.11^{+0.01}_{-0.89}$	0	$0.41 \pm 0.04^{+0.03}_{-0.18}$
Total	14	$16.03 \pm 0.41^{+1.2}_{-1.1}$	7	$5.34 \pm 0.41^{+0.43}_{-0.60}$

Table 9: Number of events selected by the squark analysis in the non-degenerate scenarios. The first errors are statistical and the second ones are systematic. (*) indicates the 2000 data taken with the sector 6 of the TPC off.

In the nearly degenerate scenario, the efficiency for the stop signal is summarised in figure 22. The figure shows the variation of the efficiency for signal selection as a function

Stop (nearly degenerate) $\Delta M \leq 10$ GeV/c^2				
$\sqrt{s}$	Preselection		Final	
(GeV)	data	MC	data	MC
189	3717	3717	3	$2.72 \pm 0.34^{+0.78}_{-0.33}$
192	527	599	0	$0.33 \pm 0.12^{+0.10}_{-0.15}$
196	1620	1623	2	$1.02 \pm 0.21^{+0.12}_{-0.17}$
200	1667	1679	0	$1.12 \pm 0.22^{+0.27}_{-0.15}$
202	867	793	0	$0.64 \pm 0.16^{+0.26}_{-0.05}$
205	1469	1492	1	$1.32 \pm 0.33^{+0.14}_{-0.21}$
207	1423	1468	2	$1.33 \pm 0.33^{+0.35}_{-0.21}$
208	138	133	1	$0.12 \pm 0.10^{+0.17}_{-0.01}$
206.5(*)	1023	1133	0	$0.55 \pm 0.19^{+0.21}_{-0.16}$
Total	12451	12637	9	$9.15 \pm 0.72^{+0.99}_{-0.55}$

Table 10: Number of events selected by the stop analysis in the nearly degenerate scenario. The first errors are statistical and the second ones are systematic. (*) indicates 2000 data taken with sector 6 of the TPC off.

of ΔM for different stop mass hypotheses for centre-of-mass energies of 189 and 206 GeV. Some examples of the detection efficiency obtained by this analysis are quoted below: for a ΔM of 2 GeV/c^2 and a stop mass of 70 GeV/c^2, an efficiency of 2.4% is obtained at $\sqrt{s} = 189$ GeV and of 4.8% at $\sqrt{s} = 206$ GeV. For a ΔM of 4 GeV/c^2 and a stop mass of 80 GeV/c^2, an efficiency of 4.0% is achieved at $\sqrt{s} = 189$ GeV and of 7.7% at $\sqrt{s} = 206$ GeV.

Table 10 gives the results for the nearly degenerate scenario in terms of number of events compared to MC expectation after the preselection (left) and the final selection (right). The systematic uncertainties were computed using the same method as for the non-degenerate case, and the same remark concerning the hadronic $\gamma\gamma$ applies.

6.5.2 Limits

Stop and sbottom cross-sections were calculated with the SUSYGEN program for two squark mixing angles. For purely left-handed squarks ($\theta_{\tilde{q}} = 0°$), the cross-section is maximal. The squark mixing angle which corresponds to the Z decoupling is 56° for the stop and 68° for the sbottom and it corresponds approximately to the minimal cross-section. The program ALRMC [33] was used to determine the confidence level in the signal hypothesis, CL_s, based on the observed events and expected backgrounds. A point is excluded if $1 - CL_s$ is greater than 95%. Systematic errors were taken into account in the definition of CL_s.

Figures 23 and 24 show the ($M_{\tilde{q}}$, $M_{\tilde{\chi}_1^0}$) regions excluded at 95% confidence level by the search for $\tilde{t} \to c\tilde{\chi}_1^0$ and $\tilde{b} \to b\tilde{\chi}_1^0$ decays, with the 100 % branching ratio assumption, both for purely left-handed states and for the states at the Z decoupling. Figure 25 shows the exclusions obtained using only the nearly degenerate analysis for ΔM values between 2 and 20 GeV/c^2.

Table 11 shows the limit on the squark masses as a function of ΔM obtained combining both analyses. The introduction of the systematics in the confidence level calculation has no effect on these numbers. Stop masses lower than 71 GeV/c^2 and sbottom masses lower than 76 GeV/c^2 are excluded if $\Delta M \geq 2$ GeV/c^2 and $\Delta M \geq 7$ GeV/c^2 respectively

for any squark mixing angle. These limits become 75 GeV/c^2 and 93 GeV/c^2 for purely left-handed squarks.

	Sbottom		Stop	
	$\theta_{\tilde{b}}=0$	$\theta_{\tilde{b}}=68°$	$\theta_{\tilde{t}}=0$	$\theta_{\tilde{t}}=56°$
ΔM $\geq$ 2 GeV/c^2	-	-	75	71
ΔM $\geq$ 3 GeV/c^2	-	-	80	78
ΔM $\geq$ 4 GeV/c^2	-	-	84	81
ΔM $\geq$ 5 GeV/c^2	-	-	91	87
ΔM $\geq$ 7 GeV/c^2	93	76	95	91
ΔM $\geq$ 10 GeV/c^2	98	87	96	92
ΔM $\geq$ 15 GeV/c^2	99	89	96	92

Table 11: Lower limits on squark masses (in GeV/c^2) as a function of ΔM from the squark analysis in the non-degenerate and nearly degenerate scenarios.

6.6 Chargino searches

6.6.1 Non-degenerate scenarios

<u>Efficiencies and selected events</u>

The total number of background events expected in the different mass windows and topologies is shown in tables 12, 13 and 14, together with the number of events selected in the data collected in 1999 and 2000. Table 15 gives the total number of events selected in data and expected from the SM simulation after the preselections and after the final selections for the different centre-of-mass energies collected during the years 1999 and 2000. The method used to compute the asymmetric statistical errors is described in [4].

The systematic errors shown in tables 12, 13 and 14 were obtained with the "re-weighting" method described in section 6.2.2.

Stable $\tilde{\chi}_1^0$				1999 data, $\mathcal{L} = 227\ pb^{-1}$	
Topology:	$jj\ell$	$\ell\ell$	$jets$	rad	Total
$3 \leq \Delta M < 5\ \mathrm{GeV}/c^2$					
Obs. events:	4	39	3	7	53
Expect. events:	$2.3^{+1.2+1.2}_{-0.2-0.1}$	$49.2^{+3.2+2.6}_{-2.0-5.7}$	$5.3^{+1.4+0.0}_{-0.5-2.7}$	$5.3^{+1.2+0.9}_{-0.3-0.2}$	$62.1^{+4.0+3.0}_{-2.2-6.3}$
$5 \leq \Delta M < 10\ \mathrm{GeV}/c^2$					
Obs. events:	4	13	1	7	25
Expect. events:	$2.3^{+1.2+1.2}_{-0.2-0.1}$	$11.9^{+1.9+0.5}_{-0.7-3.0}$	$2.5^{+1.2+0.5}_{-0.3-0.7}$	$5.3^{+1.2+0.9}_{-0.3-0.2}$	$22.0^{+2.9+1.6}_{-0.9-3.1}$
$10 \leq \Delta M < 25\ \mathrm{GeV}/c^2$					
Obs. events:	4	14	17	7	42
Expect. events:	$2.3^{+1.2+1.2}_{-0.2-0.1}$	$14.3^{+1.6+1.7}_{-0.4-3.1}$	$15.8^{+1.9+2.1}_{-0.9-1.4}$	$5.3^{+1.2+0.9}_{-0.3-0.2}$	$37.6^{+3.0+3.1}_{-1.1-3.4}$
$25 \leq \Delta M < 35\ \mathrm{GeV}/c^2$					
Obs. events:	6	21	10	7	44
Expect. events:	$2.2^{+0.4+0.7}_{-0.1-0.0}$	$25.1^{+1.6+4.2}_{-0.5-3.5}$	$8.3^{+0.4+0.8}_{-0.2-0.0}$	$5.3^{+1.2+0.9}_{-0.3-0.2}$	$40.6^{+2.2+4.4}_{-0.7-3.5}$
$35 \leq \Delta M < 50\ \mathrm{GeV}/c^2$					
Obs. events:	2	40	28	14	84
Expect. events:	$2.3^{+0.3+0.7}_{-0.0-0.1}$	$45.1^{+1.8+3.1}_{-0.6-4.2}$	$23.6^{+0.5+3.4}_{-0.4-0.4}$	$12.9^{+1.2+1.7}_{-0.3-0.2}$	$84.1^{+2.2+4.9}_{-0.8-4.2}$
$50 \leq \Delta M$					
Obs. events:	9	60	37	14	120
Expect. events:	$7.5^{+0.5+2.2}_{-0.2-0.3}$	$68.2^{+1.9+4.4}_{-0.8-6.9}$	$36.8^{+0.6+4.9}_{-0.4-0.4}$	$12.9^{+1.2+1.7}_{-0.3-0.2}$	$125.4^{+2.4+7.1}_{-1.0-6.9}$
TOTAL (logical .OR. between different ΔM windows)					
Obs. events:	14	109	54	15	192
Expect. events:	$10.7^{+1.3}_{-0.3}$	$126.1^{+3.7}_{-2.4}$	$52.8^{+2.2}_{-1.3}$	$13.9^{+1.3}_{-0.4}$	$202.6^{+4.7}_{-2.8}$

Table 12: Number of events observed in data and expected number of background events in the different chargino search channels for all the data collected in 1999. The first errors are statistical and the second ones are systematic. The "re-weighting" method used to compute the systematics is described in section 6.2.1.

The efficiencies of the chargino selection in the four topologies were computed separately for the 132 MSSM points using the $\mathcal{L_R}$ function and the $\mathcal{L_{R_{CUT}}}$ of the corresponding topology and ΔM region. To pass from the efficiencies of the chargino selection in the four topologies to the efficiencies in the four decay channels, all the migration effects were computed for all the generated points of the signal simulation. Then the efficiencies of the selection in the four decay channels were interpolated in the $(M_{\tilde{\chi}_1^\pm}, M_{\tilde{\chi}_1^0})$ plane using the same method as in [4]. These efficiencies as functions of $M_{\tilde{\chi}_1^\pm}$ and $M_{\tilde{\chi}_1^0}$ are shown in figure 26(27) for a mean centre-of-mass energy of 206(206.5) GeV with the TPC sector 6 ON(OFF).

To study the systematic effect on the estimation of the detection efficiency both the "shaking" method and the "smearing" method were used (see section 6.2.2).

Stable $\tilde{\chi}_1^0$				$< E_{cm} > = 206$ GeV, $\mathcal{L} = 164.4\ pb^{-1}$	
Topology:	$jj\ell$	$\ell\ell$	$jets$	rad	Total
$3 \leq \Delta M < 5$ GeV/c^2					
Obs. events:	0	20	5	3	28
Expect. events:	$0.4\ ^{+1.2+0.1}_{-0.1-0.0}$	$20.6\ ^{+2.6+0.3}_{-1.6-2.4}$	$7.5\ ^{+1.6+1.3}_{-0.8-0.6}$	$2.5\ ^{+1.4+1.1}_{-0.2-0.1}$	$31.0\ ^{+3.6+1.7}_{-1.8-2.5}$
$5 \leq \Delta M < 10$ GeV/c^2					
Obs. events:	0	0	2	3	5
Expect. events:	$0.4\ ^{+1.2+0.1}_{-0.1-0.0}$	$2.0\ ^{+1.4+0.1}_{-0.4-0.5}$	$1.4\ ^{+1.3+0.5}_{-0.2-0.3}$	$2.5\ ^{+1.4+1.1}_{-0.2-0.1}$	$6.4\ ^{+2.6+1.2}_{-0.5-0.6}$
$10 \leq \Delta M < 25$ GeV/c^2					
Obs. events:	0	8	4	3	15
Expect. events:	$0.4\ ^{+1.2+0.1}_{-0.1-0.0}$	$7.7\ ^{+1.7+0.9}_{-0.6-0.4}$	$5.6\ ^{+1.4+1.3}_{-0.5-0.5}$	$2.5\ ^{+1.4+1.1}_{-0.2-0.1}$	$16.3\ ^{+2.9+1.9}_{-0.8-0.6}$
$25 \leq \Delta M < 35$ GeV/c^2					
Obs. events:	1	13	3	3	20
Expect. events:	$0.4\ ^{+1.2+0.0}_{-0.0-0.0}$	$11.6\ ^{+1.6+0.7}_{-0.5-2.1}$	$4.0\ ^{+1.3+1.0}_{-0.4-0.0}$	$2.5\ ^{+1.4+1.1}_{-0.2-0.1}$	$18.5\ ^{+2.8+1.6}_{-0.7-2.1}$
$35 \leq \Delta M < 50$ GeV/c^2					
Obs. events:	2	23	10	11	46
Expect. events:	$2.4\ ^{+1.3+0.1}_{-0.2-0.1}$	$26.8\ ^{+1.7+1.2}_{-0.7-2.8}$	$8.0\ ^{+1.4+2.0}_{-0.4-0.0}$	$10.3\ ^{+1.3+1.6}_{-0.5-0.5}$	$47.5\ ^{+2.9+2.8}_{-0.9-2.8}$
50 GeV/$c^2 \leq \Delta M$					
Obs. events:	3	40	22	11	76
Expect. events:	$3.8\ ^{+1.3+0.4}_{-0.2-0.3}$	$38.9\ ^{+1.7+4.3}_{-0.7-1.1}$	$18.7\ ^{+1.4+4.2}_{-0.6-0.0}$	$10.3\ ^{+1.3+1.6}_{-0.5-0.5}$	$71.7\ ^{+2.9+6.2}_{-1.0-1.2}$
TOTAL (logical .OR. between different ΔM windows)					
Obs. events:	4	76	31	11	122
Expect. events:	$5.0\ ^{+1.4}_{-0.3}$	$69.7\ ^{+3.1}_{-2.1}$	$29.0\ ^{+1.9}_{-1.1}$	$10.9\ ^{+1.4}_{-0.5}$	$114.6\ ^{+4.1}_{-2.4}$

Table 13: Number of events observed in data and expected number of background events in the different chargino search channels for all the events recorded in 2000 with the DELPHI detector fully operational ($< E_{cm} > = 206$ GeV). The first errors are statistical and the second ones are systematic. The "re-weighting" method used to compute the systematics is described in section 6.2.1.

For the high multiplicity topologies ($jets$ & $jj\ell$) the "shaking" method was used. The systematic uncertainty is larger in the two first ΔM regions, due to the more problematic event reconstruction. For the two first ΔM regions the relative systematic uncertainty on the detection efficiency determinations is between 4% and 13%, but at the higher ΔM regions the effect is less than 4%. The relative difference for these two topologies can be seen in table 4. All the results from the "shaking" method for these topologies gave a higher efficiency, indicating that the "unshaken" efficiencies can be regarded as conservative.

For the leptonic ($\ell\ell$) topology the "smearing" method was used. The results from this study did not give consistently higher efficiencies, but since the uncertainties are less than 1% for all the ΔM regions it showed that this topology is much less sensitive to systematic effects.

In the case of the radiative topology which consists of both high and low multiplicity events both the "shaking" method and the "smearing" method were used to study the systematic uncertainty of the efficiency. The two methods gave compatible results in all the regions where they are both valid and the uncertainty is less than 2%.

All the selected events in the real data are compatible with the expectation from the background simulation. Hence, as no evidence for a signal is found, exclusion limits are set.

Limits

The simulated points were used to parameterise the efficiencies of the chargino selection criteria described in section 5.4.1 in terms of ΔM and the mass of the chargino. Then

Stable $\tilde{\chi}_1^0$				E_{cm} = 206.5 GeV, $\mathcal{L}$ = 60.0 pb^{-1}	
Topology:	$jj\ell$	$\ell\ell$	$jets$	rad	Total
			$3 \leq \Delta M < 5$ GeV/c^2		
Obs. events:	0	10	2	2	14
Expect. events:	0.2 $^{+0.5+0.1}_{-0.0-0.0}$	18.8 $^{+1.5+0.0}_{-1.1-4.0}$	2.1 $^{+0.8+0.9}_{-0.4-0.0}$	1.3 $^{+0.5+1.0}_{-0.1-0.0}$	22.5 $^{+1.8+1.3}_{-1.2-4.0}$
			$5 \leq \Delta M < 10$ GeV/c^2		
Obs. events:	0	4	4	2	10
Expect. events:	0.2 $^{+0.5+0.1}_{-0.0-0.0}$	3.6 $^{+0.8+0.0}_{-0.4-0.5}$	3.9 $^{+1.0+2.3}_{-0.6-0.1}$	1.3 $^{+0.5+1.0}_{-0.1-0.0}$	9.1 $^{+1.4+2.5}_{-0.7-0.5}$
			$10 \leq \Delta M < 25$ GeV/c^2		
Obs. events:	0	3	7	2	12
Expect. events:	0.20 $^{+0.5+0.1}_{-0.0-0.0}$	2.31 $^{+0.6+0.0}_{-0.2-0.4}$	5.4 $^{+1.0+2.7}_{-0.6-0.0}$	1.3 $^{+0.5+1.0}_{-0.1-0.0}$	9.3 $^{+1.3+2.9}_{-0.7-0.4}$
			$25 \leq \Delta M < 35$ GeV/c^2		
Obs. events:	0	3	4	2	9
Expect. events:	0.4 $^{+0.5+0.1}_{-0.0-0.1}$	5.3 $^{+0.6+0.0}_{-0.2-2.2}$	3.2 $^{+0.7+1.2}_{-0.3-0.0}$	1.3 $^{+0.5+1.0}_{-0.1-0.0}$	10.3 $^{+1.1+1.6}_{-0.4-2.2}$
			$35 \leq \Delta M < 50$ GeV/c^2		
Obs. events:	0	10	6	5	21
Expect. events:	0.7 $^{+0.4+0.0}_{-0.0-0.1}$	11.7 $^{+0.7+0.0}_{-0.3-5.2}$	5.0 $^{+0.6+2.1}_{-0.3-0.0}$	4.3 $^{+0.5+1.3}_{-0.2-0.0}$	21.6 $^{+1.1+2.5}_{-0.4-5.2}$
			50 GeV/$c^2 \leq \Delta M$		
Obs. events:	1	16	9	5	31
Expect. events:	2.0 $^{+0.5+0.0}_{-0.1-0.6}$	14.2 $^{+0.6+4.1}_{-0.3-1.1}$	6.3 $^{+0.6+2.4}_{-0.2-0.0}$	4.3 $^{+0.5+1.3}_{-0.2-0.0}$	26.8 $^{+1.1+4.9}_{-0.4-1.3}$
			TOTAL (logical .OR. between different ΔM windows)		
Obs. events:	1	31	16	5	53
Expect. events:	2.3 $^{+0.5}_{-0.1}$	38.8 $^{+1.7}_{-1.2}$	13.1 $^{+1.2}_{-0.8}$	4.5 $^{+0.5}_{-0.2}$	58.7 $^{+2.2}_{-1.5}$

Table 14: Number of events observed in data and expected number of background events in the different chargino search channels for all the events recorded in 2000 with the TPC sector 6 off ($< E_{cm} > = 206.5$ GeV). The first errors are statistical and the second ones are systematic. The "re-weighting" method used to compute the systematics is described in section 6.2.1.

$\sqrt{s}$	$\int \mathcal{L}$	Preselection		Final sel.	
(GeV)	(pb^{-1})	Data	MC	Data	MC
192	25.4	1966	2012 ± 11	21	23.7$^{+1.4}_{-0.8}$
196	76.2	5926	5818 ± 25	85	71.6$^{+3.8}_{-2.2}$
200	84.0	6433	6331 ± 22	60	72.3$^{+2.1}_{-1.5}$
202	40.4	3086	2994 ± 11	26	35.0$^{+1.0}_{-0.8}$
205	78.3	5796	5734 ± 21	56	54.6$^{+1.9}_{-1.1}$
207	78.8	5795	5770 ± 21	63	54.9$^{+1.9}_{-1.1}$
208	7.2	530	528 ± 2	3	5.1$^{+0.2}_{-0.1}$
206.5$^{(*)}$	60.0	4119	4356 ± 16	53	58.7$^{+2.2}_{-1.5}$
all		33651	33543 ± 50	367	375.9$^{+6.6}_{-4.0}$

Table 15: Numbers of events selected in data and expected from the SM simulation in the non-degenerate chargino search at the preselection and at the final selection level, for the different centre-of-mass energies collected during the years 1999 and 2000. The (∗) indicates the data collected with the TPC sector 6 off. Simulation errors are statistical.

a large number of SUSY points were investigated and the values of ΔM, the chargino and neutralino masses and the various decay branching ratios were determined for each point. By applying the appropriate efficiency (from the interpolation), branching ratios and cross-sections for each channel decay, the number of expected signal events can be calculated. Taking into account the expected background and the number of observed events, the corresponding point in the MSSM parameter space (μ, M_2, $\tan\beta$) can be excluded, if the number of expected signal events is greater than the upper limit on the number of observed events of the corresponding ΔM region computed at 95% CL using the multichannel Bayesian formula (see section 6.1).

Figure 28 shows the chargino production cross-sections as obtained in the MSSM at $\sqrt{s} = 208$ GeV for different chargino masses for the high ΔM (ΔM > 10 GeV/c^2) and low ΔM cases (ΔM $= 3$ GeV/c^2). The parameters M_2 and μ were varied randomly in the ranges 0 GeV/$c^2 < M_2 < 3000$ GeV/c^2 and -200 GeV/$c^2 < \mu < 200$ GeV/c^2 for three fixed different values of $\tan\beta$, namely 1, 1.5 and 35. The random generation of the parameters led to an accuracy on the mass limit computation of the order of 50 MeV/c^2. Two different cases were considered for the sneutrino mass: $m_{\tilde{\nu}} > 1000$ GeV/c^2 (for ΔM > 10 GeV/c^2) and $m_{\tilde{\nu}} > M_{\tilde{\chi}_1^{\pm}}$ (for ΔM $= 3$ GeV/c^2).

The chargino mass limits are summarised in table 16. The table also gives, for each case, the minimal MSSM cross-section for which $M_{\tilde{\chi}_1^{\pm}}$ is below the corresponding mass limit. These cross-section values are also displayed in figure 28. The chargino mass limit versus ΔM and M_2 assuming a heavy sneutrino are shown in figures 29 and 30. The behaviour of the curve in figure 29 depends very weakly on the relation between M_1 and M_2. Note that in figure 30, for a fixed high value of M_2, the chargino mass limit is lower for positive μ than for negative μ. This is due to higher degeneracy for positive μ than for a negative μ, for a fixed value of M_2.

For ΔM > 10 GeV/c^2 with a large sneutrino mass (> 1000 GeV/c^2), the lower limit for the chargino ranges between 102.7 GeV/c^2 (for a mostly higgsino-like chargino) and 103.4 GeV/c^2 (for a mostly wino-like chargino). The minimal excluded MSSM cross-section at $\sqrt{s} = 208$ GeV is 0.39 pb, deriving from a chargino mass limit of 102.7 GeV/c^2.

For ΔM $= 3$ GeV/c^2, the cross-section does not depend significantly on the sneutrino mass, since the chargino is higgsino-like under the assumption of gaugino mass unification. The lower limit for the chargino mass, shown in figure 28, is 97.1 GeV/c^2. The minimal excluded cross-section is in this case 1.17 pb at $\sqrt{s} = 208$ GeV.

Case	$m_{\tilde{\nu}}$ (GeV/c^2)	$M_{\chi^{\pm}}^{min}$ (GeV/c^2)	σ^{max} (pb)	N$_{95\%}$
Stable $\tilde{\chi}_1^0$ $< E_{cm} > = 191.6$-208 GeV				
ΔM > 10 GeV/c^2	> 1000	102.7	0.39	13.8
ΔM $= 5$ GeV/c^2	> 1000	101.7	0.57	7.3
ΔM $= 3$ GeV/c^2	$> M_{\tilde{\chi}_1^{\pm}}$	97.1	1.17	18.1

Table 16: 95% confidence level lower limits for the chargino mass, the corresponding pair production cross-sections at 208 GeV and the 95% confidence level upper limit on number of observed events. The scenario of a stable $\tilde{\chi}_1^0$ is considered.

The results can be translated into a limit on the mass of the lightest neutralino [4] also shown in the ($M_{\tilde{\chi}_1^{\pm}}, M_{\tilde{\chi}_1^0}$) plane in figure 31. A lower limit of 38.2 GeV/c^2 on the lightest neutralino mass is obtained, valid for $\tan\beta \geq 1$ and a heavy sneutrino. This limit is reached for $\tan\beta = 1$, $\mu = -65.1$ GeV/c^2, $M_2 = 65.0$ GeV/c^2.

6.6.2 Nearly mass-degenerate scenarios

<u>Efficiencies and selected events</u>

In the search for heavy stable charged particles, the three windows described in section 5.4.2 were searched for mass-degenerate charginos. No events were found in the 1999 and 2000 data, where 0.51 ± 0.08 and 0.15 ± 0.03 events were expected, respectively. The efficiency for selecting a single chargino track by using this technique is shown in figure 32, as a function of the mass of the chargino and at the various centre-of-mass energies.

In the search for kinks, 42000 chargino events with masses between 60 and 100 GeV/c^2 and mean decay length of 50 cm were generated at the centre-of-mass energies between 192 and 206 GeV. The events were used to map the selection and trigger efficiency for the single chargino, as a function of its mass and decay position. As an example, the efficiencies for a 75 GeV/c^2 chargino at $\sqrt{s}$=196 GeV are plotted in figure 33. In the data of 1999 (2000 with full TPC, 2000 without the sector 6 of TPC) 5 (3, 1) events passed the selection, while 3.7 ± 1.0 (1.2 ± 0.6, 0.5 ± 0.2) were expected from the standard sources.

In the search with the ISR photon tag a total of almost 3 million $\tilde{\chi}_1^+ \tilde{\chi}_1^-$ events was generated at the centre-of-mass energies between 192 and 206 GeV; about 100 000 of them had a high $p_{\rm t}$ photon within the detector acceptance and were passed through the full detector simulation. The mass of the generated charginos ranged from 60 to 95 GeV/c^2, and ΔM from 150 MeV/c^2 to 3 GeV/c^2. The selection efficiency was computed applying the selection cuts to the samples of simulated events. The trigger efficiency, instead, was parameterised on the real data, separately for the isolated photon and for the system of few low momentum particles. Compton and Bhabha events were used to assess the trigger efficiency for single photons, as a function of the photon energy and polar angle. To estimate the trigger efficiency in events with few soft charged particles, parameterised in terms of the transverse momentum of the single particles and the total transverse energy, the redundancy of the trigger in several classes of two-photon event was used instead. The overall trigger efficiency for the whole event was finally considered as the convolution of the trigger efficiency of the single photon and that of the system of low momentum charged particles. The parameterisation was then applied on the simulation (both signal and background events). Detection and trigger efficiency vary widely with $M_{\tilde{\chi}_1^\pm}$ and ΔM; they also depend on the gauge composition of the chargino, since the spectrum of the ISR radiation is different for higgsinos and gauginos. The selection times trigger efficiency for a signal (higgsino) at 206 GeV is shown in figure 34. The small probability of radiating a photon with transverse energy E_T^γ above the chosen threshold is the main reason for having such a low efficiency. As the selection cuts varied across the plane ($M_{\tilde{\chi}_1^\pm}$, ΔM), so did the number of candidate events remaining in the data and the amount of background expected from the standard MC simulations available. Figure 35 shows, as an example, the number of events remaining in data and MC for the year 2000 sample with fully operational TPC, as a function of the position on the plane ($M_{\tilde{\chi}_1^\pm}$, ΔM). In this sample, when ΔM is below 1 GeV/c^2 additional candidates are selected in the data but none in the simulated background. The number of events remaining after the dedicated preselection and at the final step after the logical OR of all selections, together with the integrated luminosity used for the analysis, are given in table 17. The excess of events seen in the data is of the same kind as the excess observed in the analyses done at lower energies [6] and, as in the past, it can be qualitatively explained by the incomplete phase space coverage of the standard simulation used, plus possibly some noise events

like beam-gas collisions, as already discussed at the end of section 5.4.2. The excess at the preselection level has been verified to be almost entirely due to the cuts done at the generator level in the (hadronic) two-photon simulation used (in 1999 tighter cuts in the generation were applied to the hadronic $\gamma\gamma$ samples). After final selection, the distribution of the 17 candidates in the data is compatible with the luminosities shown in table 17. The fewer candidates in the simulation of the background are taken to indicate missing contributions to the few selected candidates which are not included in this model for two-photon or beam-gas reactions.

$\sqrt{s}$	$\int \mathcal{L}$	Preselection		Final sel.	
(GeV)	(pb^{-1})	Data	MC	Data	MC
192	25.4	75	40 ± 2	0	0.6 ± 0.1
196	76.2	162	118 ± 4	4	1.3 ± 0.3
200	84.0	201	123 ± 4	0	1.4 ± 0.3
202	40.4	109	55 ± 2	0	0.6 ± 0.1
206	163.0	423	393 ± 18	11	3.5 ± 1.3
206$^{(*)}$	58.5	130	113 ± 4	2	1.0 ± 0.4
all		1100	842 ± 19	17	8.4 ± 1.5

Table 17: Number of events selected in data and expected from the SM simulation in the search for nearly mass-degenerate chargino and neutralino at the preselection and at the final selection level, for the different centre-of-mass energies collected during the years 1999 and 2000. All year 2000 data were considered at the mean centre-of-mass energy of 206 GeV; (∗) indicates the data collected with the TPC sector 6 off. Simulation errors are statistical.

<u>Limits</u>

Having no evidence of significant excess above the expectations in any of the three experimental methods used to search for charginos nearly mass-degenerate with the lightest neutralino, regions in the plane $(M_{\tilde{\chi}_1^\pm}, \Delta M)$ can be excluded at the 95% CL. First, the two searches for long-lived charginos were combined, assuming that in a $\tilde{\chi}_1^+ \tilde{\chi}_1^-$ event any of the two long-lived charginos can be tagged either as a kink or as a stable particle, according to its decay length. Then the search with the ISR photon was considered for all events in which the chargino decay length was shorter than that required by the two other methods. In all cases, the data collected in the years 1999 and 2000 were further combined with all previous data from the high energy phase of LEP [6].

The limits obtained in this way are certainly model dependent: cross-sections, decay modes, and the spectrum of the ISR radiation itself all depend on the gauge composition of the chargino. They were obtained in the two SUSY scenarios in which a near mass-degeneracy between the lightest chargino and neutralino is possible: the $M_2 \gg \mu$ scenario in which the lightest chargino and neutralino are both almost pure higgsinos; and the $\mu \gg M_2$ scenario in which the lightest chargino and neutralino are both almost pure gauginos. In the gaugino scenario, the gaugino mass unification at large scale must be violated in order to obtain low ΔM; in the higgsino scenario this is not mandatory, therefore this is the scenario to be taken into account in the constrained SUSY models. Those limits are shown in figure 36, separately for the different techniques. In the same figure, they are compared with the exclusion obtained in the search for higher ΔM charginos in DELPHI.

With these new results, the ΔM independent 95% CL lower limit of DELPHI on the mass of the chargino becomes $M_{\tilde{\chi}_1^\pm} > 75$ GeV/c^2 in the higgsino scenario and $M_{\tilde{\chi}_1^\pm} > 70$ GeV/c^2 in the gaugino scenario with heavy sneutrinos.

Both limits take into account a variation of $\tan\beta$ between 1 and 50, and a variation of M_1, M_2 and μ such that the mass difference between the chargino and the neutralino remains below 3 GeV/c^2 and $M_2 \le 2M_1 \le 10M_2$. In the higgsino scenario all sfermions are required to be heavier than the chargino, while in the gaugino scenario they must be heavy enough not to modify significantly the cross-section (only the sneutrino was required to be heavier than 500 GeV/c^2) or the decay modes and widths.

Uncertainties in the selection efficiencies and in the expected backgrounds were taken into account in a Bayesian way by convoluting their expected distributions with the Poissonian distribution of the number of observed events while computing the limits (see section 6.2). The most important of these systematics is the uncertainty in the background content: depending on the point, the exclusion limits may vary as much as 2-3 GeV/c^2. Such an effect comes only from the uncertainty in the simulation available, since conservatively there was no attempt to parameterize the regions of phase space not accounted for in this simulation. Other systematics, like the uncertainties in the trigger efficiencies, were similarly taken into account by considering the configuration which leads to the weakest limits.

6.7 Neutralino searches

6.7.1 Efficiencies and selected events

The number of events selected at different centre-of-mass energies and selection levels, together with the expected SM background, are given in tables 18 to 22 for the different neutralino search topologies discussed in section 5.5: the acoplanar jets and leptons $\mathcal{L}_\mathcal{R}$ searches (table 18) and the corresponding sequential searches (table 19), the multijet

search with and without photons (table 20), the multilepton and asymmetric tau search (table 21) and the search for staus in $\tilde{\chi}_2^0\tilde{\chi}_2^0$ production (table 22). The results of the sequential and likelihood ratio analyses for the acoplanar leptons and acoplanar jets were found to be comparable. The sequential analysis performed less well in the acoplanar jet search for large ΔM values, whereas their results were very similar in the acoplanar lepton channels and in the low ΔM region in general. In the search for staus in $\tilde{\chi}_2^0\tilde{\chi}_2^0$ production, all data recorded between 1998 and 2000 (at $\sqrt{s}$ from 189 to 208 GeV) were analysed. Table 23 summarises the results at the final selection level. Table 24 shows the main background sources contributing in each channel and the typical efficiency of each search for MSSM points where it is relevant.

More than 1.2 million $\tilde{\chi}_1^0\tilde{\chi}_2^0$ events were simulated for different combinations of masses with $M_{\tilde{\chi}_1^0}$ and $M_{\tilde{\chi}_2^0}$ ranging from 5 GeV/c^2 to 100 GeV/c^2 and from 10 GeV/c^2 to 200 GeV/c^2, respectively, and for different $\tilde{\chi}_2^0$ decay modes (q$\bar{\text{q}}\tilde{\chi}_1^0$, $\mu^+\mu^-\tilde{\chi}_1^0$, e$^+e^-\tilde{\chi}_1^0$, $\tilde{\tau}\tau$). The efficiencies were computed for each mass combination and parameterised as functions of the two masses. In addition, around 300 000 $\tilde{\chi}_2^0\tilde{\chi}_{3,4}^0$ events with cascade decays were simulated. For cascade processes, the efficiencies were parameterised as functions of $M_{\tilde{\chi}_1^0}$ and a second parameter chosen to be either $M_{\tilde{\chi}_{3,4}^0}$-$M_{\tilde{\chi}_2^0}$ when considering the decay modes $\tilde{\chi}_2^0 \rightarrow \tilde{\chi}_1^0\gamma$ and $\tilde{\chi}_{3,4}^0 \rightarrow$ q$\bar{\text{q}}\tilde{\chi}_2^0$, or $M_{\tilde{\chi}_{3,4}^0}$+$M_{\tilde{\chi}_2^0}$ when considering the decay modes $\tilde{\chi}_2^0 \rightarrow$ q$\bar{\text{q}}\tilde{\chi}_1^0$ and $\tilde{\chi}_{3,4}^0 \rightarrow$ q$\bar{\text{q}}\tilde{\chi}_2^0$. The dependence on remaining parameters was found to be small in the relevant mass ranges and the efficiencies were averaged over them.

The efficiency for $\tilde{\chi}_2^0\tilde{\chi}_2^0 \rightarrow \tilde{\tau}\tau\tilde{\tau}\tau$ was evaluated in a number of points with $M_{\tilde{\chi}_1^0}$ between 30 and 50 GeV/c^2 and mass differences between the stau and the $\tilde{\chi}_1^0$ ranging from 2 to 5 GeV/c^2. The $\tilde{\chi}_2^0$ mass exceeded the $\tilde{\chi}_1^0$ mass by 30 to 45 GeV/c^2. These points were chosen because they correspond to a region in the CMSSM parameter space which cannot be excluded by the chargino search, nor – due to the low mass difference – by the stau search. Efficiencies between 10 and 20% were found, varying little with the chosen masses. These values were obtained with the fast simulation and verified with the full simulation in a sub-set of points.

The effect of systematic uncertainties on background and efficiency evaluation was studied with the "shaking" method for high multiplicity topologies and with the "smearing" method for leptonic topologies (see section 6.2). The variations in the detection efficiencies were found to be small (the relative change was below 3% on average). The efficiencies for the "shaken" signal are typically larger than for the "unshaken" signal.

The background estimated with the shaking method was typically 10% higher than the "unshaken" background. The variation of both background and efficiency is consistent with "shaking" predicting slightly higher observed missing energy.

6.7.2 Limits

In the absence of a signal, limits on neutralino production cross-sections were derived, using the dependence of the calculated efficiencies on the masses involved.

The limits for $\tilde{\chi}_1^0\tilde{\chi}_2^0$ production, as obtained from the searches for acoplanar leptons and jets, are shown in figure 37 assuming different branching ratios.

Similarly, figures 38(a,b) show cross-section limits for $\tilde{\chi}_2^0\tilde{\chi}_i^0$ production ($i = 3$ or 4). Figure 38(a) shows the limit obtained using a Bayesian combination [37] of the results from the multijet and acoplanar jet searches in the case where $\tilde{\chi}_i^0\rightarrow\tilde{\chi}_2^0q\bar{\text{q}}$ and $\tilde{\chi}_2^0\rightarrow\tilde{\chi}_1^0q\bar{\text{q}}$. Figure 38(b) gives the corresponding limits when $\tilde{\chi}_2^0\rightarrow\tilde{\chi}_1^0\gamma$, as obtained from the search for multijet events with a photon signature.

$\sqrt{s}$	Acoplanar electrons search			
(GeV)	Preselection		Final	
	Data	MC	Data	MC
192	65	60 ± 1	5	6.4 ± 0.1
196	135	143 ± 3	19	15.7 ± 0.7
200	192	180 ± 2	12	16.9 ± 1.0
202	68	82 ± 1	8	9.7 ± 0.4
205	64	77 ± 1	18	14.9 ± 0.7
207	72	78 ± 1	9	15.0 ± 0.7
208	10	6.5 ± 0.1	4	1.4 ± 0.1
206.5(*)	56	62 ± 1	16	12.6 ± 0.7
$\sqrt{s}$	Acoplanar muons search			
(GeV)	Preselection		Final	
	Data	MC	Data	MC
192	102	115 ± 3	13	7.7 ± 0.1
196	298	289 ± 4	18	19.5 ± 0.4
200	340	357 ± 3	15	21.0 ± 0.6
202	200	160 ± 3	14	10.2 ± 0.2
205	179	191 ± 2	18	19.5 ± 1.0
207	180	193 ± 2	20	19.8 ± 1.1
208	24	16 ± 0.4	3	1.9 ± 0.2
206.5(*)	179	191 ± 2	14	16.3 ± 0.3
$\sqrt{s}$	Acoplanar jets search			
(GeV)	Preselection		Final	
	Data	MC	Data	MC
192	927	896 ± 6	3	3.1 ± 0.1
196	2191	2218 ± 10	13	7.9 ± 0.3
200	2886	2835 ± 12	9	10.4 ± 0.3
202	1263	1250 ± 7	7	5.1 ± 0.2
205	1458	1404 ± 8	14	12.7 ± 1.4
207	1451	1416 ± 8	15	13.0 ± 1.4
208	133	118 ± 2	2	1.2 ± 0.2
206.5(*)	1066	1014 ± 8	14	7.8 ± 0.4

Table 18: Results of the likelihood ratio acoplanar jets and acoplanar leptons searches at the different selection levels and centre-of-mass energies. The number of events selected in data and expected from the SM simulation are given. Simulation errors are statistical. The systematic uncertainties on the background were estimated to be of the order of 3% for the acoplanar leptons topologies and of the order of 10% for the acoplanar jets topologies on the final level (see section 6.2). (*) indicates the 2000 data taken with the sector 6 of the TPC off.

$\sqrt{s}$	ee selection		$\mu\mu$ selection		qq selection	
(GeV)	Data	MC	Data	MC	Data	MC
192	0	2.4 ± 0.3	3	1.2 ± 0.2	1	3.3 ± 0.2
196	11	7.5 ± 0.7	4	3.9 ± 0.5	9	10.1 ± 0.4
200	6	9.3 ± 0.9	0	4.3 ± 0.6	5	11.6 ± 0.4
202	5	4.3 ± 0.4	1	2.1 ± 0.3	5	5.5 ± 0.2
205	5	6.3 ± 0.3	5	3.4 ± 0.2	7	11.5 ± 2.8
207	6	7.4 ± 1.5	3	4.6 ± 1.2	12	10.9 ± 0.4
208	2	0.7 ± 0.1	1	0.3 ± 0.1	4	0.9 ± 0.04
206.5(*)	6	4.4 ± 0.6	3	2.5 ± 0.4	10	8.0 ± 0.5
All	41	42.3 ± 2.1	20	22.3 ± 1.5	53	61.8 ± 3.0

Table 19: Results of the acoplanar lepton and acoplanar jet sequential searches at the final selection level for the different flavours and centre-of-mass energies. The number of events selected in data and expected from the SM simulation are given. Simulation errors are statistical. The systematic uncertainties on the background were estimated to be of the order of 3% for the acoplanar leptons topologies and of the order of 10% for the acoplanar jets topologies (see section 6.2). (*) indicates the 2000 data taken with the sector 6 of the TPC off.

From the results of the search for $\tilde{\chi}_2^0 \tilde{\chi}_2^0 \to \tilde{\tau}\tau\tilde{\tau}\tau$ described in section 5.2.3, an equivalent production cross-section at $\sqrt{s} = 206.7$ GeV larger than 63 fb can be excluded. This limit is valid for 30 GeV$/c^2 \leq M_{\tilde{\chi}_1^0} \leq 50$ GeV$/c^2$ and $M_{\tilde{\tau}} - M_{\tilde{\chi}_1^0} \leq 5$ GeV$/c^2$ in the

$\sqrt{s}$	Multijets without γ search					
(GeV)	Preselection		Intermediate		Final	
	Data	MC	Data	MC	Data	MC
192	873	916 ± 6	114	130.9 ± 2.0	3	6.7 ± 0.3
196	2683	2664 ± 9	383	368.5 ± 2.7	23	19.3 ± 0.6
200	2837	2733 ± 8	417	392.1 ± 2.5	20	21.4 ± 0.6
202	1359	1323 ± 4	208	188.5 ± 1.4	8	10.0 ± 0.3
205	2469	2412 ± 15	378	349.8 ± 4.7	15	17.5 ± 0.3
207	2471	2415 ± 6	405	355.6 ± 1.9	20	17.9 ± 0.4
208	213	212 ± 1	33	31.2 ± 0.2	3	1.6 ± 0.04
206.5(*)	1701	1248 ± 6	265	225.3 ± 1.8	17	12.9 ± 0.5
All	14606	13923 ± 22	2203	2042 ± 7	109	107.3 ± 1.2
$\sqrt{s}$	Multijets with γ search					
(GeV)	Preselection		Intermediate		Final	
	Data	MC	Data	MC	Data	MC
192	11	10.5 ± 0.7	4	2.8 ± 0.4	0	0.4 ± 0.2
196	29	31.1 ± 0.8	6	7.9 ± 0.4	0	1.0 ± 0.1
200	33	31.6 ± 0.7	8	8.7 ± 0.4	1	1.3 ± 0.2
202	17	15.5 ± 0.4	4	4.1 ± 0.2	0	0.6 ± 0.1
205	28	29.2 ± 0.6	8	7.8 ± 0.3	2	1.0 ± 0.1
207	28	29.2 ± 0.7	7	7.8 ± 0.3	0	1.2 ± 0.1
208	1	2.5 ± 0.1	0	0.6 ± 0.02	0	0.1 ± 0.01
206.5(*)	24	14.2 ± 0.5	8	4.0 ± 0.2	2	0.7 ± 0.1
All	171	164 ± 2	43	44 ± 1	5	6.3 ± 0.4

Table 20: Results of the multijets without γ and multijets with γ searches at the different selection levels and centre-of-mass energies. The numbers of events selected in data and expected from the SM simulation are given. Simulation errors are statistical. The systematic uncertainties on the background were estimated to be of the order of 10% on the final level (see section 6.2). (*) indicates the 2000 data taken with the sector 6 of the TPC off.

$\sqrt{s}$	Multilepton search					
(GeV)	Preselection		Intermediate		Final	
	Data	MC	Data	MC	Data	MC
192	1710	1608 ± 12	26	22.6 ± 0.8	3	4.2 ± 0.4
196	5158	4862 ± 35	64	69.3 ± 2.0	13	11.5 ± 1.0
200	5923	5339 ± 37	61	68.3 ± 1.8	11	11.3 ± 0.5
202	2900	2600 ± 18	36	33.0 ± 0.9	4	5.7 ± 0.3
205	5532	5135 ± 48	57	62.0 ± 3.3	13	10.8 ± 1.0
207	5553	5126 ± 34	55	62.5 ± 3.5	13	11.1 ± 1.1
208	486	455 ± 3	7	5.6 ± 0.3	0	1.0 ± 0.1
206.5(*)	3911	4135 ± 26	46	44.8 ± 1.3	9	8.7 ± 0.7
All	31173	29260 ± 85	352	368.1 ± 5.8	66	64.3 ± 2.1
$\sqrt{s}$	Asymmetric tau search					
(GeV)	Preselection		Intermediate		Final	
	Data	MC	Data	MC	Data	MC
192	1637	1828 ± 14	23	19.1 ± 1.0	1	0.6 ± 0.3
196	5118	5536 ± 42	57	57.5 ± 2.7	4	1.7 ± 0.9
200	5773	6139 ± 45	58	53.4 ± 2.3	1	2.1 ± 1.2
202	2819	2994 ± 22	34	24.6 ± 1.1	2	0.9 ± 0.6
205	5288	5804 ± 44	45	45.0 ± 3.9	0	1.1 ± 0.8
207	5319	5873 ± 39	48	50.4 ± 3.0	4	1.9 ± 1.0
208	491	521 ± 3	4	4.3 ± 0.3	0	0.2 ± 0.1
206.5(*)	3318	4613 ± 29	32	31.1 ± 1.6	1	1.5 ± 0.6
All	29763	33308 ± 94	301	285.4 ± 6.5	13	10.0 ± 2.2

Table 21: Results of the multilepton and asymmetric tau searches at the different selection levels and centre-of-mass energies. The numbers of events selected in data and expected from the SM simulation are given. Simulation errors are statistical. The systematic uncertainties on the background were estimated to be of the order of 3% on the final level (see section 6.2). (*) indicates the 2000 data taken with the sector 6 of the TPC off.

gaugino region $|\mu| >> M_2$, where this channel is important for setting a limit on the

$\sqrt{s}$ (GeV)	Data	Background
189	0	0.42 ± 0.17
192	0	0.02 ± 0.06
196	0	0.06 ± 0.02
200	0	0.25 ± 0.11
202	0	0.13 ± 0.05
205−208	0	0.21 ± 0.04
All	0	1.10 ± 0.19

Table 22: Background and candidates in the $\tilde{\chi}_2^0 \tilde{\chi}_2^0 \to \tilde{\tau}\tau\tilde{\tau}\tau$ analysis. This analysis did not include data from the period in 2000 when one sector of the TPC was off. The total expected background over the three years was 1.10 ± 0.19 events, 55 % of which were two-fermion events, the remainder being four-fermion events. The systematic uncertainties on the background were estimated to be of the order of 5% on the final level (see section 6.2.2).

1999	192 GeV		196 GeV		200 GeV		202 GeV	
Search	Data	Tot bkg.	Data	Tot bkg.	Data	Tot bkg.	Data	Tot bkg.
Acopl jets	3	3.1 ± 0.1	13	8.0 ± 0.3	9	10.3 ± 0.3	7	5.1 ± 0.2
Acopl electrons	5	6.3 ± 0.1	19	16.1 ± 0.7	12	14.8 ± 0.8	8	7.7 ± 0.3
Acopl muons	13	7.7 ± 0.1	18	19.5 ± 0.4	15	21.0 ± 0.5	14	10.2 ± 0.2
Multijets, γ's	0	0.4 ± 0.2	0	1.0 ± 0.1	1	1.3 ± 0.2	0	0.6 ± 0.1
Multijets, no γ	3	6.7 ± 0.3	23	19.3 ± 0.6	20	21.4 ± 0.6	8	10.0 ± 0.3
Multileptons	3	4.2 ± 0.4	13	11.5 ± 1.0	11	11.3 ± 0.5	4	5.7 ± 0.3
Asym tau cascades	1	0.6 ± 0.3	4	1.7 ± 0.9	1	2.1 ± 1.2	2	0.9 ± 0.6
All	28	29 ± 1	90	77 ± 2	69	82 ± 2	43	40 ± 1
2000	205 GeV		207 GeV		208 GeV		206.5 GeV(*)	
Search	Data	Tot bkg.	Data	Tot bkg.	Data	Tot bkg.	Data	Tot bkg.
Acopl jets	14	12.7 ± 1.4	15	13.0 ± 1.4	2	1.2 ± 0.2	14	8.0 ± 0.4
Acopl electrons	18	14.9 ± 0.7	9	15.0 ± 0.7	3	1.4 ± 0.1	16	13.0 ± 0.7
Acopl muons	18	19.5 ± 1.0	20	19.8 ± 1.1	3	1.8 ± 0.2	15	15.4 ± 0.3
Multijets, γ's	2	1.0 ± 0.1	0	1.2 ± 0.1	0	0.1 ± 0.01	2	0.7 ± 0.1
Multijets, no γ	15	17.5 ± 0.3	20	17.9 ± 0.4	3	1.6 ± 0.04	17	12.9 ± 0.5
Multileptons	13	10.8 ± 1.0	13	11.1 ± 1.1	0	1.0 ± 0.1	9	8.7 ± 0.7
Asym tau cascades	0	1.1 ± 0.8	4	1.9 ± 1.0	0	0.2 ± 0.1	1	1.5 ± 0.6
All	80	78 ± 2	81	80 ± 2	11	7.3 ± 0.3	74	60 ± 1

Table 23: Results of the different searches. For any given search, events are explicitly rejected if accepted by one of the searches appearing earlier in the table. (*) indicates the 2000 data taken with the sector 6 of the TPC off.

LSP mass. The cross-section dependence on $\sqrt{s}$ as given by SUSYGEN was assumed. The corresponding expected limit was 68 fb.

The effect of the systematic and statistical errors of background and efficiency on the cross-section limits was evaluated using the method described in section 6.2.3 and found to be very small.

Search	Main bkg.	Eff. (%)
Acopl jets	W^+W^-, ZZ	$10-30$
Acopl electrons	$W^+W^-, \gamma\gamma \to e^+e^-$	$10-40$
Acopl muons	$W^+W^-, \gamma\gamma \to \mu^+\mu^-$	$10-40$
Multijets, γ's	$Z\gamma$	$10-20$
Multijets, no γ	$W^+W^-, Z\gamma$	$10-40$
Multileptons	W^+W^-	$30-50$
Asym tau cascades	$W^+W^-, \gamma\gamma \to \mu^+\mu^-$	$13-19$
Double tau cascades	$ZZ, ZZ^*, Z\gamma^*$	$10-20$

Table 24: The main backgrounds and the typical efficiency of each search for MSSM points where it is relevant is shown. The efficiencies depend typically on the masses of the sparticles involved in the process.

7 Combined exclusions and mass limits in MSSM with gauge and sfermion mass unification

7.1 The method

The method employed to set lower mass limits on the LSP mass and on the masses of other SUSY particles is to convert the negative results of the searches for charginos, neutralinos, sleptons and squarks into exclusion regions in the (M_2, μ) plane for different $\tan\beta$ values, and then to find the minimal allowed sparticle masses as a function of $\tan\beta$. It is described in detail in [8,9]. The Higgs boson search in the conservative maximal M_{h^0} scenario was used to exclude low values of $\tan\beta$ [11].

Unless stated otherwise, the limits presented in the following are valid for $M_2 \leq 1000$ GeV/c^2 and for the μ region in which the lightest neutralino is the LSP. The μ range depends on the values of $\tan\beta$ and m_0, and on the mixing parameters in the third family (A_τ, A_t, A_b). Unless stated otherwise, for high values of m_0 (above 500 GeV/c^2) the μ range between -2000 and 2000 GeV/c^2 was scanned, but the scan range was increased if any limit point was found to be close to the scan boundary.

7.1.1 Method of combining different searches

In the scan of the SUSY parameter space the efficiencies of the different searches, as obtained in the previous sections, were parameterised for the dominant channels, and used together with the information on the number of events selected in data and the expected number of background events. The 95% confidence level exclusion regions obtained with the different searches were then simply superimposed.

In previous publications [8,9] we have verified that our parameterisations led to conservative results by comparing with a parallel approach, where these searches were applied to samples produced combining the very fast detector simulation program (SGV) with SUSYGEN (see section 4) to simulate simultaneously all channels of chargino, neutralino, slepton and squark production and decay.

The typical scan step size in μ and M_2 was 1 GeV/c^2 except in the region of the LSP mass limit, where the step size was decreased to 0.5 GeV/c^2. The step size in m_0 was variable, the density of points being increased in regions of potentially difficult mass configurations. Special care was taken to set up the scan logic in such a way that no such configuration was overlooked. In particular, whenever two nearby scan points were

excluded by different searches, the scan was performed with smaller steps between these points to check the continuity of the exclusion.

7.1.2 The influence of the m_0 value and of the mixing in the third family

The unification of sfermion masses to a common m_0 at the GUT scale allows sfermion masses at the Electroweak Scale to be calculated as functions of $\tan\beta$, M_2 and m_0. In particular the masses of the sneutrino ($\tilde{\nu}$), the left-handed selectron and smuon ($\tilde{e}_L, \tilde{\mu}_L$), and the right-handed selectron and smuon ($\tilde{e}_R, \tilde{\mu}_R$) can be expressed as [20]:

1) $m_{\tilde{\nu}}^2 = m_0^2 + 0.77 M_2^2 + 0.5 m_Z^2 \cos 2\beta$
2) $M_L^2 = m_0^2 + 0.77 M_2^2 - 0.27 m_Z^2 \cos 2\beta$
3) $M_R^2 = m_0^2 + 0.22 M_2^2 - 0.23 m_Z^2 \cos 2\beta$

In the high m_0 scenario, $m_0 = 1000$ GeV/c^2 was assumed, which implied sfermion masses of the same order. In this case only charginos, neutralinos and the Higgs boson could be produced at LEP [21] and the limits arise from a combination of the searches for these particles described in the previous sections of this paper and in [11].

For high m_0, the chargino pair-production cross-section is large and the chargino is excluded nearly up to the kinematic limit, provided $M_2 < 200$ GeV/c^2.

It may also be remarked that at low M_2, $\Delta M = M_{\tilde{\chi}_1^\pm} - M_{\tilde{\chi}_1^0}$ is large, resulting in increased background from W^+W^- production. However, if $|\mu|$ is low as well, the chargino tends to decay via $\tilde{\chi}_1^\pm \to \tilde{\chi}_2^0 W^*$ to the next-to-lightest neutralino $\tilde{\chi}_2^0$, which then decays by $\tilde{\chi}_2^0 \to \tilde{\chi}_1^0 \gamma$ or $\tilde{\chi}_2^0 \to \tilde{\chi}_1^0 Z^*$. For setting the mass limits, it is therefore important that the chargino search includes topologies with photons stemming from the decays $\tilde{\chi}_1^\pm \to \tilde{\chi}_2^0 W^* \to \tilde{\chi}_1^0 \gamma W^*$, since the search for topologies with photons does not suffer from W^+W^- background and is effective for large ΔM (close to m_W).

Of the detectable neutralino production channels (i.e. excluding $\tilde{\chi}_1^0 \tilde{\chi}_1^0$), the $\tilde{\chi}_1^0 \tilde{\chi}_2^0$ and $\tilde{\chi}_1^0 \tilde{\chi}_3^0$ channels are dominant for large regions in the parameter space, but in order to cover as much as possible channels like $\tilde{\chi}_2^0 \tilde{\chi}_3^0$ and $\tilde{\chi}_2^0 \tilde{\chi}_4^0$ must also be considered, giving cascade decays with multiple jets or leptons in the final state. At high m_0 the production cross-section for all these neutralino production channels drops to very low values for $|\mu| \gtrsim 75$ GeV/c^2. This is because the two lightest neutralinos have very small higgsino component (photino $\tilde{\chi}_1^0$ and zino $\tilde{\chi}_2^0$) and their s-channel pair-production is therefore suppressed, while pair-production of heavier neutralinos is not kinematically accessible. Nevertheless, for $\tan\beta < 1.5$ and $M_2 > 68$ GeV/c^2 the neutralino exclusion reaches beyond the kinematic limit for chargino production at negative μ (see figure 39). This region of $\tan\beta$ is now also excluded by searches for the production for the lightest Higgs boson [11].

For medium m_0, 100 GeV/$c^2 \lesssim m_0 \lesssim 1000$ GeV/c^2, the $\tilde{\chi}_1^0 \tilde{\chi}_2^0$ production cross-section in the gaugino-region ($|\mu| \gtrsim 75$ GeV/c^2) grows quickly as m_0 falls, due to the rapidly rising contribution from the selectron t-channel exchange. Meanwhile the chargino production cross-section in the gaugino region drops slowly, but it remains high enough to allow chargino exclusion nearly up to the kinematic limit for $m_0 \gtrsim 200$ GeV/c^2. For lower m_0 (~ 100 GeV/c^2), the chargino production cross-section in the gaugino region is close to its minimum, while the neutralino production cross-section is very much enhanced. Consequently the region of the (μ, M_2) parameter space excluded by searches for neutralino production at low m_0 is larger than the one excluded by the search for

---

[20]It is worth noting that for $\tan\beta \geq 1$ ($\tan\beta < 1$) we have $\cos 2\beta \leq 0$ ($\cos 2\beta > 0$), so the $\tilde{\nu}$ is never heavier (lighter) than the $\tilde{e}_L$.

[21]If $|\mu|$ and/or mixing terms for the third family sfermions are sufficiently high, they can be light for high m_0 as well, this case will be discussed further on.

chargino and neutralino production at high m_0 as shown in [7–9].

For low m_0, $m_0 \lesssim 100$ GeV/c^2, and low M_2, $M_2 \lesssim 200$ GeV/c^2, the situation is much more complicated because light sfermions affect not only the production cross-sections but also the decay patterns of charginos and neutralinos. Sleptons can also be searched for in direct pair-production. Exclusion regions at low m_0 arise from the combination of searches for chargino, neutralino and slepton production.

For low m_0 and M_2 the sneutrino is light, and for $M_{\tilde{\chi}_1^\pm} > m_{\tilde{\nu}}$ the chargino decay mode $\tilde{\chi}_1^\pm \to \tilde{\nu}\ell$ is dominant, leading to an experimentally undetectable final state if $M_{\tilde{\chi}_1^\pm} \simeq m_{\tilde{\nu}}$. In the gaugino region, for every value of M_2 and μ, an m_0 can be found such that $M_{\tilde{\chi}_1^\pm} \simeq m_{\tilde{\nu}}$, therefore the search for charginos cannot be used to exclude regions in the (μ, M_2) plane if very low m_0 values are allowed. The search for selectron production is used instead to put a limit on the sneutrino mass (and thus on the chargino mass), the selectron and the sneutrino masses being related by equations 1)-3). The selectron pair production cross-section is typically larger than the smuon pair production cross-section, due to the contribution of t-channel neutralino exchange. However, at $|\mu| \lesssim 200$ GeV/c^2 the selectron production cross-section tends to be small and the exclusion arises mainly from the search for neutralino pair-production.

Mixing between the left-handed and right-handed sfermion states can be important for the third family sfermions and can lead to light $\tilde{\tau}_1$, $\tilde{b}_1$ and $\tilde{t}_1$. Mass splitting terms at the Electroweak Scale proportional to $m_\tau(A_\tau - \mu\tan\beta)$, $m_b(A_b - \mu\tan\beta)$, and $m_t(A_t - \mu/\tan\beta)$ were considered for $\tilde{\tau}$, $\tilde{b}$, and $\tilde{t}$ respectively. In the first instance $A_\tau = A_t = A_b = 0$ was assumed, then the dependence of the results on A_τ, A_b and A_t was studied. These terms lead to $\tilde{\tau}_1$, $\tilde{b}_1$ or $\tilde{t}_1$ being degenerate in mass with $\tilde{\chi}_1^0$ or being the LSP for large values of $|\mu|$. The terms A_τ, A_t, A_b are arbitrary unless further constraints on the model are imposed. To derive a conservative limit on the LSP mass, which is valid for any stau mixing scenario, a model was used with no mixing in the sbottom or stop sector, but only in the stau sector. This maximises the region in the parameter space where the stau can be close in mass to the LSP. Moreover the trilinear coupling A_τ was adjusted in every point of the parameter space to get the stau close in mass to the LSP mass.

The results presented in this paper are limited to the range of the μ parameter where the lightest neutralino is the LSP.

7.2 Results

7.2.1 The LSP mass limit for high m_0

From charginos searches alone a limit of 38.2 GeV/c^2 on the lightest neutralino mass is obtained, valid for $\tan\beta \geq 1$ and a heavy sneutrino ($m_{\tilde{\nu}} > 300$ GeV/c^2). The limit is reached for $\tan\beta = 1$, $\mu = -65.7$ GeV/c^2, $M_2 = 65.0$ GeV/c^2. This limit improves by ~ 1 GeV/c^2 due to the constraint from the search for neutralino production, thus from chargino and neutralino searches the LSP mass can be constrained to be $M_{\tilde{\chi}_1^0} > 39.2$ GeV/c^2 and the limit occurs at $\tan\beta = 1.0$. Figure 39 shows the region in the (μ, M_2) plane for $\tan\beta = 1$ excluded by the chargino and neutralino searches, relevant for the LSP mass limit at $m_0 = 1000$ GeV/c^2. The lowest value of $M_{\tilde{\chi}_1^0}$ not excluded by chargino and neutralino searches occurs for $\tan\beta = 1$, $\mu = -76.5$ GeV/c^2 and $M_2 = 67.0$ GeV/c^2. For these parameters, $\tilde{\chi}_4^0 \tilde{\chi}_2^0$ production and chargino pair production are important.

Figure 40 gives the lower limit on $M_{\tilde{\chi}_1^0}$ as a function of $\tan\beta$. At $\tan\beta \gtrsim 1.2$ the neutralino search no longer contributes, the LSP limit is given by the chargino search, and its value reaches about half the limit on the chargino mass at high $\tan\beta$, where the isomass contours of $\tilde{\chi}_1^\pm$ and $\tilde{\chi}_1^0$ in the (μ, M_2) plane become parallel. The rise of the LSP limit for small $\tan\beta$ can be explained by the change of the shape of these contours with $\tan\beta$ as illustrated in [8,9]. It should be noted that, because the chargino and neutralino masses are invariant under the exchange $\tan\beta \leftrightarrow 1/\tan\beta$, the point $\tan\beta = 1$ is the real minimum and the LSP limit for $\tan\beta < 1$ can be obtained by replacing $\tan\beta$ with $1/\tan\beta$ in figure 40.

For $M_A \leq 1000$ GeV/c^2, A_t-$\mu/\tan\beta = \sqrt{6}$ TeV/c^2 (maximal M_{h^0} scenario used in [11]), and $m_t = 174.3$ GeV/c^2, the $\tan\beta$ region $0.5 \leq \tan\beta \leq 2.36$ is excluded by the Higgs searches. Thus including Higgs searches imposes the limit on $M_{\tilde{\chi}_1^0}$ (see figure 40) of $M_{\tilde{\chi}_1^0}$ > 49.0 GeV/c^2 for $\tan\beta \geq 2.36$ and $M_{\tilde{\chi}_1^0}$ > 48.5 GeV/c^2 for $\tan\beta < 0.5$.

Thus the lightest neutralino is constrained to have a mass:

$$M_{\tilde{\chi}_1^0} > 49.0 \text{ GeV}/c^2$$

for $m_0 = 1000$ GeV/c^2 and $M_2 \leq 1000$ GeV/c^2 and $\tan\beta \geq 1.0$. The limit occurs at the edge of the $\tan\beta$ exclusion given by searches for the Higgs boson. However, if $m_t = 179$ GeV/c^2, the $\tan\beta$ area excluded by searches for the Higgs boson shrinks to $0.6 \leq \tan\beta \leq 2.0$ and these limits worsen to $M_{\tilde{\chi}_1^0} > 48.5$ GeV/c^2 for $\tan\beta \geq 2.0$ and $M_{\tilde{\chi}_1^0} > 47.0$ GeV/c^2 for $\tan\beta < 0.6$. Thus the above limit worsens by 2 GeV if $m_t = 179$ GeV/c^2 and the $\tan\beta < 1.0$ region is included.

7.2.2 The LSP mass limit for any m_0

Figure 40 also gives the lower limit on $M_{\tilde{\chi}_1^0}$ as a function of $\tan\beta$ for any m_0. The "any m_0" limit resulting from chargino, neutralino and slepton searches follows the high m_0 limit up to $\tan\beta = 1.4$; then it increases more slowly due to the opening of the possibility of the chargino-sneutrino degeneracy, reaching 46 GeV/c^2 at $\tan\beta \geq 2.36$ (edge of the region excluded by Higgs boson searches); finally, as discussed in more detail below, it falls to its lowest value, 45.5 GeV/c^2, at $\tan\beta \geq 5$, due to small $M_{\tilde{\tau}_1}$-$M_{\tilde{\chi}_1^0}$, if mixing in the stau sector is of the form $A_\tau - \mu\tan\beta$, and $A_\tau = 0$. This limit is set by searches for $\tilde{\chi}_1^0\tilde{\chi}_2^0$ and $\tilde{\chi}_2^0\tilde{\chi}_2^0$ production with $\tilde{\chi}_2^0 \to \tilde{\tau}_1\tilde{\chi}_1^0$.

Thus

$$M_{\tilde{\chi}_1^0} > 46.0 \text{ GeV}/c^2$$

independent of m_0, for $\tan\beta \geq 1$ if there is no mixing in the third family ($A_\tau = \mu\tan\beta$, $A_b = \mu\tan\beta$, $A_t = \mu/\tan\beta$), or if the mixing parameters leading to $M_{\tilde{\tau}_1} - M_{\tilde{\chi}_1^0} < 5$ GeV/c^2 are avoided. The Higgs boson search in the conservative maximal M_{h^0} scenario was used to exclude $0.5 \leq \tan\beta \leq 2.36$.

LSP mass limits obtained with various assumptions are summarised in table 25.

7.2.3 The dependence of the LSP limit on the mixing in the third family.

Mixing in the third family affects in a complicated way exclusion regions obtained from Higgs, chargino, neutralino and squark searches, and a consistent discussion of the mixing is difficult.

For example the maximal M_{h^0} scenario used to set $\tan\beta$ limits from Higgs searches implies A_t-$\mu/\tan\beta = \sqrt{6}$ TeV/c^2, thus a different A_t for every μ. Such a scenario implies

as well that low m_0 values are forbidden for M_2 sufficiently low to be of interest from the point of view of the LSP mass limit [22]. Thus to be consistent we should consider only the high m_0 scenario for the LSP limit (thus higher limit), when we use $\tan\beta$ limits from the maximal M_{h^0} scenario.

In the no-mixing scenario ($A_\tau = \mu\tan\beta$, $A_b = \mu\tan\beta$, $A_t = \mu/\tan\beta$), the LSP limit occurs in the chargino-sneutrino degeneracy region, at $\tan\beta> 1.5$, where both the chargino and sneutrino mass limits are given by the selectron exclusion (see section 7.3). If there is no mixing in the stop sector, the $\tan\beta$ region excluded from the Higgs searches grows to $\tan\beta\leq 9.4$, compared to $0.5\leq \tan\beta \leq 2.36$ for the maximal M_{h^0} scenario. However, there is no improvement of the LSP limit as compared to $M_{\tilde{\chi}_1^0} > 46.0$ GeV/c^2 given above, as the $\tan\beta$ dependence of the limit "flattens out" at high $\tan\beta$ (see figure 40).

As discussed in previous papers [8,9], mixing in the stau sector can lead to a configuration where $M_{\tilde{\tau}_1}$-$M_{\tilde{\chi}_1^0}$ is small enough to make the $\tilde{\tau}_1$ undetectable and cause a blind spot both in $\tilde{\tau}_1$ and chargino exclusion. For $A_t=A_\tau=A_b=0$ with the present data, the LSP mass limit occurs a) at high enough M_2 that already for $\tan\beta\geq 3$ both $M_{\tilde{b}_1}$ and $M_{\tilde{t}_1}$ are pushed above $M_{\tilde{\tau}_1}$[23], and $\tilde{\tau}_1$ can become degenerate in mass with $\tilde{\chi}_1^0$, and b) at high enough m_0 that selectron and sneutrino pair-production are not allowed by kinematics.

For the above mixing assumptions, the mass of the lightest Higgs boson corresponding to the LSP limit point varies between 109 and 120 GeV/c^2, depending on the $\tan\beta$ region. However, when the stau is light the lightest Higgs boson decays predominantly to $\tilde{\tau}_1\overline{\tilde{\tau}_1}$, thus "invisibly". The mass limit $M_h > 113.1$ GeV/c^2 set for an invisibly decaying Higgs boson [11] can be used to exclude some of these points, but it is enough to change slightly the mixing in the stop sector (A_t) to push the Higgs mass above 113.1 GeV/c^2.

For such a mixing configuration and for $\tan\beta \gtrsim 3$, the LSP limit is therefore set by the searches for stop and sbottom and those for $\tilde{\chi}_1^0\tilde{\chi}_2^0$ production with $\tilde{\chi}_2^0 \to \tilde{\tau}_1\tau$, and it falls to $M_{\tilde{\chi}_1^0} > 45.5$ GeV/c^2 (see dot-dashed line in figure 40). This limit was verified to be robust when varying independently A_t, A_τ and A_b in the range $\pm$ 1000 GeV/c^2.

As noted in previous papers [8,9], it is the appearance of the light sbottom and stop which protects the stau from being degenerate in mass with the LSP for very high m_0 values, where the $\tilde{\chi}_1^0\tilde{\chi}_2^0$ and $\tilde{\chi}_2^0\tilde{\chi}_2^0$ production cross-sections are small. This is illustrated on figure 41 where the stop, sbottom, and stau masses at the highest allowed $|\mu|$ value at the lowest non-excluded M_2 are plotted. At high $\tan\beta$, the highest $|\mu|$ value occurs when the sbottom and stop masses have their lowest non-excluded (see section 6.5) values. In a pathological model where there is no mixing in the sbottom or stop sector ($A_b = \mu\tan\beta$, $A_t = \mu/\tan\beta$) but only in the stau sector, can $\tilde{\tau}_1$ be made degenerate with $M_{\tilde{\chi}_1^0}$ even at high values of m_0 and $|\mu|$ so that the $\tilde{\chi}_1^0\tilde{\chi}_2^0$ and $\tilde{\chi}_2^0\tilde{\chi}_2^0$ production cross-section at LEP are very small and the production of the Higgs boson and other sfermions is not accessible kinematically. However, for high m_0 values the $\tilde{\chi}_1^\pm\tilde{\chi}_1^\pm$ cross-section is sufficiently large to set a limit on the production of "invisibly" decaying charginos ($\tilde{\chi}_1^\pm \to \tilde{\tau}_1 \nu$, $\tilde{\tau}_1\to \tilde{\chi}_1^0\tau$) from the search for the ISR photons (see section 5.4.2). The limit set on the neutralino mass in such a scenario is 39 GeV/c^2 for $\tan\beta>2$ and it is illustrated in figure 42.

---

[22] To avoid "tachyonic" mass solutions for the squarks and sleptons we must have $m_{ll} + m_{rr} > \sqrt{(m_{ll} - m_{rr})^2 + 4*m_{lr}^2}$ where m_{lr} is the off-diagonal mixing term, and m_{ll}, m_{rr} are the diagonal mass terms. For example, for the stop we have: $m_{lr} = m_{top}(A_t - \mu/\tan\beta)$ and $m_{ll} \simeq m_0^2 + 9M_2^2 + m_{top}^2 + m_Z^2 \cos 2\beta(0.5 - 2/3sin^2\theta_W)$, $m_{rr} \simeq m_0^2 + 8.3M_2^2 + m_{top}^2 + 2/3m_Z^2 \cos 2\beta sin^2\theta_W$;

for an example value of $A_t - \mu/\tan\beta = \sqrt{6}$ TeV/c^2, the condition above sets a lower limit on a combination of m_0^2 and M_2^2: $m_0{}^2 + 8.5M_2{}^2 > 0.39$ TeV/c^2 [2]. Thus, if $M_2 < 190$ GeV/c^2 we must have $m_0 > 300$ GeV/c^2.

[23] The "mixing -independent" (diagonal) terms of the mass matrices grow faster with M_2 for squarks than for sleptons, and they have different dependence on $\tan\beta$. For example, for $A_t=A_\tau=A_b=0$, $\mu=0$, and $\tan\beta=1$, both the $\tilde{t}_1$ and $\tilde{b}_1$ are heavier than the $\tilde{\tau}_1$; but they become lighter than the $\tilde{\tau}_1$ for large $|\mu|$ values. The mass hierarchy between $\tilde{\tau}_1$, $\tilde{b}_1$, and $\tilde{t}_1$ depends on M_2, $\tan\beta$, μ, and m_0.

In mSUGRA (as defined in section 2), $|\mu|^2$ is in the range $3.3\,m_{1/2}^2 - 0.5 m_Z^2 < \mu^2 < m_0^2 + 3.8 m_{1/2}^2$ for $\tan\beta > 2$ and a light stau cannot be degenerate with neutralino for large m_0. Thus neutralino searches set a limit on the LSP (and the lightest chargino) mass for small $M_{\tilde{\tau}_1} - M_{\tilde{\chi}_1^0}$ which is close to the one obtained for heavy sleptons.

7.2.4 The influence of radiative corrections to the gauge mass relations on the LSP limit.

The relations between chargino, neutralino and gluino masses and $|\mu|$ and M_2 are affected by radiative corrections of the order of 2%-20% [48]. However, only the relative relations between chargino, neutralino and gluino masses are important from the experimental point of view, and here the corrections are much smaller. For example, the relation $M_{\tilde{\chi}_1^\pm}(M_{\tilde{\chi}_2^\pm})/M_{\tilde{\chi}_1^0} \simeq 2$ in the gaugino region, which is exploited to set a limit on the LSP mass, receives corrections only of the order of 2%. Thus, it is enough to lower the LSP limits presented here by 1 GeV/c^2 to account for the effects of radiative corrections conservatively.

7.3 $\tilde{\chi}_1^\pm$ mass limits for any m_0

Figure 43 shows the chargino mass limit as a function of $\tan\beta$ for $M_2 < 200$ GeV/c^2. The lowest non-excluded chargino mass is found at MSSM points very close to those giving the LSP mass limit, and the arguments presented in section 7.2.2 also apply to explain the dependence of the chargino mass limit on $\tan\beta$. For $\tan\beta \lesssim 1.4$ the limit occurs at high m_0 values. For $1.4 \lesssim \tan\beta \lesssim 3$ and $M_2 < 200$ GeV/c^2, the limit occurs at low m_0 in the chargino-sneutrino degeneracy region. It falls at $\tan\beta \gtrsim 4$ because of the small $\Delta M = M_{\tilde{\tau}} - M_{\tilde{\chi}_1^0}$.

The lightest chargino is constrained to have a mass:

$$M_{\tilde{\chi}_1^\pm} > 94 \text{ GeV}/c^2,$$

independently of m_0, for $\tan\beta \leq 40$, $M_2 \leq 1000$ GeV/c^2, if either there is no mixing in the third family ($A_\tau = \mu\tan\beta$, $A_b = \mu\tan\beta$, $A_t = \mu/\tan\beta$) or the mixing parameters leading to $M_{\tilde{\tau}_1} - M_{\tilde{\chi}_1^0} < 5$ GeV/c^2 are avoided.

If mixing in the stau sector is of the form $A_\tau - \mu\tan\beta$, and $A_\tau = 0$, the limit falls to 90 GeV/c^2, at $\tan\beta \geq 3$, due to small $M_{\tilde{\tau}_1}$-$M_{\tilde{\chi}_1^0}$. This limit is robust when varying A_t, A_τ and A_b independently in the range $\pm$ 1000 GeV/c^2. In the "arbitrary" mixing scenario described above, where there is no mixing in the stop and sbottom sector, but only in the stau sector this limit falls to 80 GeV/c^2 and it is independent of the stau mixing.

The chargino mass limits for high M_2 values where the chargino can be degenerate in mass with the LSP presented in 6.6.2, are close to 75 GeV/c^2.

Chargino mass limits obtained with various assumptions are summarised in table 25.

7.4 $\tilde{\nu}$ and $\tilde{e}_R$ mass limits for any m_0

The sneutrino and the $\tilde{e}_R$ mass limits are:

$$m_{\tilde{\nu}} > 94 \text{ GeV}/c^2 \text{ and } M_{\tilde{e}_R} > 94 \text{ GeV}/c^2.$$

These limits, shown in figure 43, were obtained assuming no mass splitting in the third sfermion family ($A_\tau = \mu\tan\beta$), implying $M_{\tilde{e}_R}=M_{\tilde{\tau}_R}=M_{\tilde{\tau}_1}=M_{\tilde{\mu}_R}$, as this gives the lowest values.

These limits result from the combination of slepton and neutralino searches. The selectron mass limit (see figure 43, dotted curve) is valid for -1000 GeV/$c^2 \leq \mu \leq 1000$ GeV/c^2 and $1 \leq \tan\beta \leq 40$ provided that $M_{\tilde{e}_R} - M_{\tilde{\chi}_1^0} > 10$ GeV/c^2, and it allows a limit to be set on the sneutrino mass as shown in figure 43 (dashed curve). The sneutrino mass limit is expected to rise for $\tan\beta < 1$, the sneutrino being heavier than the $\tilde{e}_R$ for small $\tan\beta$. The selectron mass limit for $\tan\beta = 1.5$ and $\mu = -200$ GeV/c^2 was shown in section 6.4.1.

Slepton mass limits obtained with different assumptions are summarised in table 25.

7.5 MSSM parameter space exclusion

Limits on Higgs, chargino, neutralino, slepton and squark production used in the previous sections to set a mass limit on the LSP and other particles can be also used to exclude regions in a parameter space of the CMSSM. The exclusion regions in the (μ, M_2) plane for $\tan\beta = 35$ and two assumptions about m_0 and mixing in the third family are shown in figure 44.

8 Summary

Searches for charginos, neutralinos, sleptons and squarks in e^+e^- collisions at centre-of-mass energies up to 208 GeV were performed with the DELPHI detector at LEP. No evidence for a signal was found in any of the channels and 95% CL upper limits on the production cross-sections were derived.

Under assumptions that depend on the channel, such results were translated into lower limits on the masses of SUSY particles. In particular, in the framework of constrained SUGRA-broken MSSM scenarios (section 2) regions of the parameter space can be excluded and these exclusions can be translated into limits on the masses of SUSY particles. The combination of the results of the different search channels is crucial to ensure a complete coverage of the parameter space.

A summary of the limits obtained on the masses of SUSY particles is presented in table 25. The results presented extend and confirm previous exclusions set by DELPHI (see [2] to [9]) and by the other LEP experiments [49].

Particle	Validity conditions	Mass limit (GeV/c^2)
$\tilde{e}_R$	$\tan\beta$=1.5, μ=-200, ΔM>15	94
	CMSSM, ΔM>10	94
$\tilde{\mu}_R$	BR($\tilde{\mu}\rightarrow \mu\tilde{\chi}^0$)=1 , ΔM>5	88
	CMSSM, ΔM>10	94
$\tilde{\tau}$	BR($\tilde{\tau}\rightarrow \tau\tilde{\chi}^0$)=1, ΔM$\geq m_\tau$	26
$\tilde{\tau}_R$	BR($\tilde{\tau}\rightarrow \tau\tilde{\chi}^0$)=1, ΔM>15, no mixing	85
$\tilde{\tau}_{min}$	BR($\tilde{\tau}\rightarrow \tau\tilde{\chi}^0$)=1, ΔM>15, minimal cross-section	82
$\tilde{\nu}$	CMSSM, $(M_{\tilde{e}_R}-M_{\tilde{\chi}_1^0})$>10	94
$\tilde{b}$	BR($\tilde{b}\rightarrow$ b $\tilde{\chi}^0$)=1,ΔM>7, no mixing	93
	BR($\tilde{b}\rightarrow$ b $\tilde{\chi}^0$)=1, ΔM>7, minimal cross-section	76
$\tilde{t}$	BR($\tilde{t}\rightarrow$ c $\tilde{\chi}^0$)=1, ΔM>10, no mixing	96
	BR($\tilde{t}\rightarrow$ c $\tilde{\chi}^0$)=1, ΔM>2, no mixing	75
	BR($\tilde{t}\rightarrow$ c $\tilde{\chi}^0$)=1, ΔM>10, minimal cross-section	92
	BR($\tilde{t}\rightarrow$ c $\tilde{\chi}^0$)=1, ΔM>2, minimal cross-section	71
$\tilde{\chi}^\pm$	$m_{\tilde{\nu}}$>1000, ΔM>10, $M_1 =\sim 0.5M_2$,	102.7
	$M_{\tilde{f}} > M_{\tilde{\chi}^\pm}$, ΔM>3	97
	$M_{\tilde{f}} > M_{\tilde{\chi}^\pm}$, any ΔM, $M_1 =\sim 0.5M_2$	75
	$m_{\tilde{\nu}}$> 300, $|\mu| \geq M_2$, no gaugino mass unification, any ΔM	70
	CMSSM, ΔM>3, any m_0, no mixing or ΔM($\tilde{\tau}$-$\tilde{\chi}^0$)>6	94
	CMSSM, any m_0, any M_2, $\tan\beta$ <40, mixing A_τ=A_b=A_t=0	90
$\tilde{\chi}^0$	CMSSM, high m_0, $\tan\beta$ >1, maximal mixing in $\tilde{t}$ sector	49
	CMSSM, any m_0, $\tan\beta$ <40 no mixing or ΔM($\tilde{\tau}$-$\tilde{\chi}^0$)>6	46
	CMSSM, any m_0, $\tan\beta$ <40, mixing A_τ=A_b=$A_t = 0$	46
	CMSSM, any m_0, 1<$\tan\beta$ <40, mix. A_τ=A_b=0, $A_t = \sqrt{6}$ TeV/c^2	49

Table 25: Summary of mass limits for supersymmetric particles and their validity conditions. In each line of the table ΔM is the mass difference between the corresponding sparticle and the LSP. All masses and ΔM values are in GeV/c^2. CMSSM refers to a model with gauge and sfermion mass unification, where μ however is a free parameter (see section 2). Neutralino mass limits should be lowered by 1 GeV/c^2 if the radiative corrections of [48] are taken into account.

9 Acknowledgements

References

[1] P. Fayet and S. Ferrara, Phys. Rep. **32** (1977) 249;
H.P. Nilles, Phys. Rep. **110** (1984) 1;
H.E. Haber and G.L. Kane, Phys. Rep. **117** (1985) 75.

[2] DELPHI Coll., P. Abreu *et al.*, E. Phys. J. **C19** (2001) 29;
DELPHI Coll., P. Abreu *et al.*, E. Phys. J. **C6** (1999) 385.

[3] DELPHI Coll., P. Abreu *et al.*, Phys. Lett. **B496** (2000) 59.

[4] DELPHI Coll., P. Abreu *et al.*, Phys. Lett. **B479** (2000) 118;
T. Alderweireld, I. Gil, P. Rebecchi, *Review of the chargino search in DELPHI. Latest results at $E_{\mathrm{cm}} = 189$ GeV*, CERN-OPEN-2002-031;
DELPHI Coll., P. Abreu *et al.*, Phys. Lett. **B446** (1999) 75.

[5] DELPHI Coll., P. Abreu *et al.*, Phys. Lett. **B503** (2001) 34.

[6] DELPHI Coll., P. Abreu *et al.*, Phys. Lett. **B485** (2000) 65;
DELPHI Coll., P. Abreu *et al.*, E. Phys. J. **C11** (1999) 1.

[7] DELPHI Coll., P. Abreu *et al.*, E. Phys. J. **C19** (2001) 201.

[8] DELPHI Coll., P. Abreu *et al.*, Phys. Lett. **B489** (2000) 38.

[9] M. Espirito Santo, K. Hultqvist, P. Johansson, A. Lipniacka, F. Mazzucato, *Limits on the masses of supersymmetric particles at $\sqrt{s}$ up to 202 GeV*, CERN-OPEN-2002-014.

[10] R. Arnowitt, A. Chamseddine and P. Nath, *N=1 Supergravity*, World Scientific, Singapore, 1984.

[11] DELPHI Coll., P. Abreu *et al.*,Phys. Lett. **B499** (2001) 23.

[12] C.H. Chen, M. Drees, J.F. Gunion, Phys. Rev. **D55** (1997) 330, erratum/addendum *ibid.* **D60**:039901 (1999).

[13] DELPHI Coll., P. Aarnio *et al.*, Nucl. Instr. and Meth. **303** (1991) 233;
DELPHI Coll., P. Abreu *et al.*, Nucl. Instr. and Meth. **378** (1996) 57.

[14] P. Rebecchi, *Optimisation de l'herméticité du détecteur DELPHI pour la recherche de particules supersymétriques à LEP2*, Ph.D. thesis, LAL 96-30 (May 1996), Université Paris XI Orsay, CERN THESIS-96-003.

[15] T. Sjöstrand, Comp. Phys. Comm. **39** (1986) 347;
T. Sjöstrand, `PYTHIA 5.6` *and* `JETSET 7.3`, CERN-TH/6488-92.

[16] J.E. Campagne and R. Zitoun, Z. Phys. **C43** (1989) 469.

[17] S. Jadach, B.F.L. Ward and Z. Was, Comp. Phys. Comm. **79** (1994) 503.

[18] S. Jadach, W. Placzek and B.F.L. Ward, Phys. Lett. **B390** (1997) 298.

[19] F.A. Berends, R. Pittau, R. Kleiss, Comp. Phys. Comm. **85** (1995) 437.

[20] J.Fujimoto *et al.*, Comp. Phys. Comm. **100** (1997) 128

[21] S. Nova, A. Olshevski, and T. Todorov, *A Monte Carlo event generator for two photon physics*, DELPHI note 90-35 (1990).

[22] R. Engel, Z. Phys. **C66** (1995) 203;
R. Engel and J. Ranft, Phys. Rev. **D54** (1996) 4244.

[23] F.A. Berends, P.H. Daverveldt, R. Kleiss, Comp. Phys. Comm. **40** (1986) 271, Comp. Phys. Comm. **40** (1986) 285, Comp. Phys. Comm. **40** (1986) 309.

[24] S.Katsanevas and P.Morawitz, Comp. Phys. Comm. **112** (1998) 227.

[25] G. Altarelli *et al.*, *Physics at LEP2*, Yellow Report CERN 96-01, vol. 2. (1996)

[26] DELPHI Coll., P. Abreu *et al.*, Z. Phys. **C73** (1996) 11.

[27] R. Keranen, A. Sopczak, H. Nowak, M. Berggren, E. Phys. J. **C7** (2000) 1.

[28] S. Catani *et al.*, Phys. Lett. **B269** (1991) 432.

[29] F. Cossutti, A. Tonazzo, F. Mazzucato, *REMCLU : a package for the Reconstruction of Electromagnetic CLUsters at LEP200*, DELPHI note 2000-164 PROG 242 (2000).

[30] DELPHI Coll., P. Abreu *et al.*, Z. Phys. **C70** (1996) 531;
G. Borisov, C. Mariotti, Nucl. Instr. and Meth. **372** (1996) 181.

[31] T.W. Anderson, An Introduction to multivariate analysis, New York Wiley, 1958.

[32] A. Zell *et al.*, SNNS user manual : Version 4.1 (1995),
"http://www.ra.informatik.uni-tuebingen.de/SNNS/".

[33] A. Read *et al.*, *1st Workshop on Confidence Limits*, Yellow report CERN 2000-005, (May 2000) 81-103;
A. Read, note DELPHI 97-158 PHYS 737.

[34] DELPHI Coll., P. Abreu *et al.*, Phys. Lett. **B444** (1998) 491.

[35] A.V. Oppenheim and R.W. Schafer, Discrete-time signal processing, Prentice-Hall, 1989

[36] Particle Data Group, R.M. Barnett *et al.*, Phys. Rev. **D54** (1996) .

[37] V.F. Obraztsov, Nucl. Instr. and Meth. **316** (1992) 388;
V.F. Obraztsov, Nucl. Instr. and Meth. **399** (1997) 500.

[38] S. Jadach *et al.*, *LEP2 Monte Carlo Workshop : Report of the Working Groups on Precision Calculations for LEP2 Physics*, Yellow Report CERN 2000-009, (September 2000).

[39] T. Alderweireld, S. Todorovova and P. Verdier, *Study of the hadronic $\gamma\gamma$ interactions at $\sqrt{s} = 200 GeV$*, CERN-OPEN-2002-032.

[40] DELPHI, Coll., J. Abdallah *et al.*, *ZZ production in e^+e^- interactions at $\sqrt{s} = 183 - 209$ GeV*, to be submitted to E. Phys. J. C.

[41] A. Perrotta, *Confidence limits with multiple channels and arbitrary probability distributions for sensitivity and expected background*, accepted by Int. J. Mod. Phys **C**.

[42] ALEPH Coll., D.Decamp *et al.*, Phys. Rep. **216** (1992) 253;
L3 Coll., M. Acciari *et al.*, Phys. Lett. **B350** (1995) 109;
OPAL Coll., G. Alexander *et al.*, Phys. Lett. **B377** (1996) 273;
DELPHI Coll., A. Lopez-Fernandez, *Search for Z^0 decays into sleptons and neutralinos using the DELPHI detector*, DELPHI note 92-95 (Dallas) PHYS 206.

[43] DELPHI Coll., P. Abreu *et al.*, E. Phys. J. **C16** (2000) 371:
ALEPH, DELPHI, L3, OPAL Coll., D. Abbaneo *et al.*, *A combination of preliminary electroweak measurements and constraints on the Standard Model*, CERN-EP/2001-098.

[44] Particle Data Group, J. Bartels *et al.*, E. Phys. J. **C15** (2000) 1.

[45] K.Mönig, *Model independent limit of the Z-decay-width into unknown particles*, CERN-OPEN-97-040 and DELPHI 97-174 PHYS 748.

[46] ASP Collaboration: C. Hearty *et al.*, Phys. Rev. **D39** (3207) 1989.

[47] A. Bartl *et al.*, Z. Phys. **C76** (1997) 549.

[48] D. Pierce and A. Papadopoulos, Phys. Rev. D **50** (1994) 565; D. Pierce and A. Papadopoulos, Nucl. Phys. B **430** (1994) 278.

[49] ALEPH Coll., D. Abbaneo *et al.*, Phys. Lett. **B499** (2001) 67;
ALEPH Coll., D. Abbaneo *et al.*, *Search for Charginos and Neutralinos in $e+e-$ Collisions at $\sqrt{s}$ up to 208 GeV and Mass Limit for the Lightest Neutralin o*, ALEPH 2001-009, February 2001;
L3 Coll., P. Achard *et al.*, *Search for Supersymmetry in $e+e-$ collisions at $\sqrt{s}= 202$-208 GeV*, L3 note 2644, February 2001;
OPAL Coll., G. Abbiendi *et al.*, *New Particle Searches in e^+e^- Collisions at $\sqrt{s} = 200$-209 GeV*, Opal Physics note PN470, February 2001.
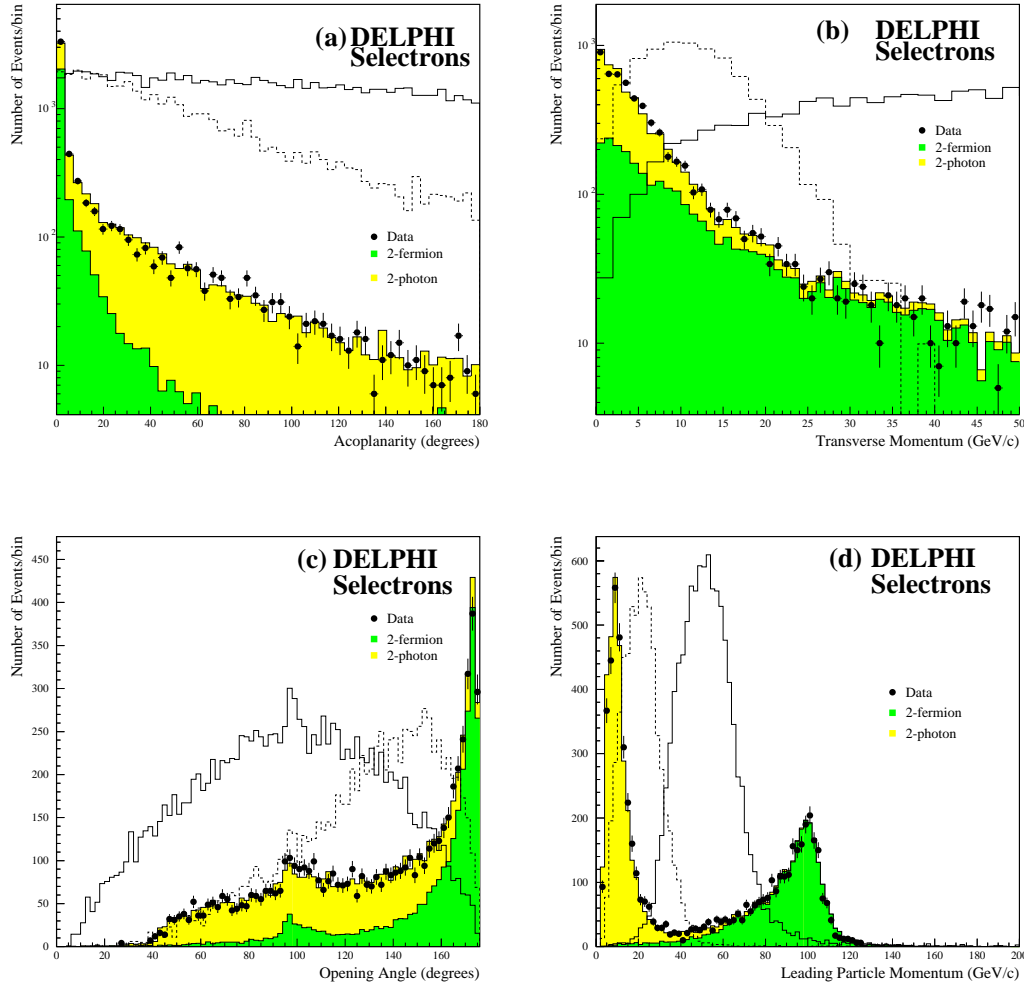
Figure 1: Comparison of data and simulation in the selectron channel at preselection level. The dots with error bars show the data, shaded histograms show the simulation. Plots include data taken in the year 2000 when the DELPHI detector was fully operational. The plots show: (a) the acoplanarity, (b) the transverse momentum, (c) the opening angle, (d) the momentum of the leading charged particle. Possible signals corresponding to the mass combinations $M_{\tilde{e}}$=90 GeV/c^2,$M_{\tilde{\chi}_1^0}$=10 GeV/c^2 (solid) and $M_{\tilde{e}}$=50 GeV/c^2,$M_{\tilde{\chi}_1^0}$=40 GeV/c^2 (dashed) are shown by the superimposed open histograms. The signal normalisation is arbitrary.
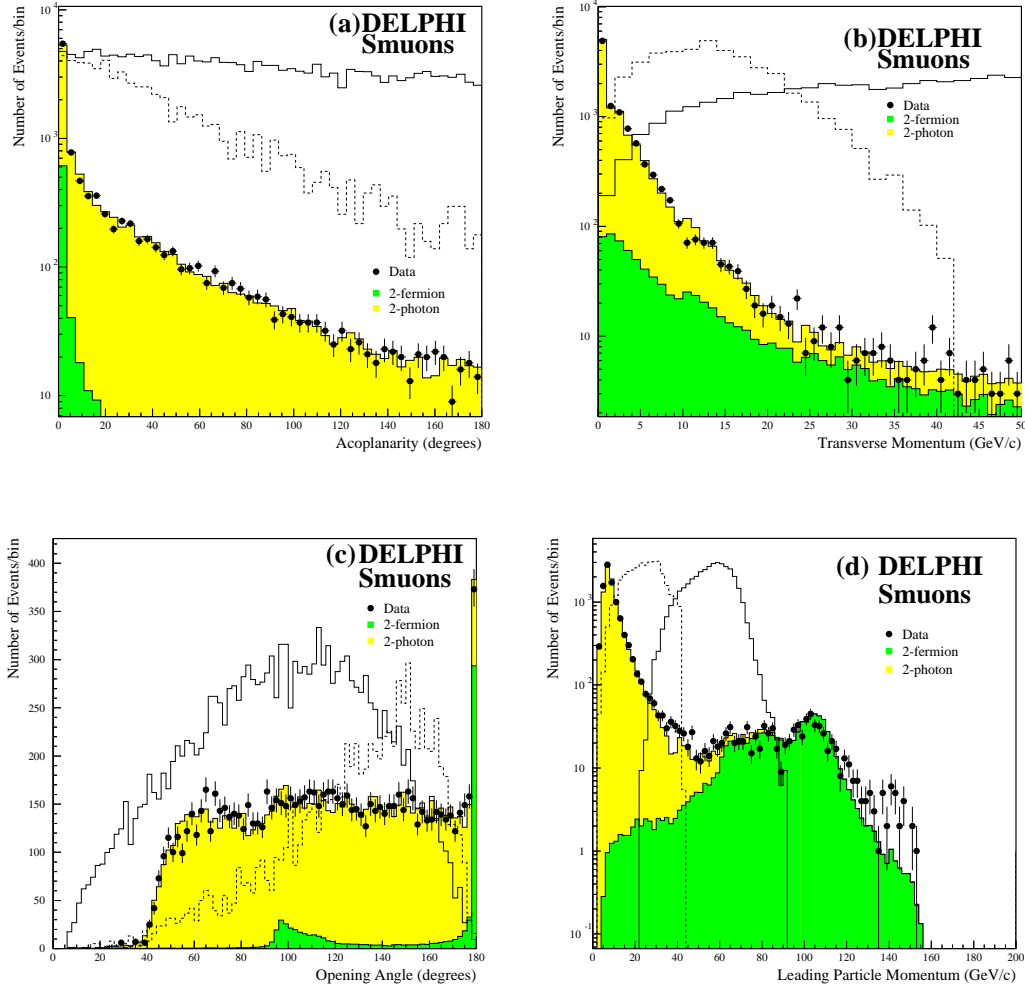
Figure 2: Comparison of data and simulation in the smuon channel at preselection level. The dots with error bars show the data, shaded histograms show the simulation. Plots include data taken in the year 2000 when the DELPHI detector was fully operational . The plots show: (a) the acoplanarity, (b) the transverse momentum, (c) the opening angle, (d) the momentum of the leading charged particle. Possible signals corresponding to the mass combinations $M_{\tilde{\mu}}$=90 GeV/c^2,$M_{\tilde{\chi}_1^0}$=10 GeV/c^2 (solid) and $M_{\tilde{\mu}}$=50 GeV/c^2,$M_{\tilde{\chi}_1^0}$=40 GeV/c^2 (dashed) are shown by the superimposed open histograms. The signal normalisation is arbitrary.
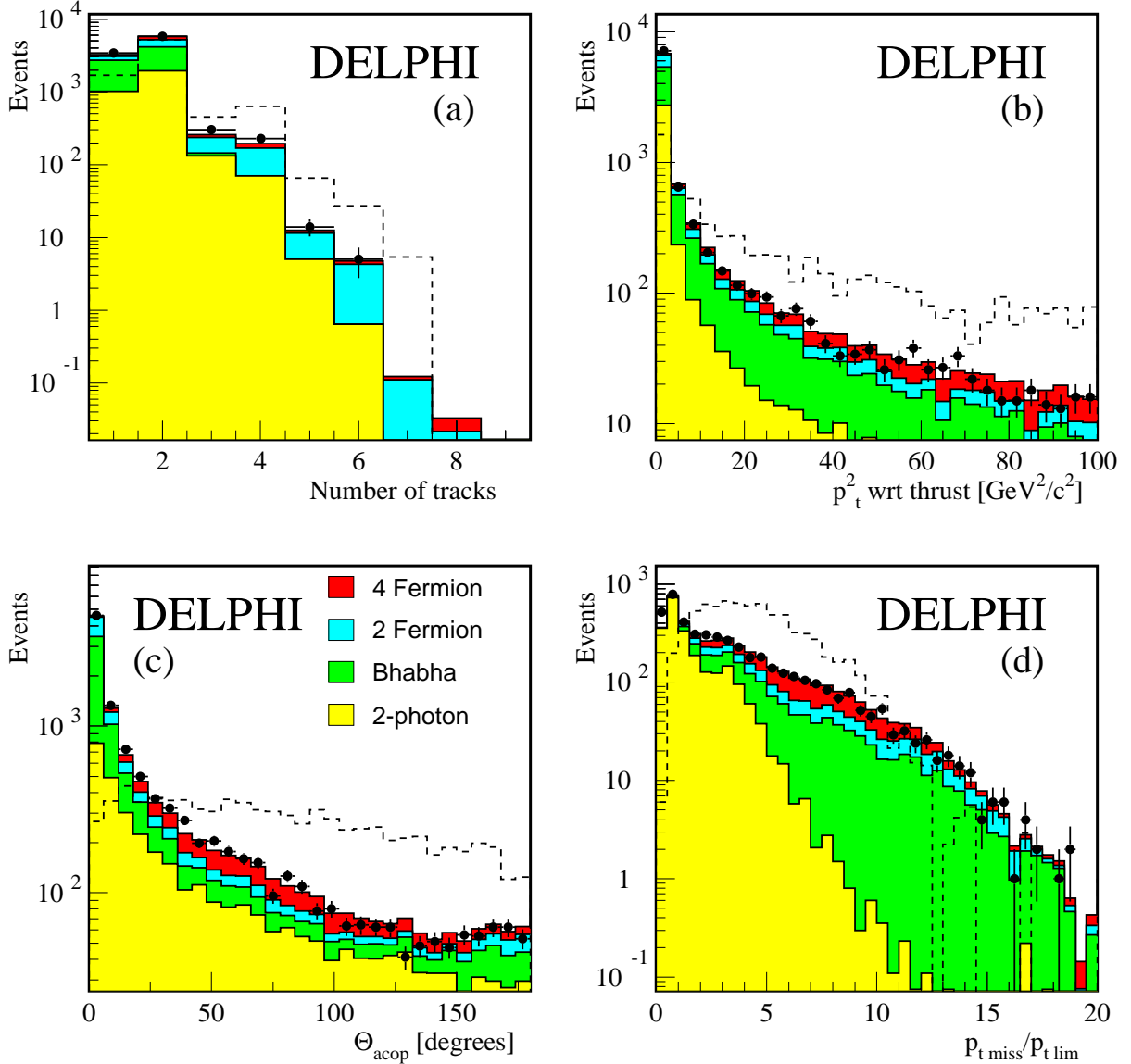
Figure 3: A preselection comparison of data and simulation in the stau analysis. The plots show: (a) the number of charged particles, (b) the square of the transverse momentum with respect to the thrust axis, (c) the acoplanarity, (d) the missing transverse momentum divided by the maximum missing transverse momentum in two-photon events with no beam-remnant electrons in the detector acceptance (ie. in "no-tag" events). The dots with error bars show the data, while the simulation is shown shaded. A typical signal ($M_{\tilde{\tau}} = 83$ GeV/c^2, $M_{\mathrm{LSP}} = 0$ GeV/c^2) is shown by the superimposed open histogram, with arbitrary normalisation.
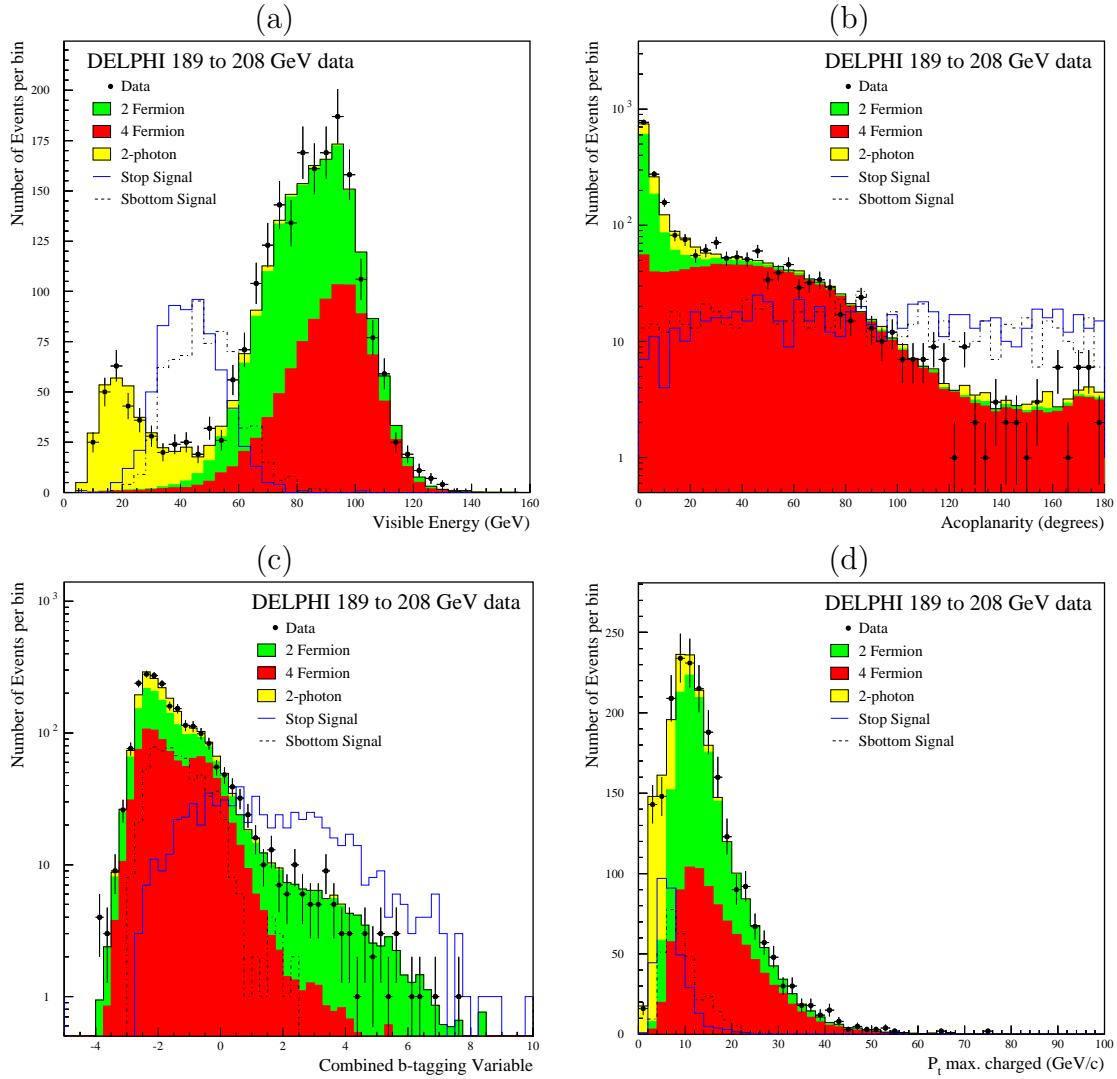
Figure 4: Comparison of data and simulation at the preselection level in the non-degenerate squark analysis. Plots include all DELPHI data from 189 to 208 GeV: (a) visible energy, (b) combined b-tagging variable, (c) acoplanarity, (d) maximal transverse momentum of a charged particle. The expected signal distributions at $\sqrt{s} = 200$ GeV are shown for one possible stop and sbottom signal ($M_{\tilde{q}} = 90$ GeV/c^2, $M_{\tilde{\chi}_1^0} = 60$ GeV/c^2), with arbitrary normalisation.
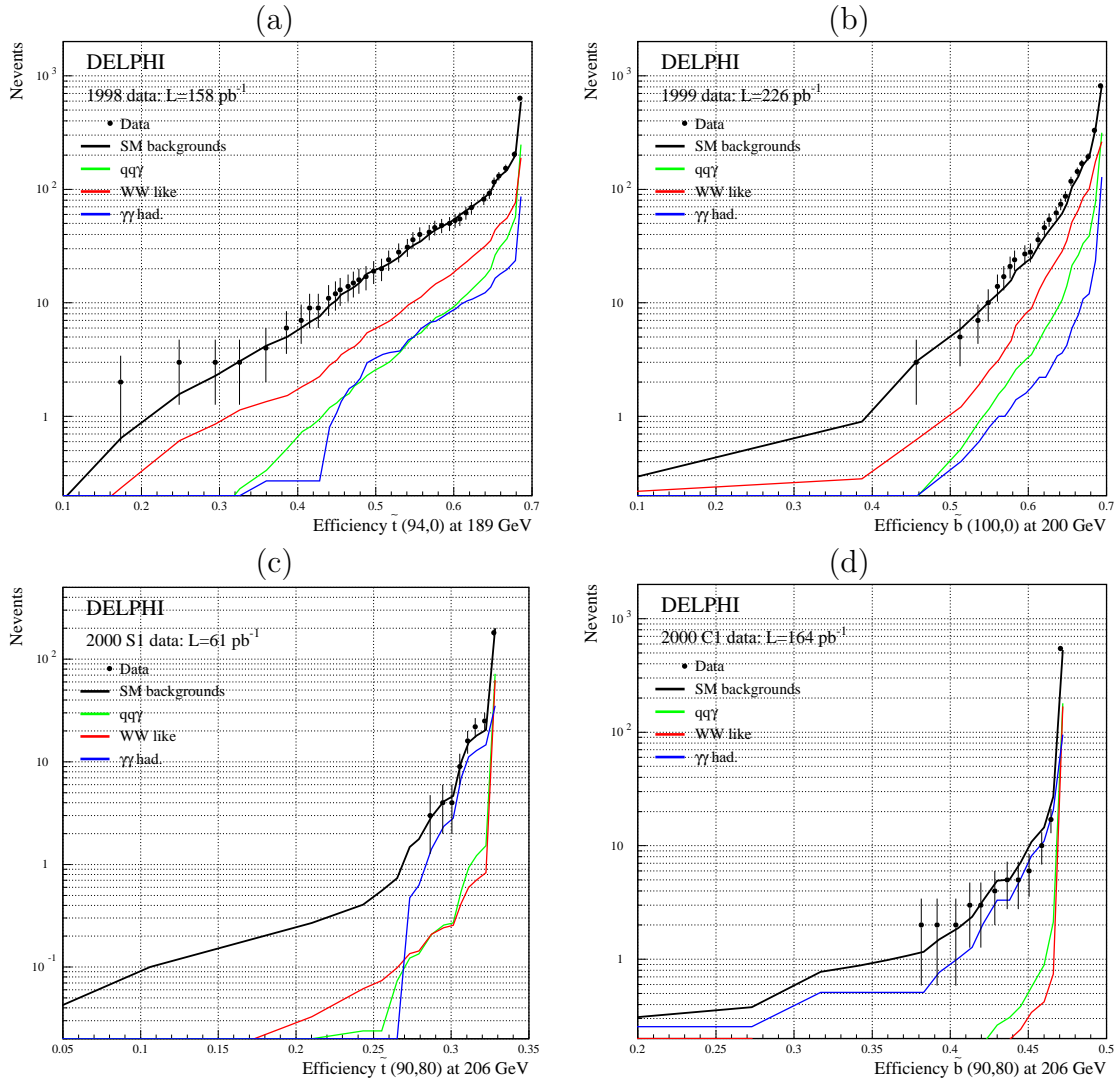
Figure 5: Number of events as a function of the signal detection efficiencies in the non-degenerate squark analysis: (a) 1998 data at 189 GeV: stop analysis for $\Delta M > 20$ GeV/c^2, (b) 1999 data from 192 to 202 GeV: sbottom analysis for $\Delta M > 20$ GeV/c^2, (c) 2000 data with TPC sector 6 off: stop analysis for $5 \leq \Delta M \leq 20$ GeV/c^2, (d) 2000 data with TPC sector 6 on: sbottom analysis for $5 \leq \Delta M \leq 20$ GeV/c^2.

(a)

(b)

(c)

(d)

(e)

(f)
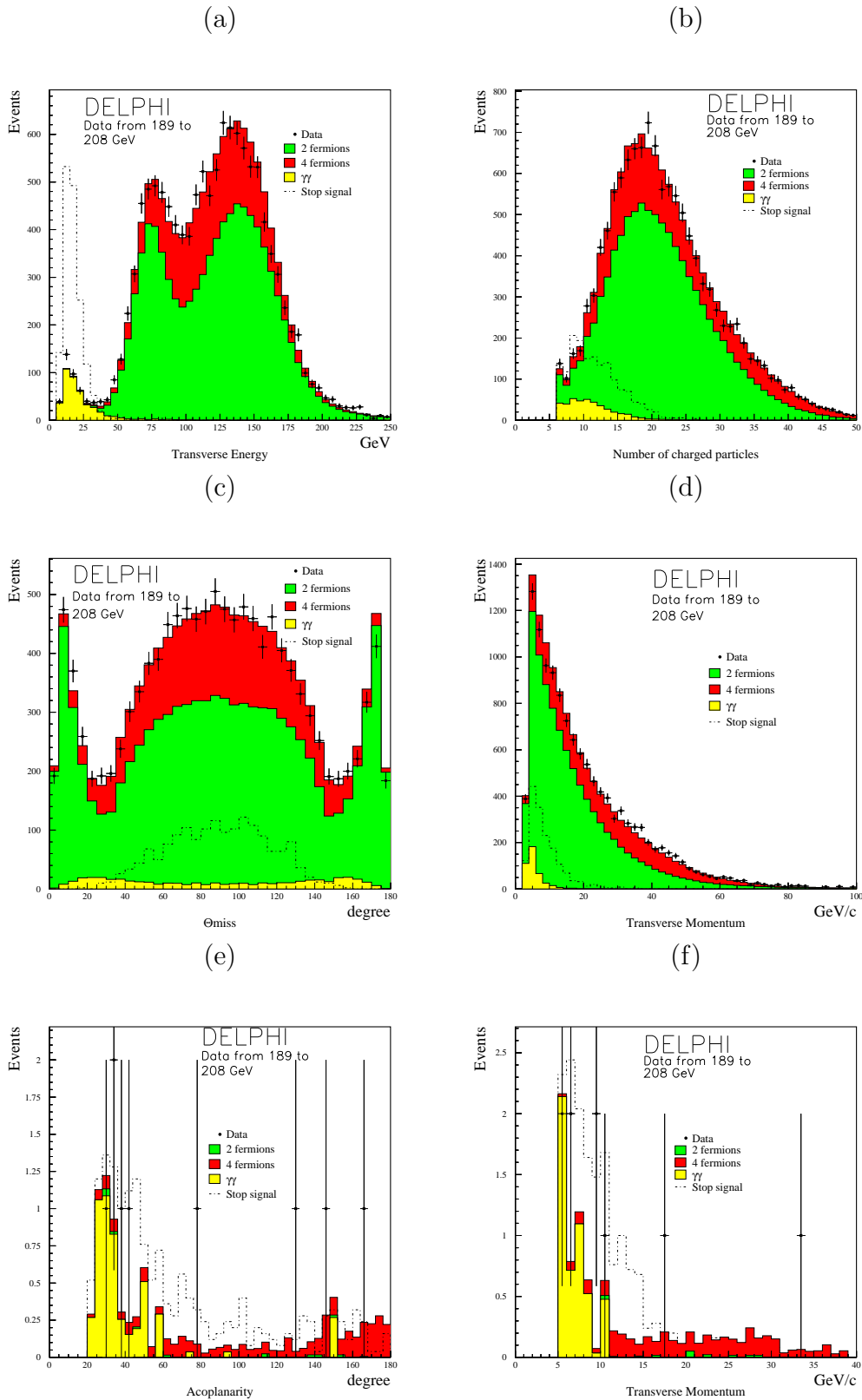
Figure 6: Comparison of data and simulation in the nearly degenerate squark analysis at preselection and final selection level. The distributions of (a) the total transverse energy, (b) total number of charged particles, (c) angle between the missing momentum and the beam axis and (d) transverse momentum are shown at preselection level. At the final selection level the distributions of (e) the acoplanarity and (f) the transverse momentum are shown. All DELPHI data from 189 to 208 GeV is included. A signal corresponding to $M_{\tilde{t}}$ =60 GeV/c^2 and ΔM =4 GeV/c^2 is also shown (with arbitrary normalisation at preselection level and normalised to a cross-section of 0.16 pb in (e) and (f)).
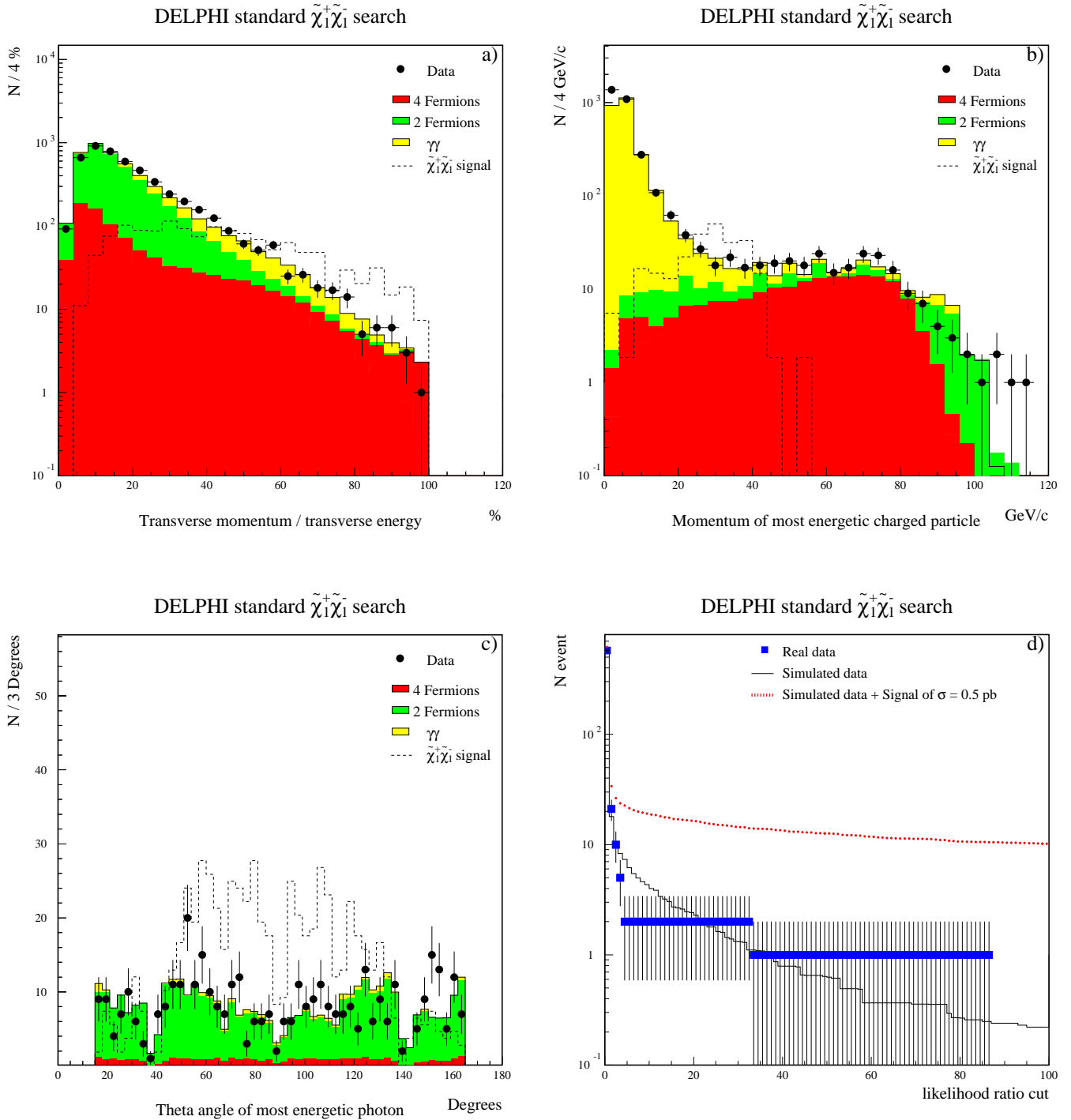
Figure 7: a), b) and c) show comparisons between real data (dots) and simulated background events (histogram) for the $jets$, $\ell\ell$ and rad topologies respectively, using a logical OR of the 6 preselection cut functions of the corresponding topology. The dashed lines indicate how a characteristic chargino signal would appear (arbitrary normalisation). d) shows the number of events selected by the standard chargino analysis as a function of the $\mathcal{L}_{\mathcal{R}_{CUT}}$ cut in the $jj\ell$ topology for $25 \leq \Delta M < 35$ GeV/c^2. The squares are the data and the solid line is the background simulation. The dotted curve shows a possible signal, $M_{\tilde{\chi}_1^\pm}$=102.8 GeV/c^2 $M_{\tilde{\chi}_1^0}$=73 GeV/c^2, of 0.5 pb. In all cases the data collected in the year 2000 with the TPC sector 6 on are shown.

Figure 8: a), b) and c) show comparisons between real data (dots) and simulated background events (histogram) for the $jets$, $\ell\ell$ and rad topologies respectively, using a logical OR of the 6 preselection cut functions of the corresponding topology. The dashed lines indicate how a characteristic chargino signal would appear (arbitrary normalisation). d) shows the number of events selected by the standard chargino analysis as a function of the $\mathcal{L}_{\mathcal{R}_{CUT}}$ cut in the $jj\ell$ topology for $25 \leq \Delta M < 35 \text{ GeV}/c^2$. The squares are the data and the solid line is the background simulation. The dotted curve shows a possible signal, $M_{\tilde{\chi}_1^\pm}=102.8 \text{ GeV}/c^2$ $M_{\tilde{\chi}_1^0}=73 \text{ GeV}/c^2$, of 0.5 pb. In all cases the data collected in the year 2000 with the TPC sector 6 off are shown.

DELPHI
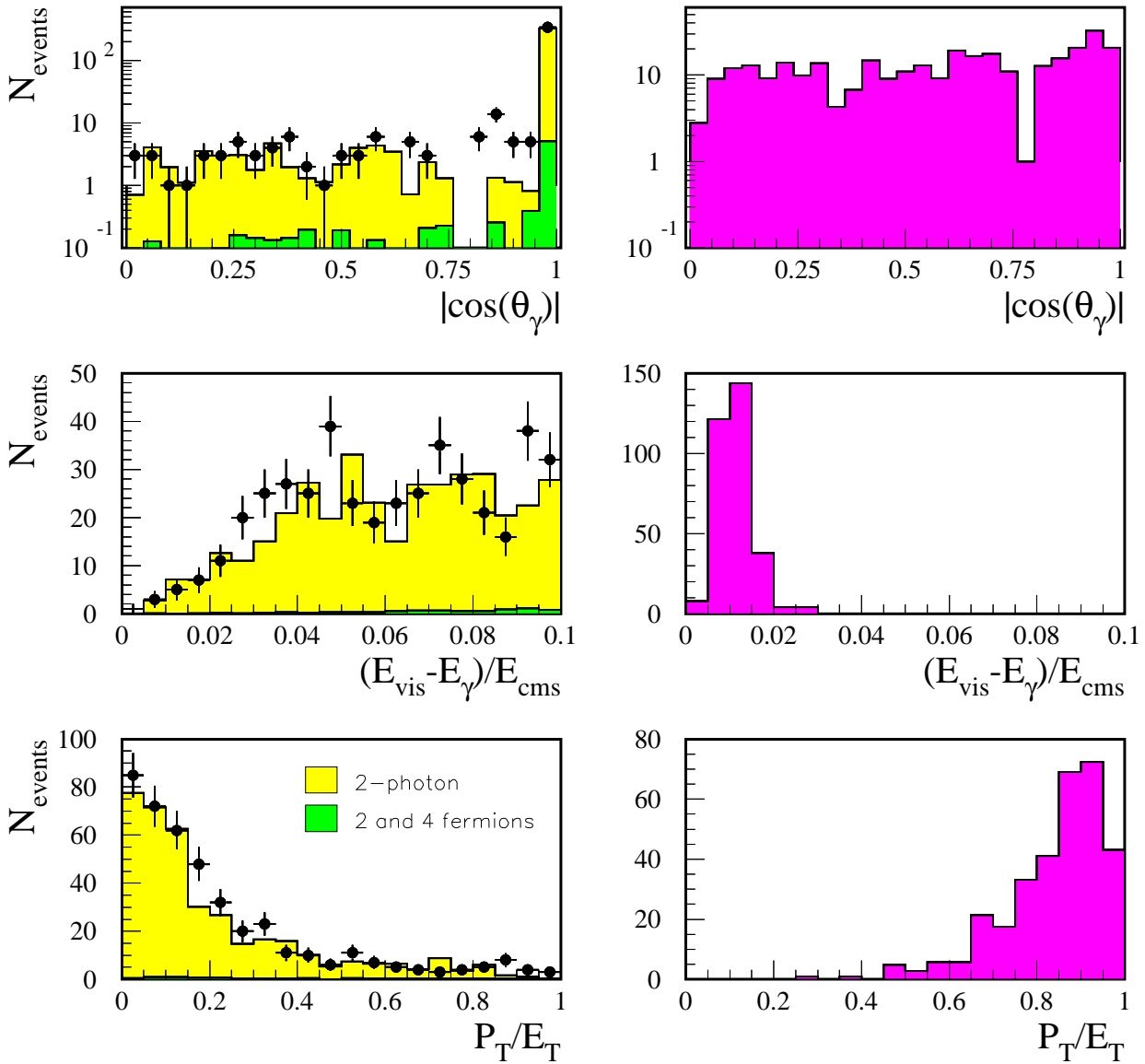
Figure 9: Some of the variables used in the selection for mass-degenerate charginos with an ISR photon tag. In the plots on the left the data (dots) are compared with the SM expectations. On the right, as an example, the corresponding distributions (with arbitrary normalisation) are shown for the signal with $M(\tilde{\chi}_1^+) = 80$ GeV/c^2 and $\Delta M = 1$ GeV/c^2.
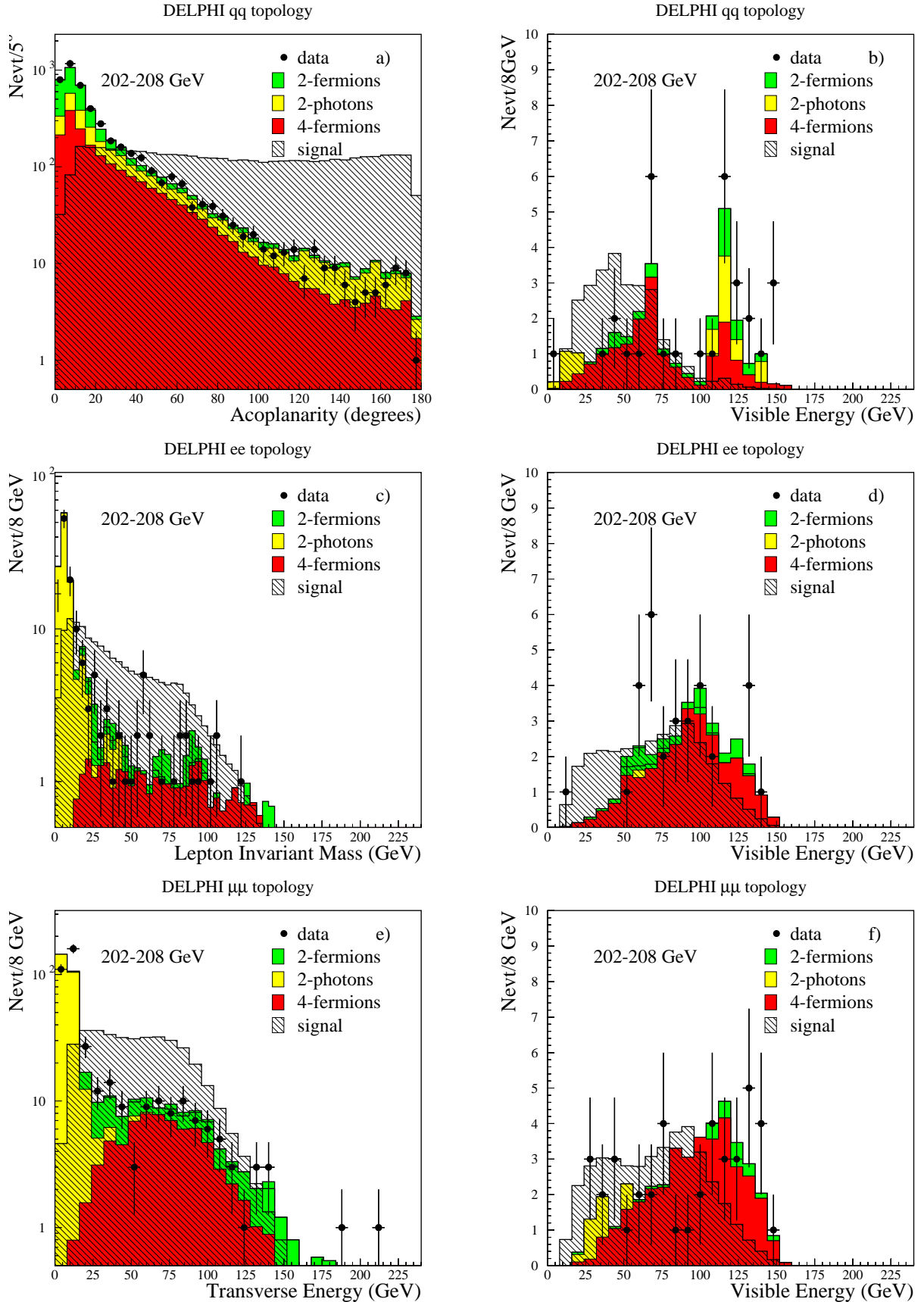
Figure 10: On the left the comparison between the real and simulated data is shown at preselection level for different variables for the q q̄, ee, and μμ topologies in the neutralino search. On the right the visible energy distribution is shown for the events selected at the final stage, after the likelihood selection. The signal distribution contains the contribution of all generated mass combinations and is arbitrarily normalised.
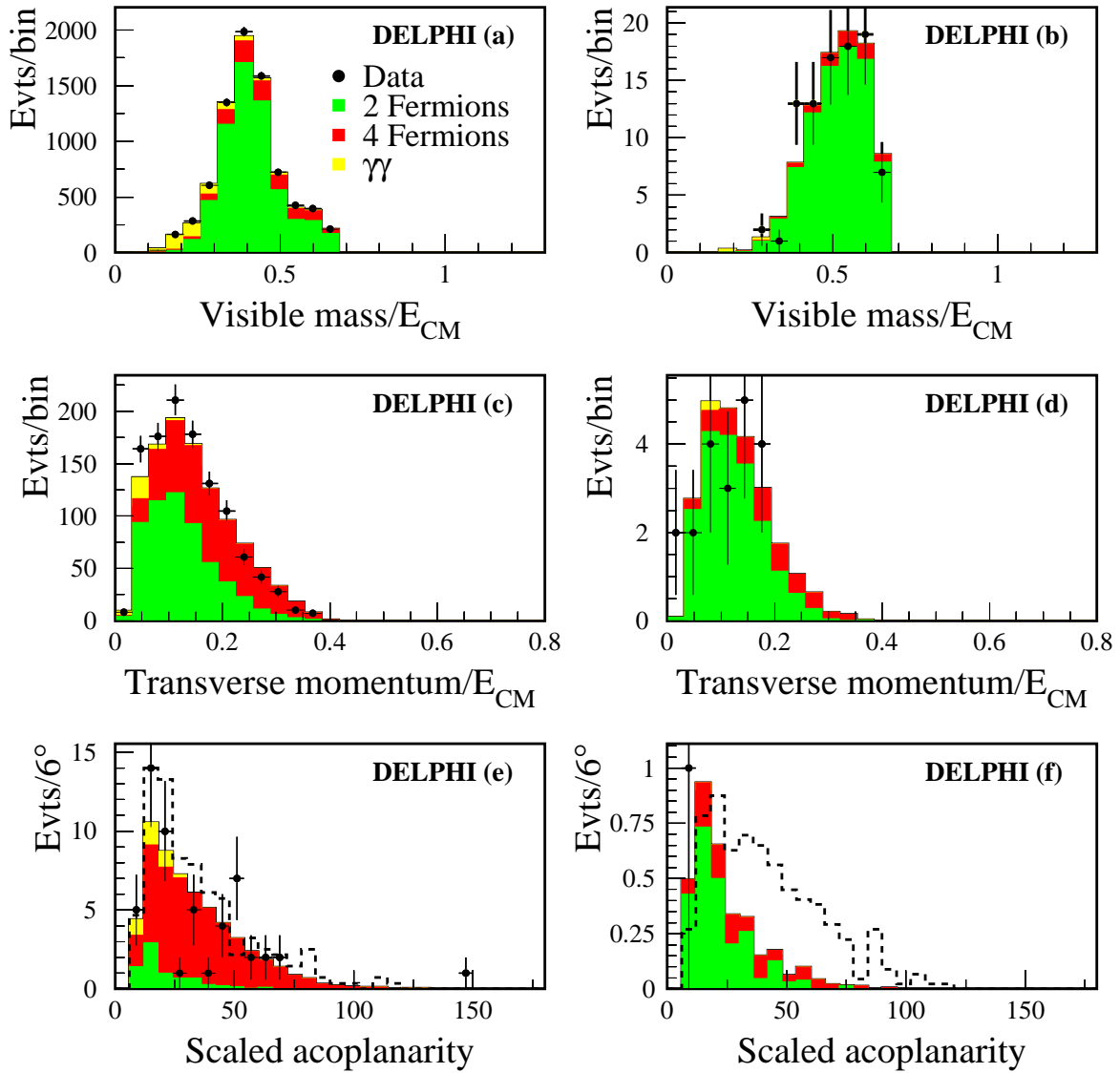
Figure 11: Comparison of real data from 1999 ($\sqrt{s}$ in the range 192–202 GeV) and simulation for the neutralino multijet selection without photons (a,c,e) and with photons (b,d,f), at the preselection (a,b), intermediate (c,d), and final selection (e,f) stages. The distributions expected for $\tilde{\chi}_3^0 \tilde{\chi}_2^0$ production with $\tilde{\chi}_3^0 \to \tilde{\chi}_2^0 q \bar{q}$ and $\tilde{\chi}_2^0$ decaying to $\tilde{\chi}_1^0 q \bar{q}$ or $\tilde{\chi}_1^0 \gamma$ are shown as dashed histograms where $M_{\tilde{\chi}_3^0} = 112$ GeV/c^2, $M_{\tilde{\chi}_2^0} = 75$ GeV/c^2 and $M_{\tilde{\chi}_1^0} = 41$ GeV/c^2. The signals are normalised to cross-sections of 0.8 pb (e) and 0.1 pb (f).
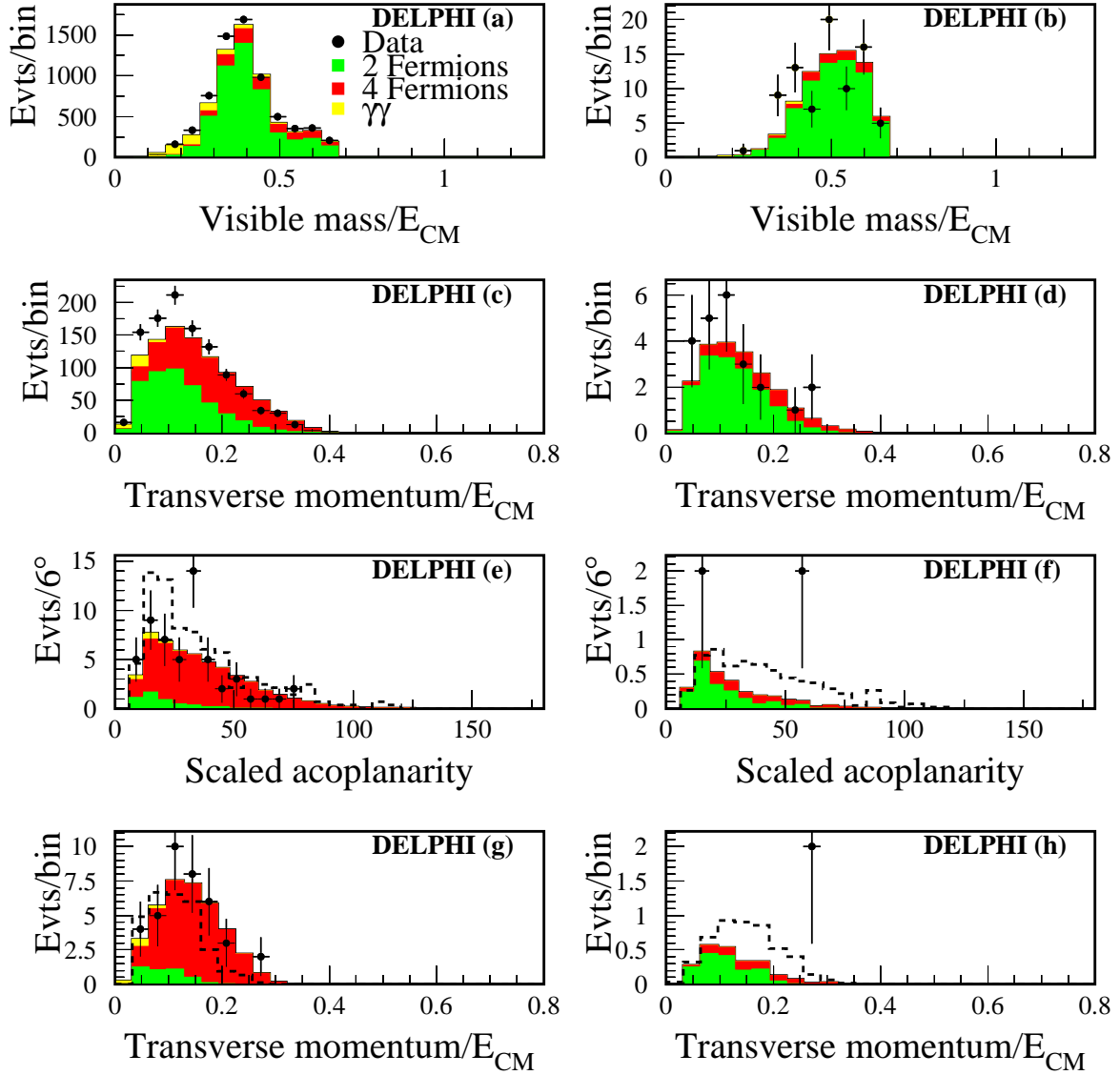
Figure 12: Comparison of real data from 2000 ($\sqrt{s}$ in the range 204–208 GeV) and simulation for the neutralino multijet selection without photons (a,c,e,g) and with photons (b,d,f,h), at the preselection (a,b),intermediate (c,d), and final selection(e,f,g,h) stages. In (g,h) only the data collected with the TPC sector 6 on are shown. The distributions expected for $\tilde{\chi}_3^0\tilde{\chi}_2^0$ production with $\tilde{\chi}_3^0 \to \tilde{\chi}_2^0 q\bar{q}$ and $\tilde{\chi}_2^0$ decaying to $\tilde{\chi}_1^0 q\bar{q}$ or $\tilde{\chi}_1^0\gamma$ are shown as dashed histograms where $M_{\tilde{\chi}_3^0}$=112 GeV/c^2, $M_{\tilde{\chi}_2^0}$=75 GeV/c^2 and $M_{\tilde{\chi}_1^0}$=41 GeV/c^2. The signals are normalised cross-sections of 0.8 pb (e), 0.1 pb (f,h) and 0.4 pb (g).
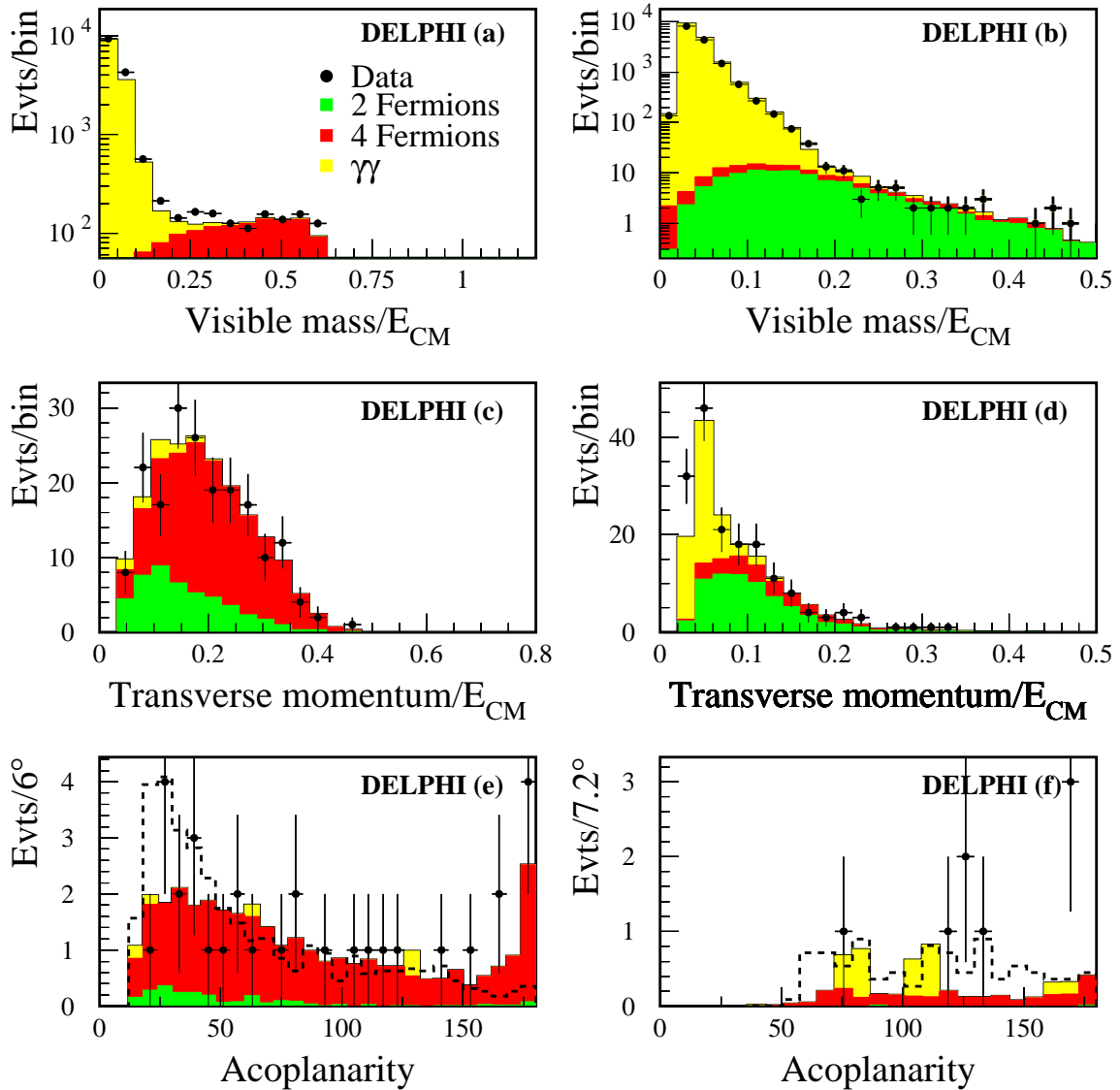
Figure 13: Comparison of real data from 1999 ($\sqrt{s}$ in the range 192–202 GeV) and simulation for the neutralino multilepton search (a,c,e) and asymmetric tau search (b,d,f), at the preselection (a,b), intermediate (c,d), and final selection (e,f) stages. The dashed line in (e) shows the multilepton signal expected for $\tilde{\chi}_3^0 \tilde{\chi}_2^0$ production with $\tilde{\chi}_3^0 \to \tilde{\chi}_2^0 \ell^+\ell^-$ and $\tilde{\chi}_2^0$ decaying to $\tilde{\chi}_1^0 \ell^+\ell^-$ where $M_{\tilde{\chi}_3^0}$=103 GeV/c^2, $M_{\tilde{\chi}_2^0}$=51 GeV/c^2 and $M_{\tilde{\chi}_1^0}$=45 GeV/c^2. In (f) the dashed line shows the tau cascade signal for $\tilde{\chi}_2^0 \tilde{\chi}_1^0$ production with $\tilde{\chi}_2^0 \to \tilde{\tau}\tau$ and $\tilde{\tau} \to \tilde{\chi}_1^0 \tau$ where $M_{\tilde{\chi}_2^0}$=75 GeV/c^2, $M_{\tilde{\tau}}$=44 GeV/c^2 and $M_{\tilde{\chi}_1^0}$=37.5 GeV/c^2. The signals are normalised to a cross-section of 0.4 pb.

Figure 14: Comparison of real data from 2000 ($\sqrt{s}$ in the range 204–208 GeV) and simulation for the neutralino multilepton search (a,c,e) and asymmetric tau search (b,d,f), at the preselection (a,b), intermediate (c,d), and final selection (e,f) stages. The dashed line in (e) shows the multilepton signal expected for $\tilde{\chi}_3^0 \tilde{\chi}_2^0$ production with $\tilde{\chi}_3^0 \to \tilde{\chi}_2^0 \ell^+ \ell^-$ and $\tilde{\chi}_2^0$ decaying to $\tilde{\chi}_1^0 \ell^+ \ell^-$ where $M_{\tilde{\chi}_3^0}=103$ GeV/c^2, $M_{\tilde{\chi}_2^0}=51$ GeV/c^2 and $M_{\tilde{\chi}_1^0}=45$ GeV/c^2. In (f) the dashed line shows the tau cascade signal for $\tilde{\chi}_2^0 \tilde{\chi}_1^0$ production with $\tilde{\chi}_2^0 \to \tilde{\tau}\tau$ and $\tilde{\tau} \to \tilde{\chi}_1^0 \tau$ where $M_{\tilde{\chi}_2^0}=75$ GeV/c^2, $M_{\tilde{\tau}}=44$ GeV/c^2 and $M_{\tilde{\chi}_1^0}=37.5$ GeV/c^2. The signals are normalised to a cross-section of 0.4 pb.

Figure 15: 95% CL exclusion region in the ($M_{\tilde{e}_R}$ M_{LSP}) plane. The solid line shows the expected limit and the shaded region shows the obtained exclusion limit. The cross-section and the branching ratios for each mass point were determined with the SUSY parameters $\tan \beta{=}1.5$ and $\mu = -200\,\mathrm{GeV}/c^2$ (for a discussion on the low selectron mass region see section 6.3).
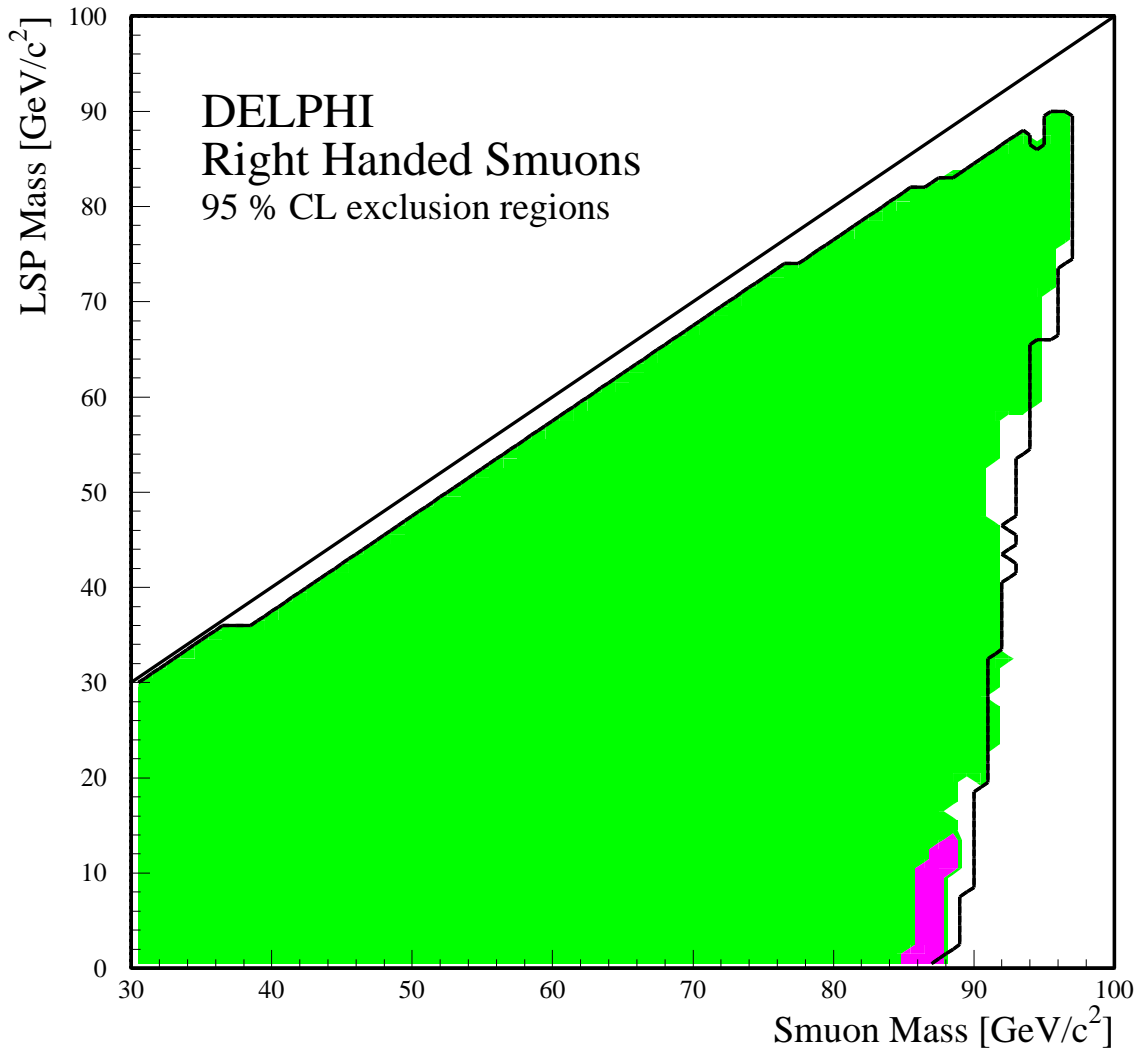
Figure 16: 95% CL exclusion region in the $(M_{\tilde{\mu}_R}\ M_{LSP})$ plane. The solid line shows the expected limit and the shaded region shows the obtained exclusion limit. The lighter shaded region is excluded taking the branching ratios for each mass point with the SUSY parameters $\tan\beta$=1.5 and $\mu=-200\,\mathrm{GeV}/c^2$. If the branching ratio of $\tilde{\mu}\rightarrow\mu\chi_1^0$ is set to 1, the darker shaded region is also excluded (for a discussion on the low smuon mass region see section 6.3).
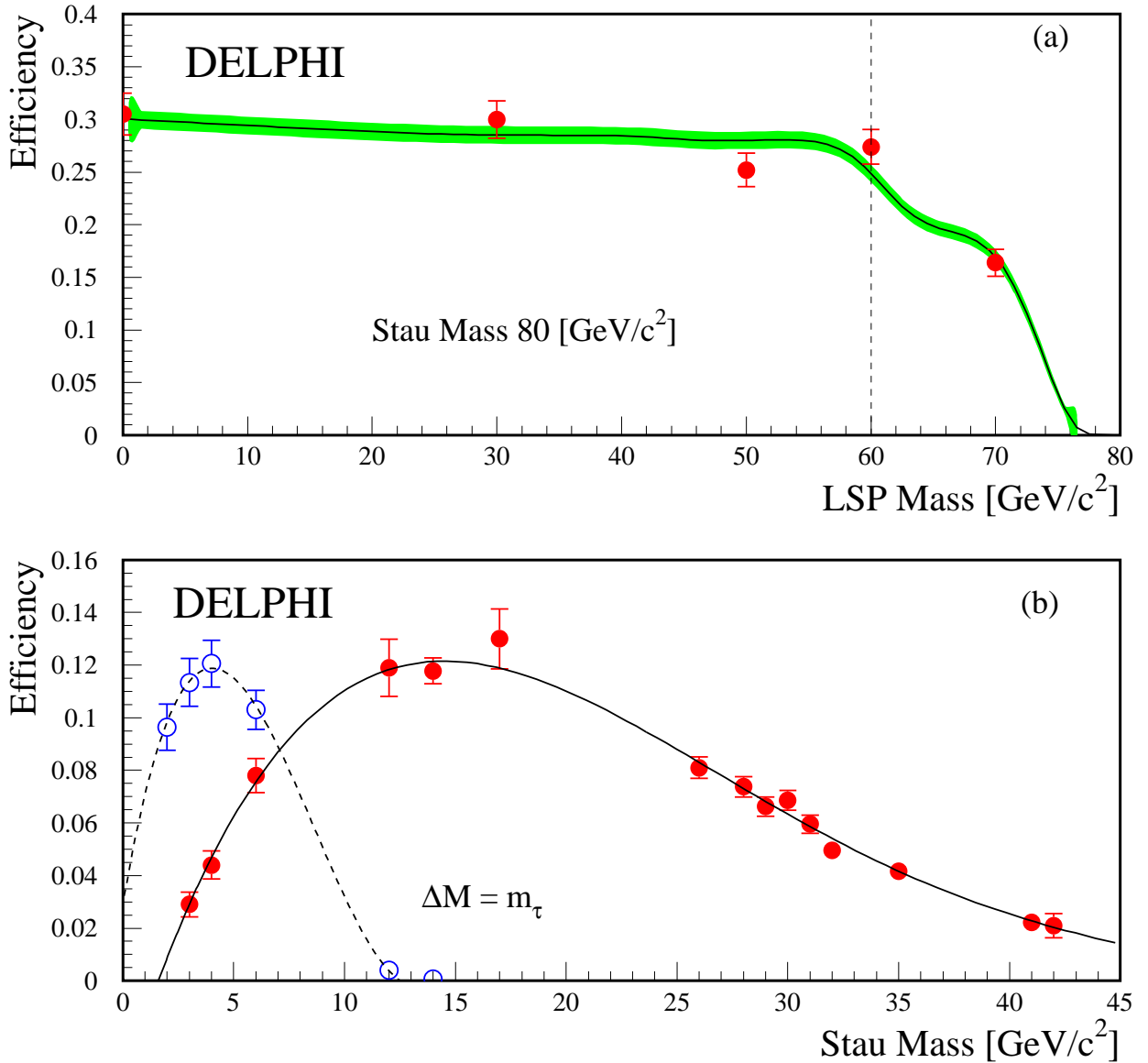
Figure 17: The selection efficiency in the stau analysis. The plots show: (a) Efficiency as a function of M_{LSP} at $M_{\tilde{\tau}} = 80$ GeV/c^2. The line shows the result of the fast simulation, and the points with error bars show the result of the full simulation. The shaded area indicates the statistical uncertainty of the estimate, and the vertical line shows the position of the transition between the two ΔM-regions. (b) Efficiency as a function of $M_{\tilde{\tau}}$ at $\Delta M = m_\tau$ for the low mass analysis (filled circles) and the very low mass analysis (open circles). The points show the results of the full simulation. The lines are polynomial fits to the points.
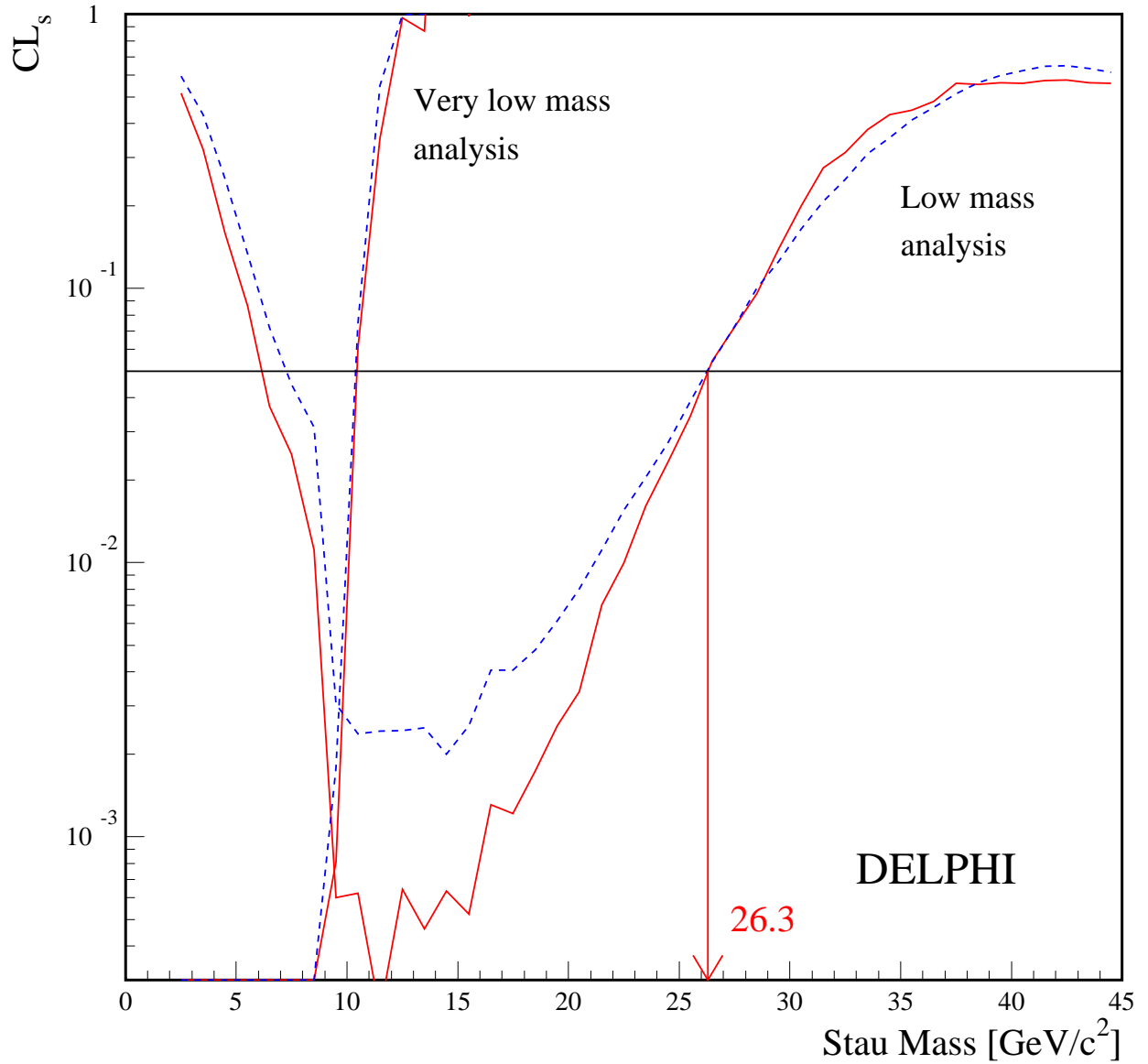
Figure 18: The value of CL_s versus $M_{\tilde{\tau}}$ obtained for the minimal $\tilde{\tau}$ pair-production cross-section, and $\Delta M = m_{\tau}$, which corresponds to the weakest limit. The solid curve shows the obtained CL_s, and the dashed line shows the corresponding expected value. The two sets of curves correspond to the "very low mass analysis" and the "low mass analysis", as indicated in the figure.
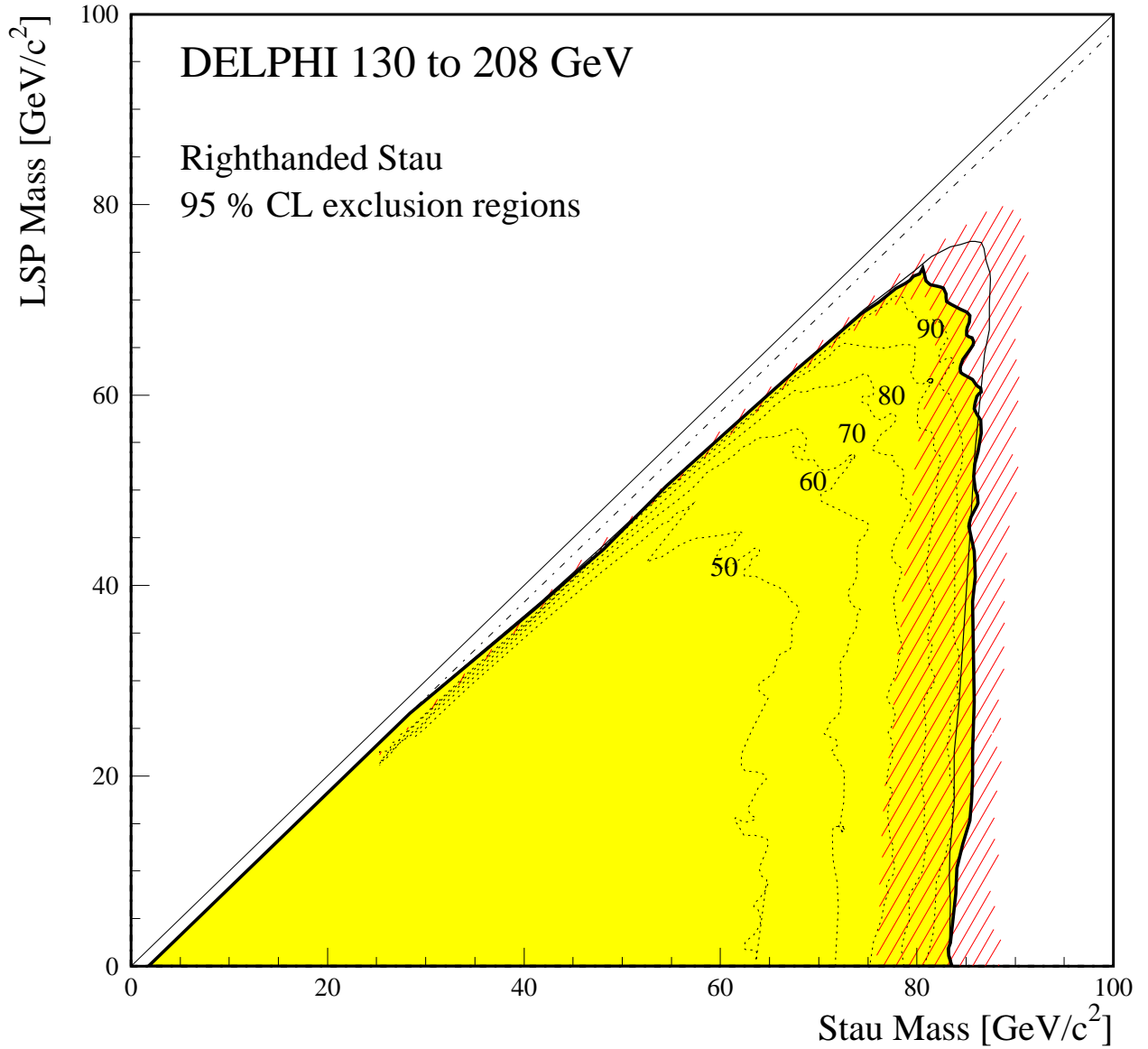
Figure 19: 95% CL exclusion region in the $(M_{\tilde{\tau}_R}, M_{LSP})$ plane. The shaded region shows the exclusion limit obtained if $\tilde{\tau} \to \tau$ LSP is the only allowed channel, and the thin solid line shows the corresponding expected limit. The dotted lines show the seen exclusion regions obtained if the branching-ratio of $\tilde{\tau} \to \tau$ LSP has the values indicated in percent next to the lines, and it is assumed that the analysis has no sensitivity to other decay-modes. The dash-dotted line indicates $\Delta M = m_\tau$. The observed limit is everywhere within the 90% CL band for the expected limit shown as the hatched area.
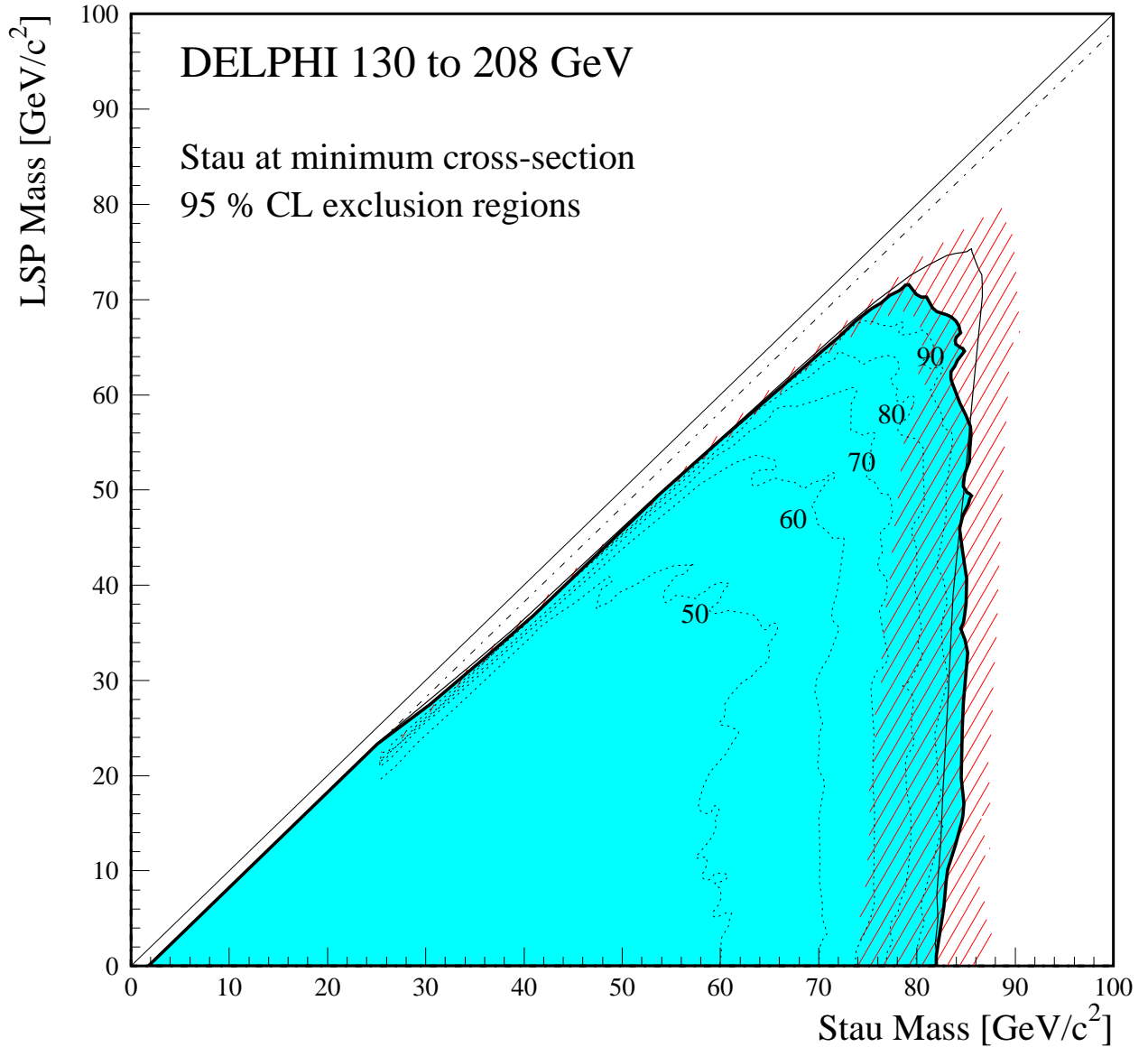
Figure 20: 95% CL exclusion region in the ($M_{\tilde{\tau}}$, M_{LSP}) plane obtained for the minimal $\tilde{\tau}$ pair-production cross-section. The shaded region shows the exclusion limit obtained if $\tilde{\tau} \to \tau$ LSP is the only allowed channel, and the thin solid line shows the corresponding expected limit. The dotted lines show the seen exclusion regions obtained if the branching-ratio of $\tilde{\tau} \to \tau$ LSP has the values indicated in percent next to the lines, and it is assumed that the analysis has no sensitivity to other decay-modes. The dash-dotted line indicates $\Delta M = m_{\tau}$. The observed limit is everywhere within the 90% CL band for the expected limit shown as the hatched area.
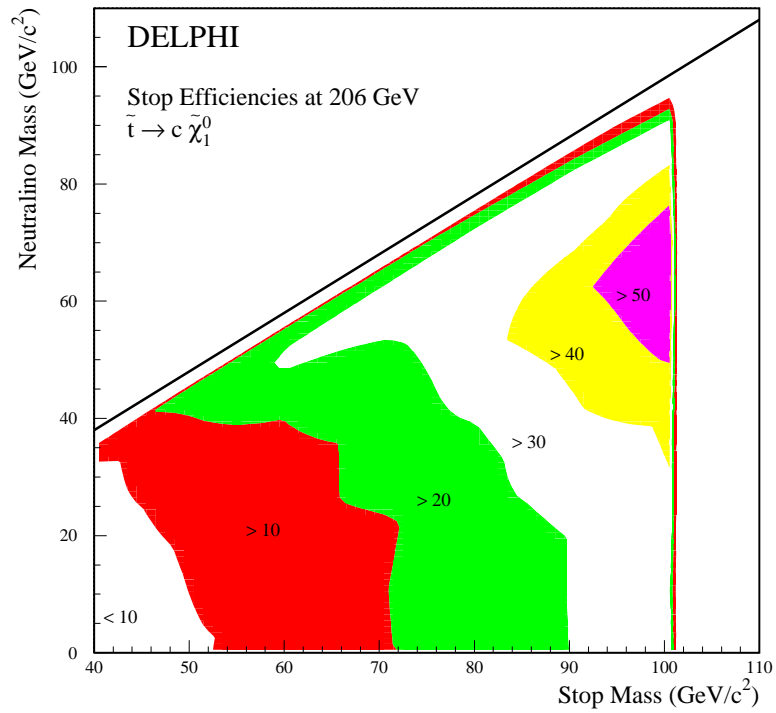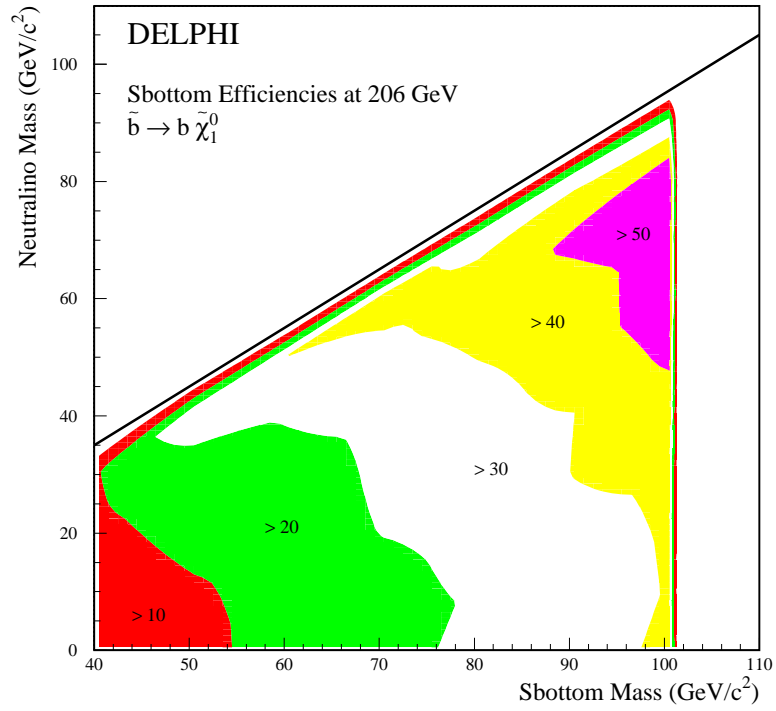
Figure 21: Squark signal detection efficiencies (in %) in the plane $(M_{\tilde{q}_1}, M_{\tilde{\chi}_1^0})$ in the non-degenerate scenario.

DELPHI; Stop efficiencies at 189 GeV

DELPHI; Stop efficiencies at 206 GeV
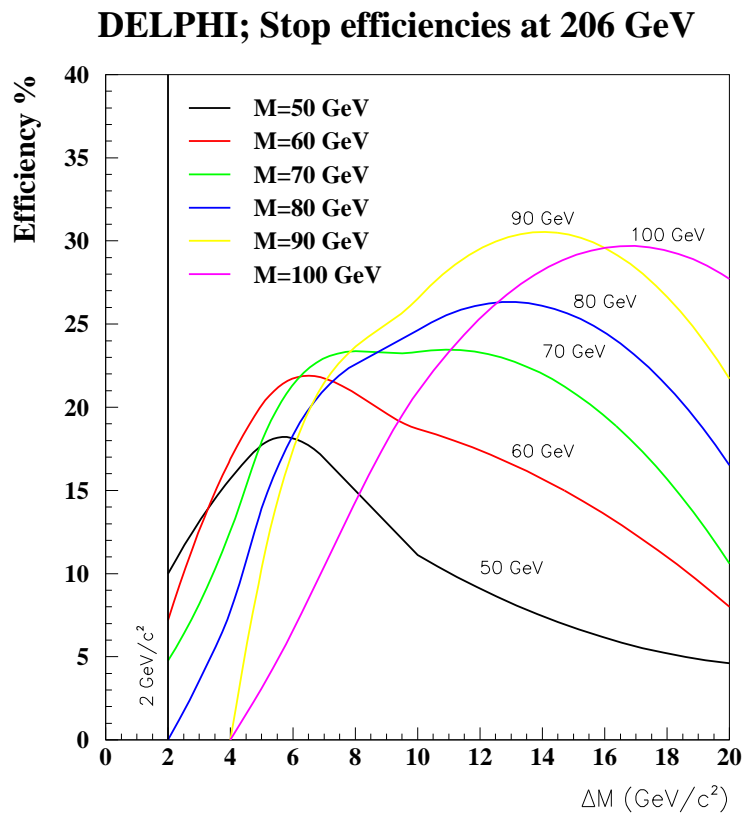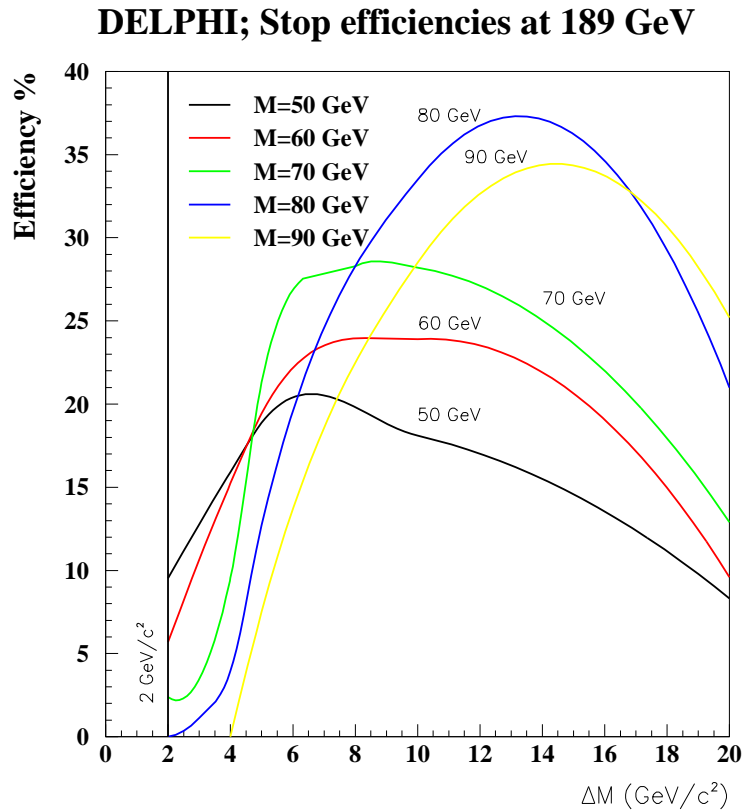
Figure 22: Signal efficiency of the stop search in the nearly degenerate scenario for different mass hypothesis as a function of $\Delta M = M_{\tilde{t}_1} - M_{\tilde{\chi}_1^0}$, for $\sqrt{s}$=189 and 206 GeV.
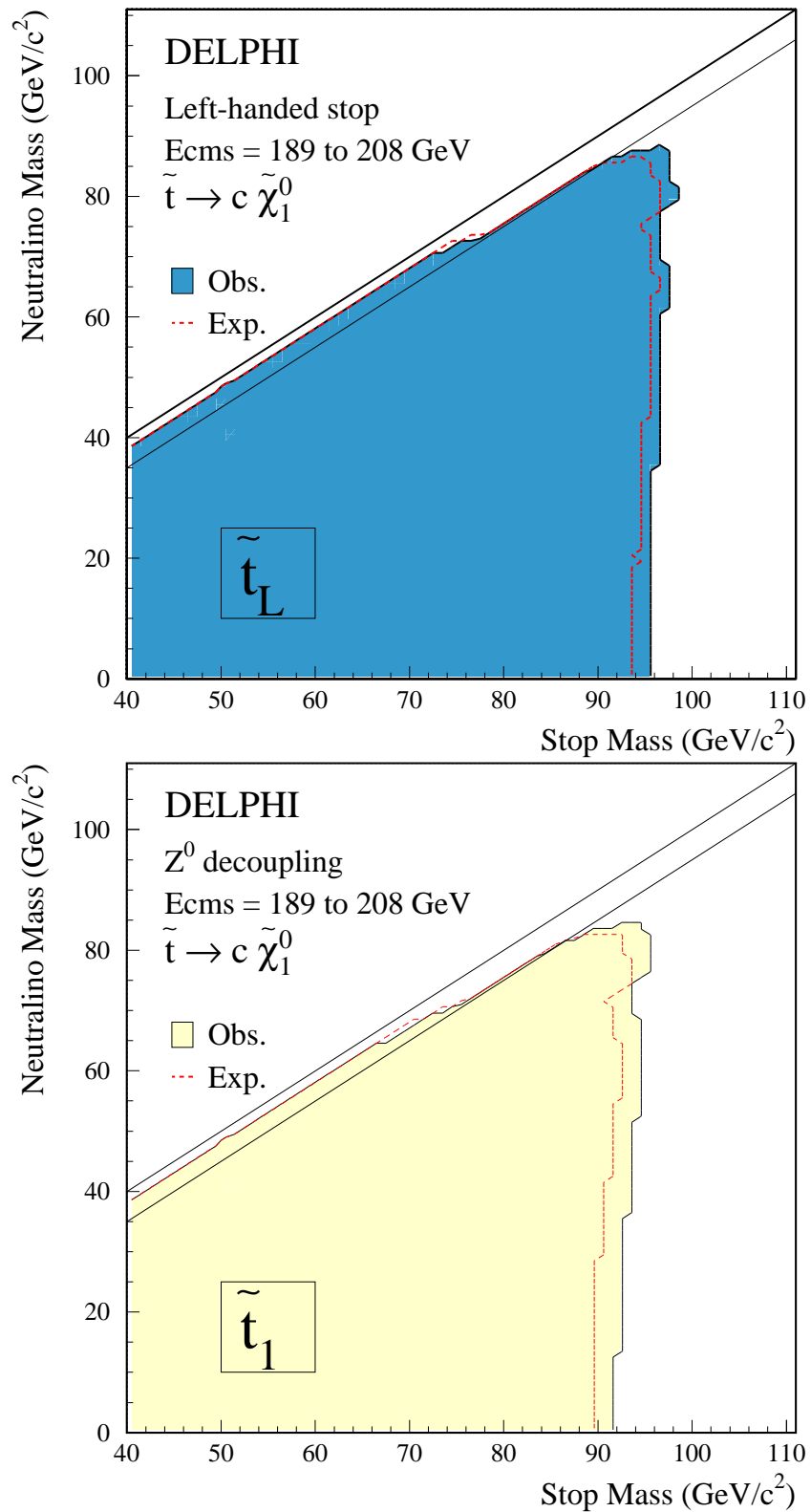
Figure 23: Excluded regions at 95% confidence level for the stop search in the plane $(M_{\tilde{t}_1}, M_{\tilde{\chi}_1^0})$ for purely left handed stops (top) and for the states at the Z decoupling (bottom). The shaded areas show the observed excluded regions and the lines correspond to the expected exclusions (for a discussion on the low stop mass region see section 6.3).
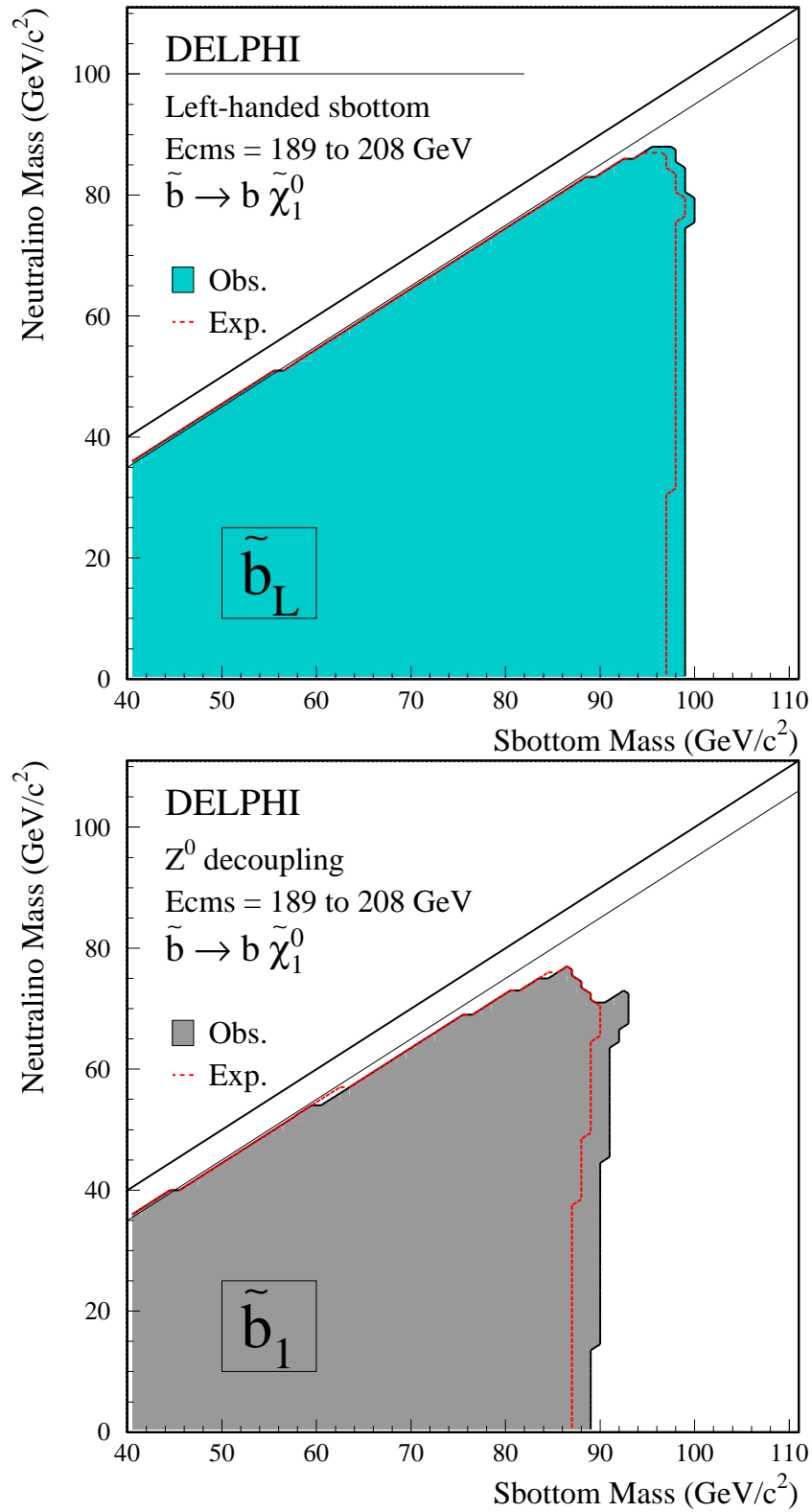
Figure 24: Excluded regions at 95% confidence level for the sbottom search in the plane $(M_{\tilde{b}_1}, M_{\tilde{\chi}_1^0})$ for purely left handed sbottoms (top) and for the states at the Z decoupling (bottom). The shaded areas show the observed excluded regions and the lines correspond to the expected exclusions (for a discussion on the low sbottom mass region see section 6.3).

DELPHI 189 to 208 GeV at 95% CL

DELPHI 189 to 208 GeV at 95% CL
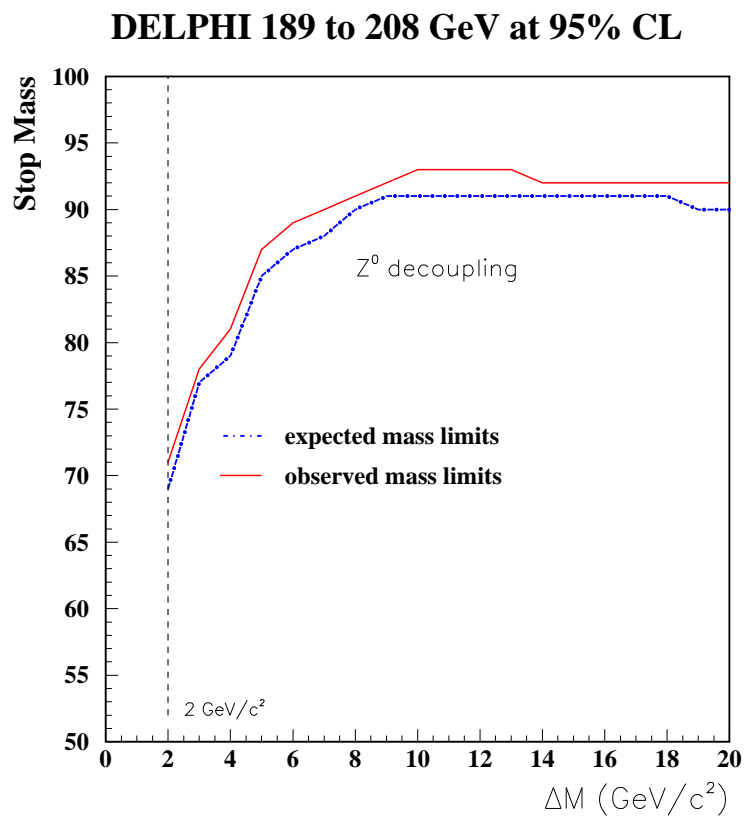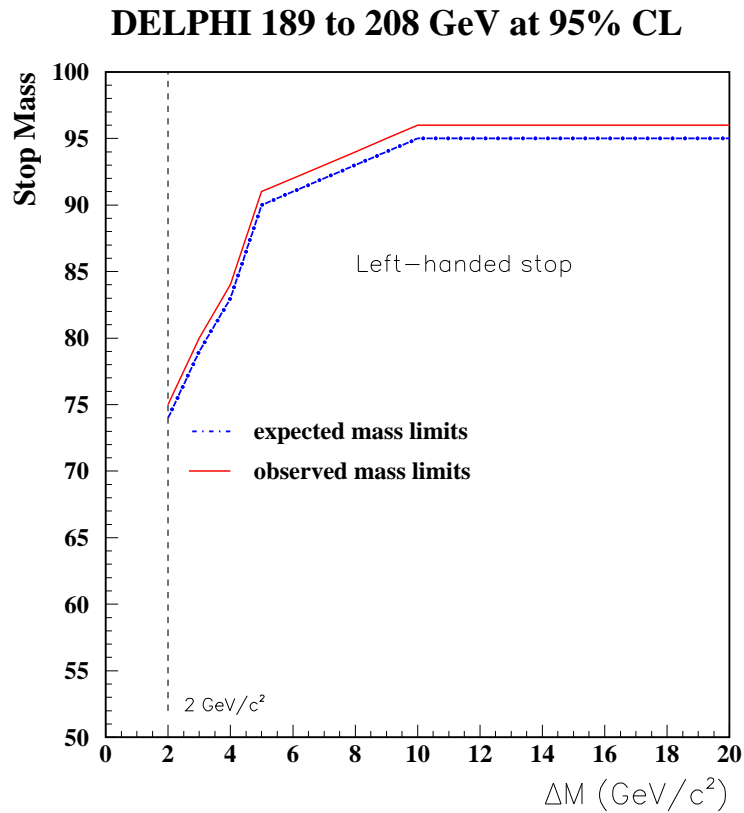
Figure 25: Stop mass limit as a function of ΔM for a purely left-handed stop and for the stop mixing angle which minimises the cross-section.

DELPHI $\tilde{\chi}_1^+\tilde{\chi}_1^-$ efficiencies at 206 GeV
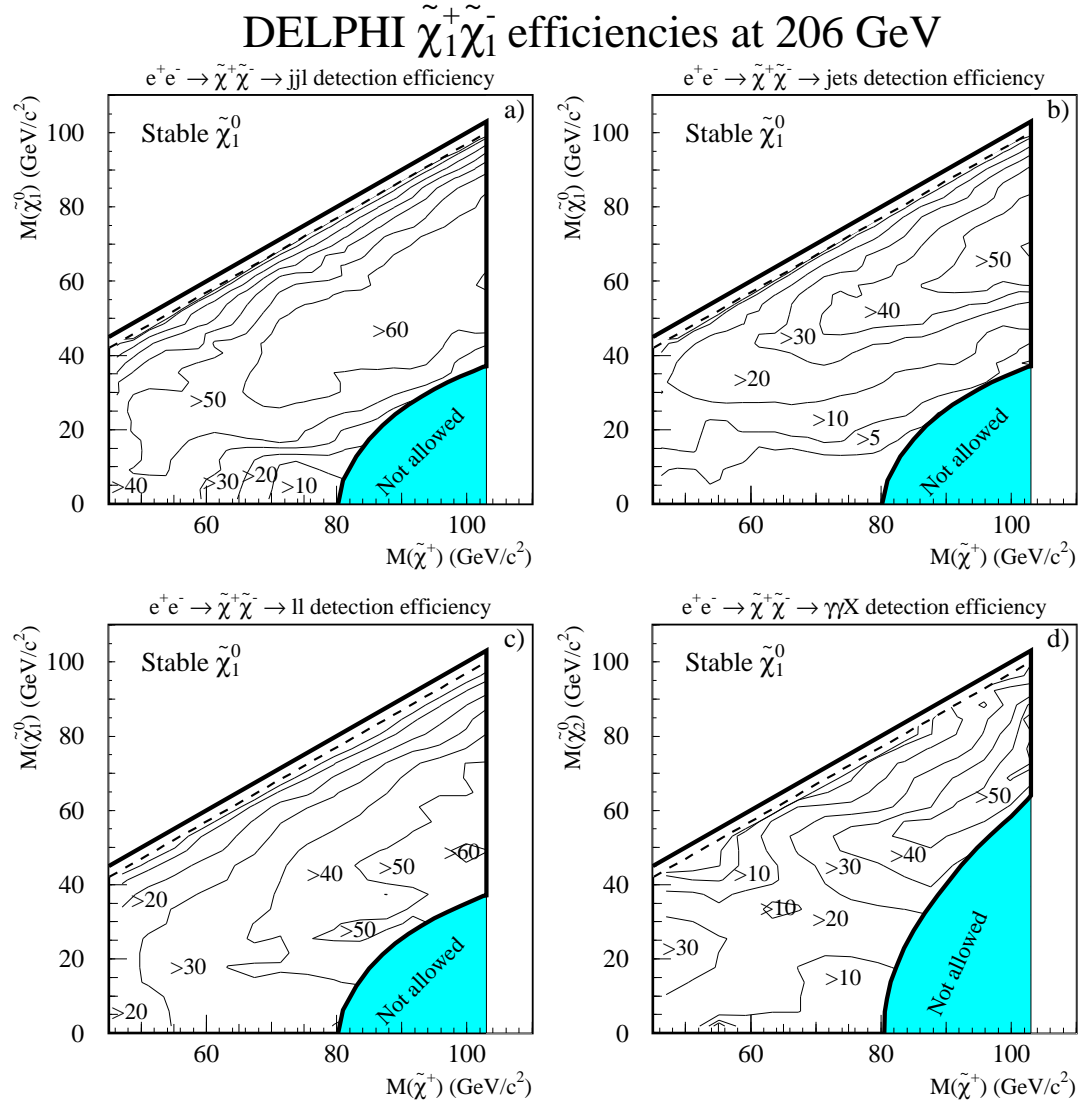
Figure 26: Chargino pair production detection efficiencies (%) for the four decay channels a) $jj\ell$, b) *jets*, c) $\ell\ell$ and d) *rad*, at 206 GeV in the $(M_{\tilde{\chi}^\pm}, M_{\tilde{\chi}^0})$ plane. TPC sector 6 on and a stable $\tilde{\chi}_1^0$ are assumed. The shaded areas are disallowed in the MSSM scheme.

DELPHI $\tilde{\chi}_1^+\tilde{\chi}_1^-$ efficiencies at 206.5 GeV
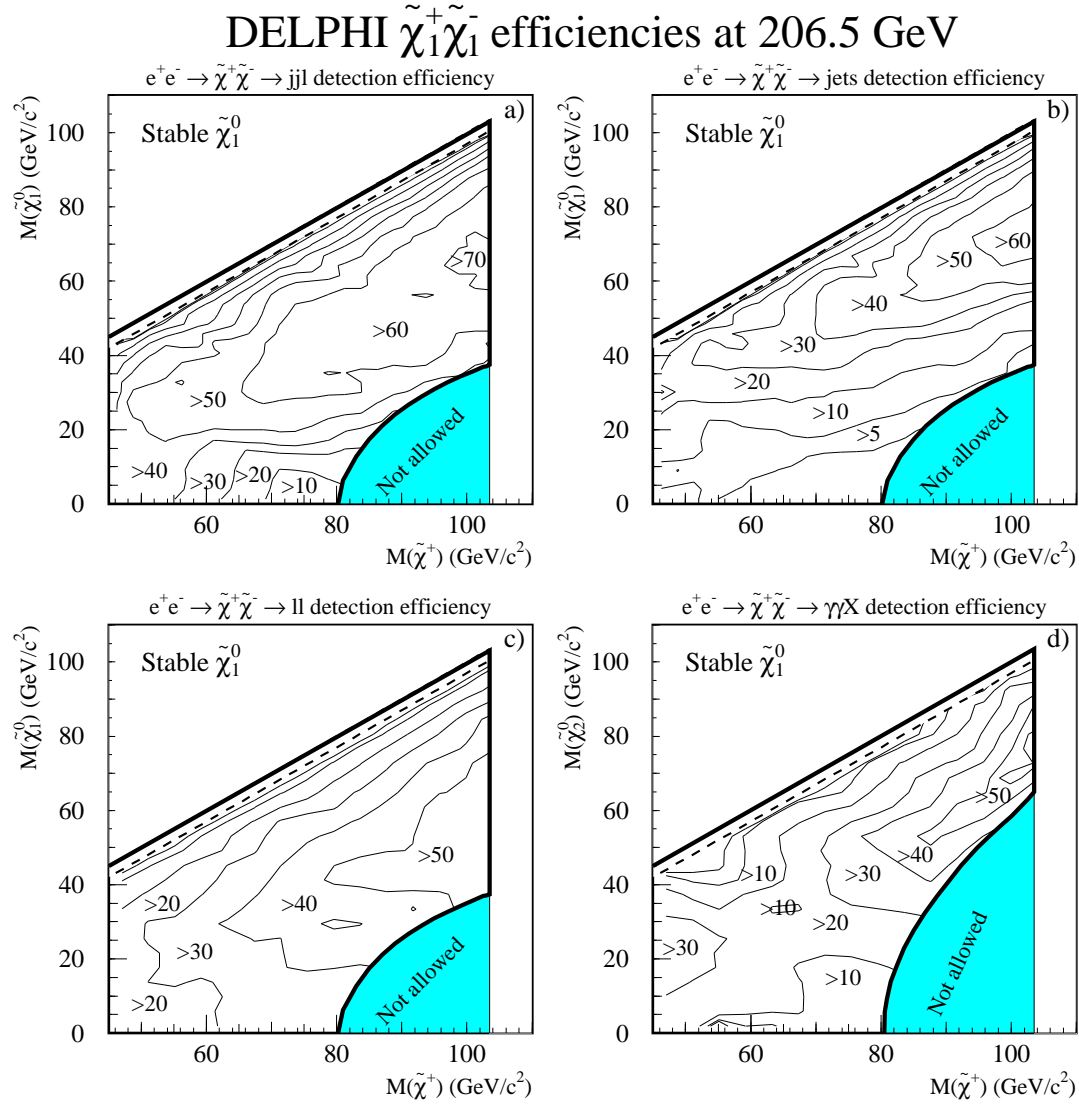
Figure 27: Chargino pair production detection efficiencies (%) for the four decay channels a) $jj\ell$, b) *jets*, c) $\ell\ell$ and d) *rad*, at 206.5 GeV in the $(M_{\tilde{\chi}^\pm}, M_{\tilde{\chi}^0})$ plane. TPC sector 6 off and a stable $\tilde{\chi}_1^0$ are assumed. The shaded areas are disallowed in the MSSM scheme.

DELPHI $\tilde{\chi}_1^+\tilde{\chi}_1^-$ cross-section limits
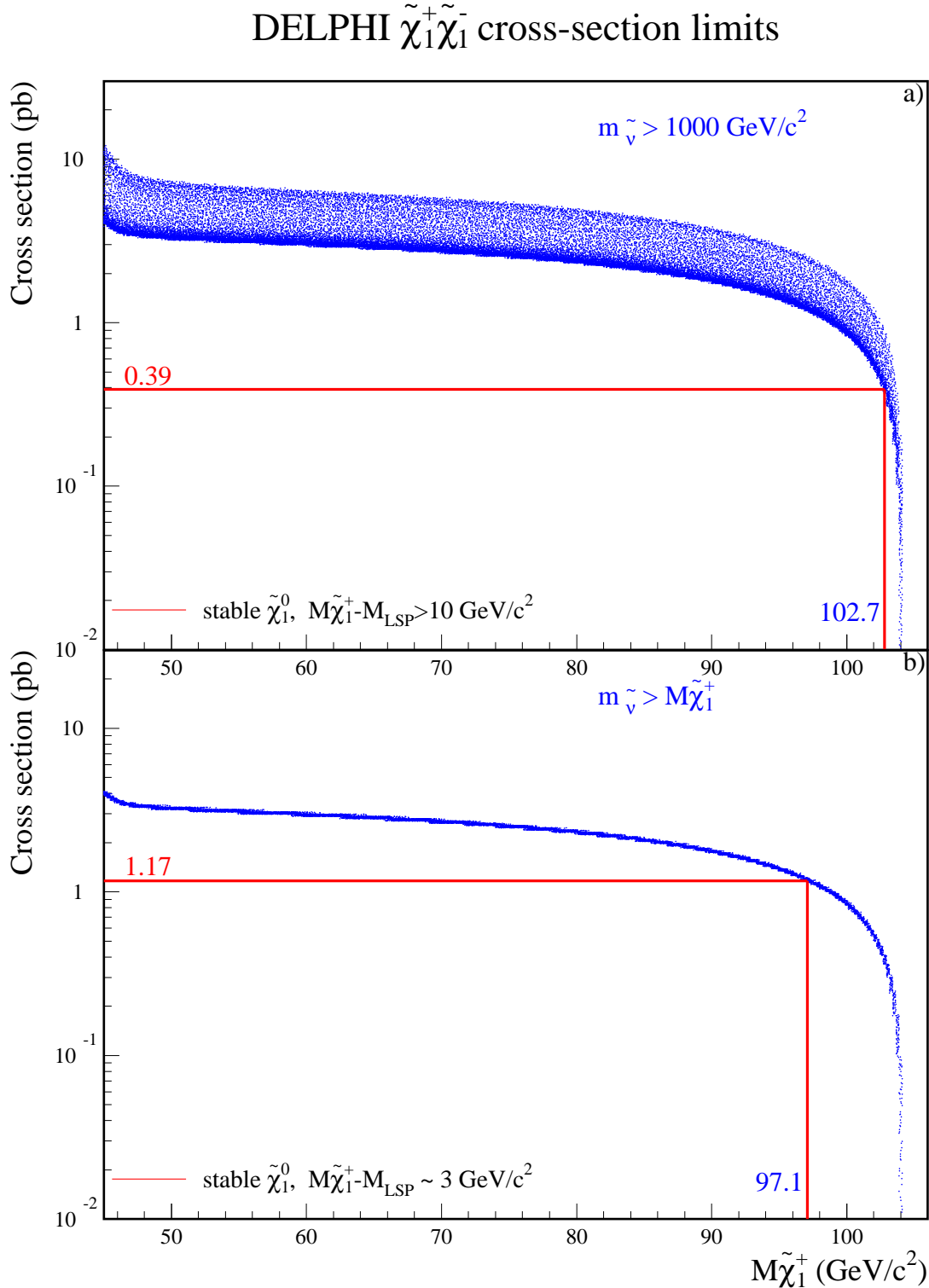
Figure 28: Expected cross-sections in pb at 208 GeV (dots) versus the chargino mass in a) for $\Delta M > 10$ GeV/c^2 and b) for $\Delta M \sim 3$ GeV/c^2. The spread in the dots originates from the random scan over the parameters μ and M_2. A heavy sneutrino ($m_{\tilde{\nu}} > 1000$ GeV/c^2) has been assumed in a) and $m_{\tilde{\nu}} > M_{\tilde{\chi}_1^\pm}$ in b). The minimal cross-sections below the mass limits are indicated by the horizontal lines.
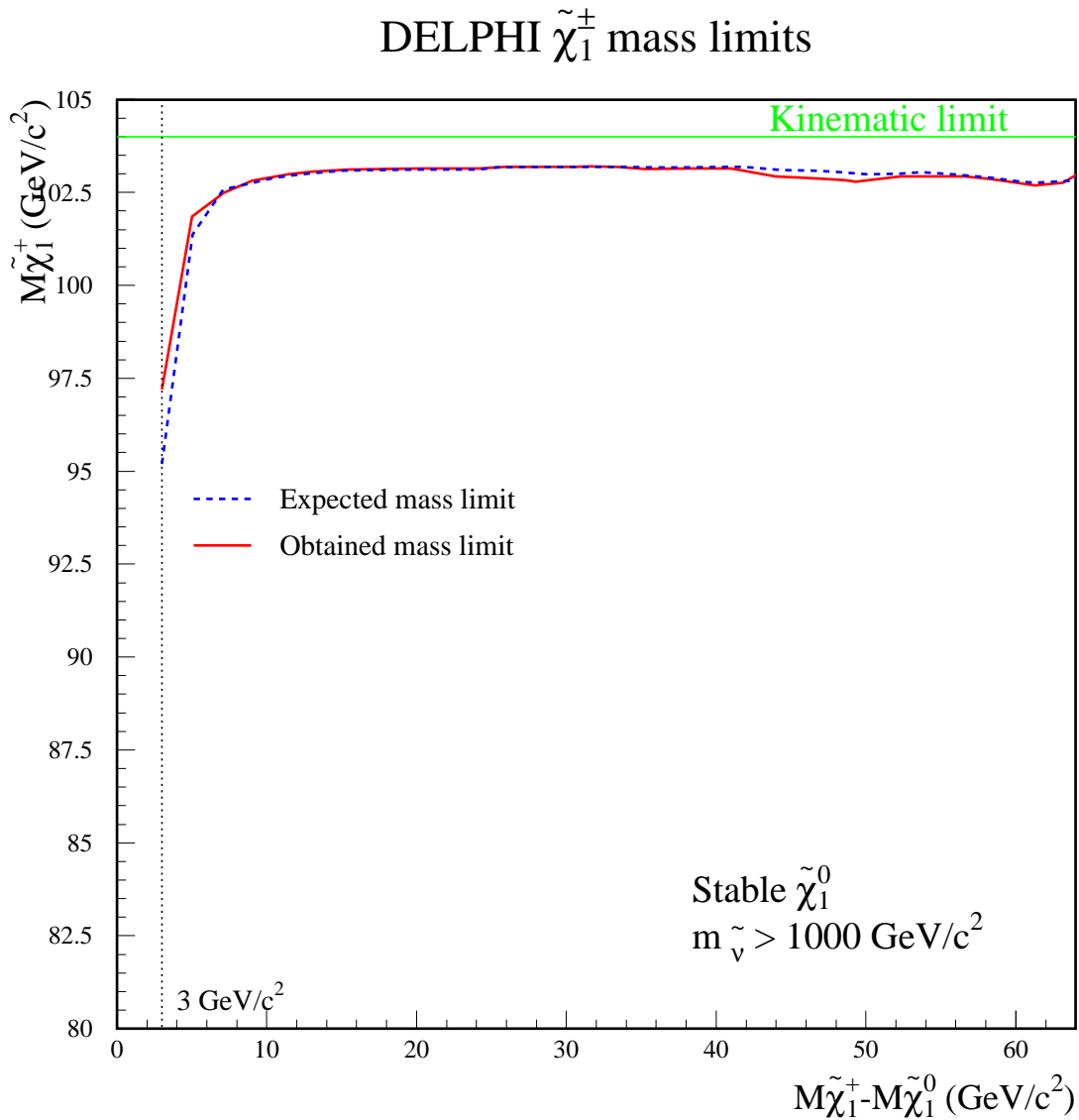
Figure 29: The chargino mass limit as function of the ΔM value under the assumption of a heavy sneutrino. The limit applies to the case of a stable $\tilde{\chi}_1^0$. The straight horizontal line shows the kinematic limit.

DELPHI $\tilde{\chi}_1^\pm$ mass limits
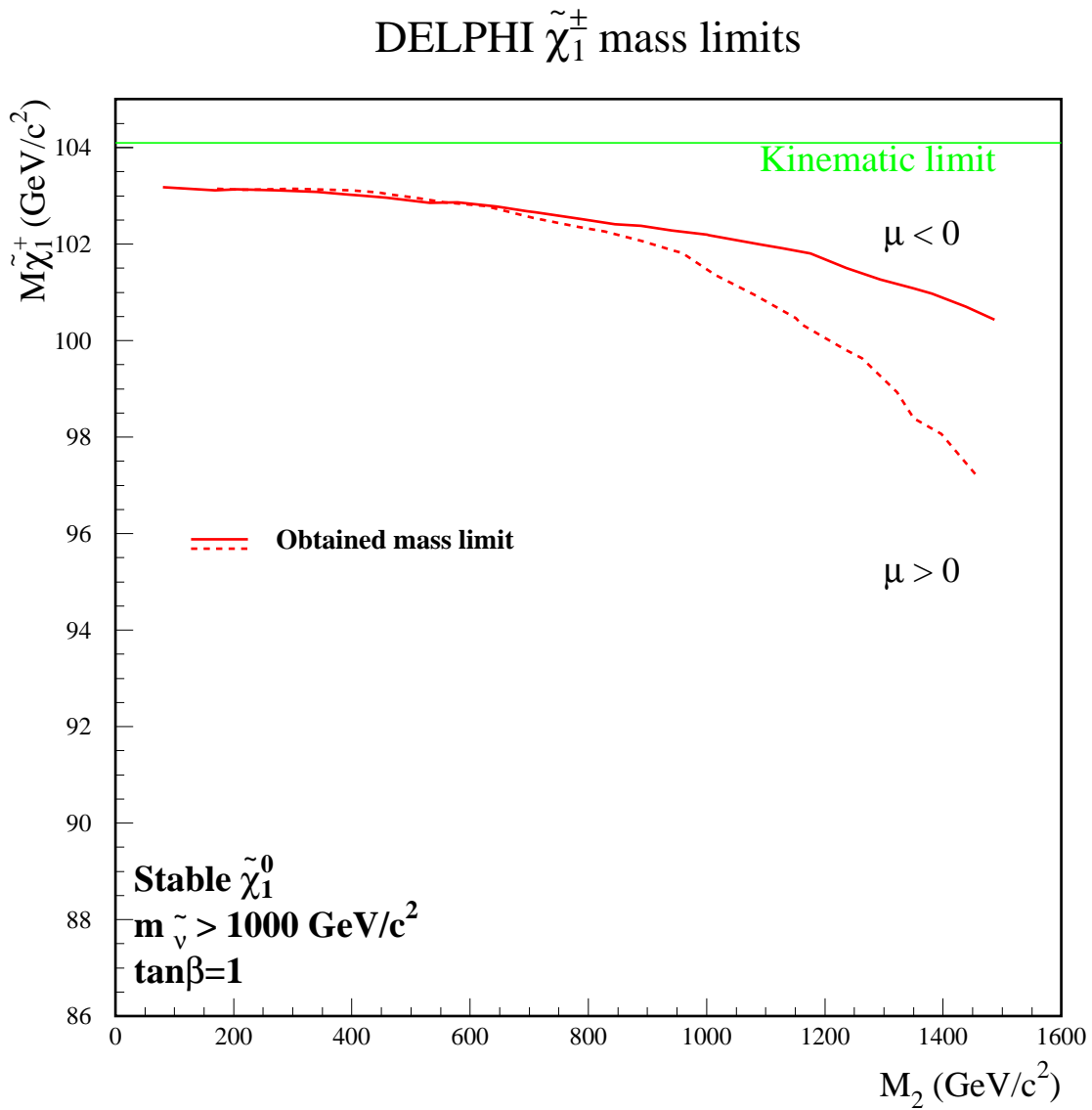
Figure 30: The chargino mass limit as function of M_2 for $\tan \beta = 1$, under the assumption of a heavy sneutrino. The straight horizontal line shows the kinematic limit of the chargino production. The limit applies in the case of a stable $\tilde{\chi}_1^0$.
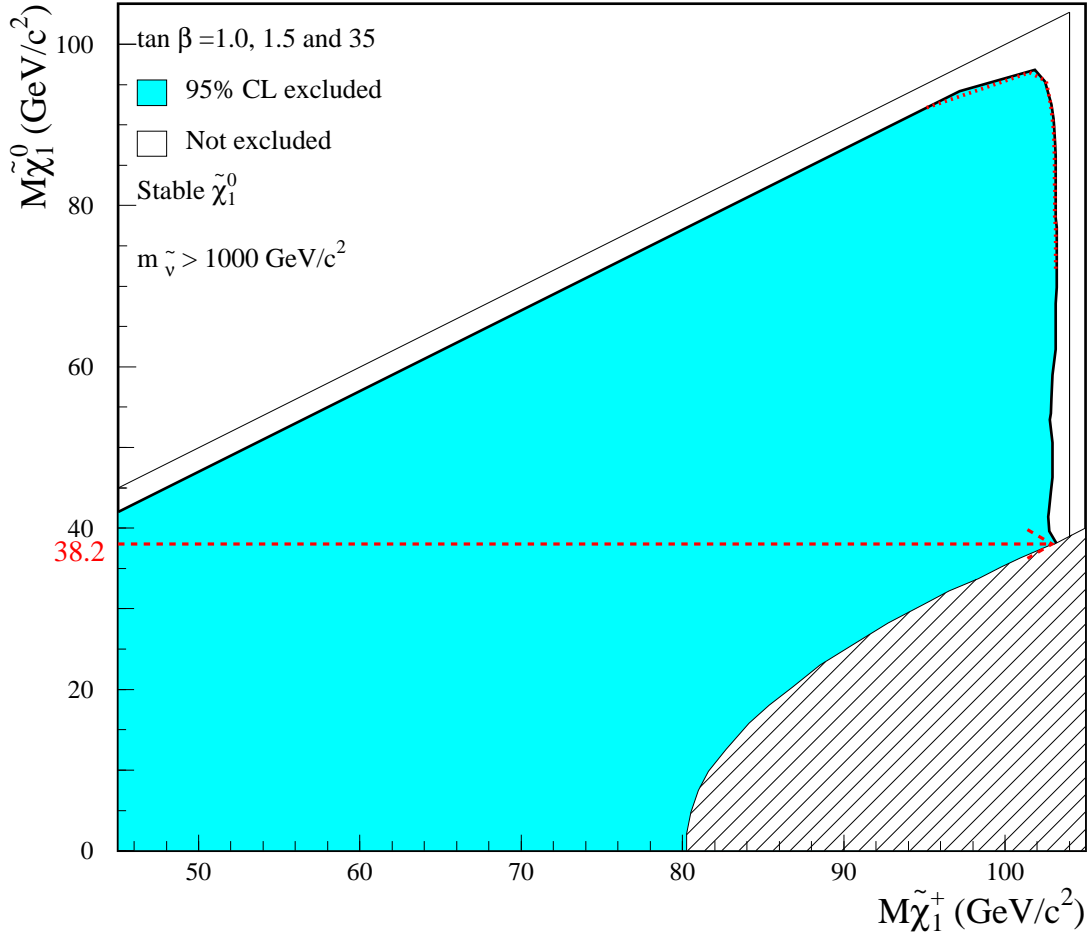
Figure 31: Region excluded at 95% confidence level in the plane of the mass of the lightest neutralino versus that of the lightest chargino under the assumption of a heavy sneutrino, for $\tan \beta = 1.0$, 1.5 and 35. The thin lines show the kinematic limits in the production and the decay. The dotted line (partly hidden by the shading) shows the expected exclusion limit. The dashed region is not allowed in the MSSM. The limit applies in the case of a stable $\tilde{\chi}_1^0$. The mass limit on the lightest neutralino is indicated by the horizontal dashed line (for a discussion on the low mass region see section 6.3).
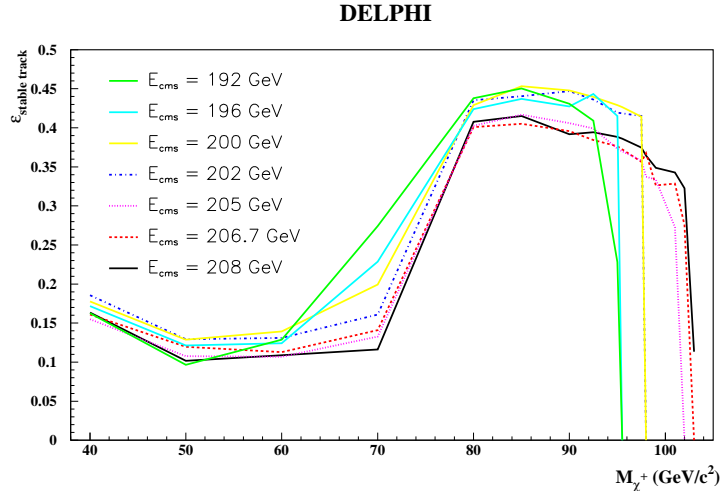
DELPHI

Figure 32: Efficiency for selecting a single almost stable chargino, as function of its mass, at the reference centre-of-mass energies collected by DELPHI in the years 1999 and 2000.

DELPHI E_{cms}=196 GeV
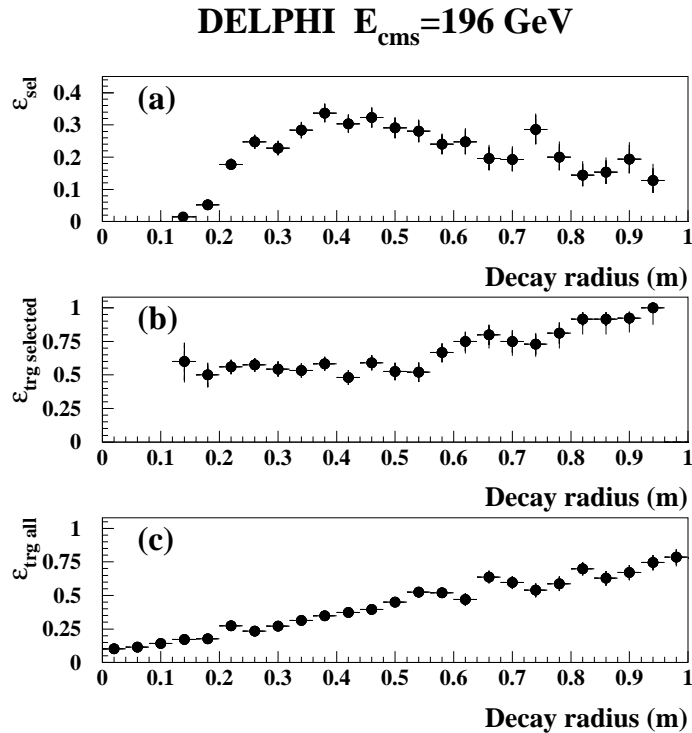
Figure 33: (a) Efficiency for selecting a single 75 GeV/c^2 chargino in the search for displaced decay vertices (kinks) at the centre-of-mass energy of 196 GeV, as function of its decay radius. (b) Trigger efficiency for the selected charginos. (c) Trigger efficiency for all 75 GeV/c^2 charginos, whether or not they were selected.
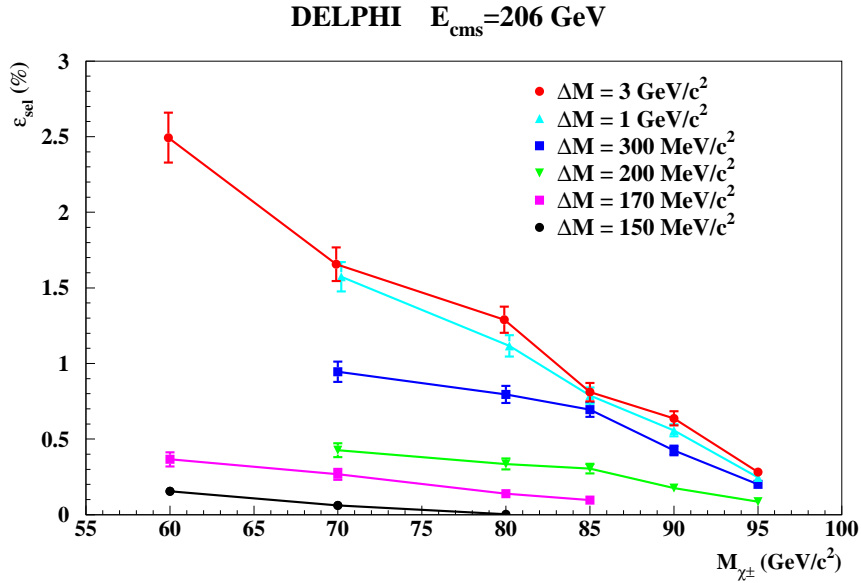
Figure 34: Selection times trigger efficiency in the search for nearly mass-degenerate charginos in the search with an ISR photon. The efficiency for higgsinos at $\sqrt{s} = 206$ GeV at the different chargino masses and ΔM values fully simulated is given as an example.
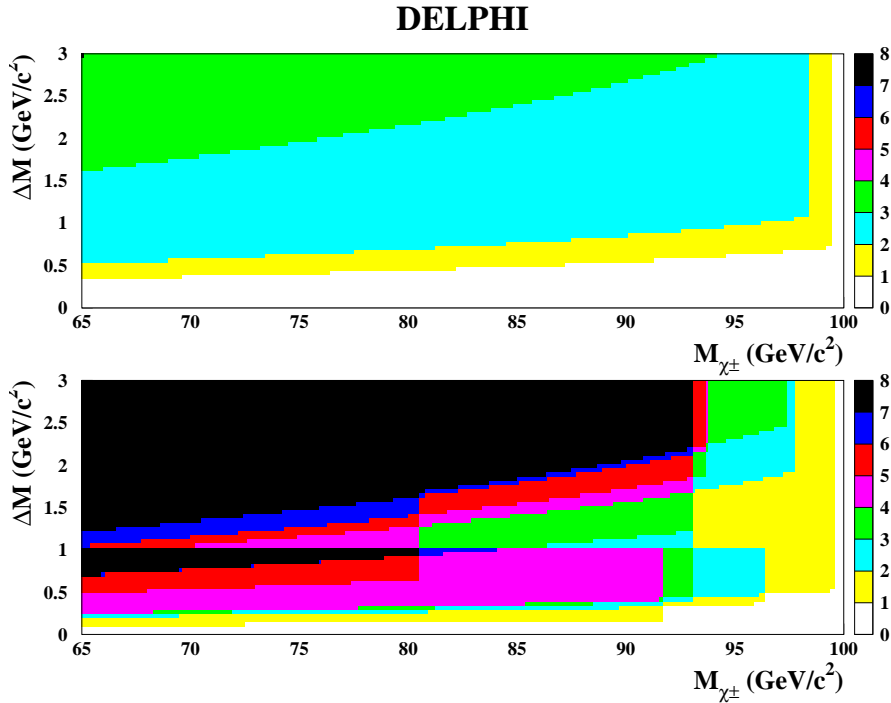
Figure 35: Expected number of background events (top) and number of selected events in the real data (bottom) after the final selection, for the year 2000 data with the TPC fully operational, as function of the points in the plane $(M_{\tilde{\chi}_1^\pm}, \Delta M)$ considered in the chargino search with an ISR photon.
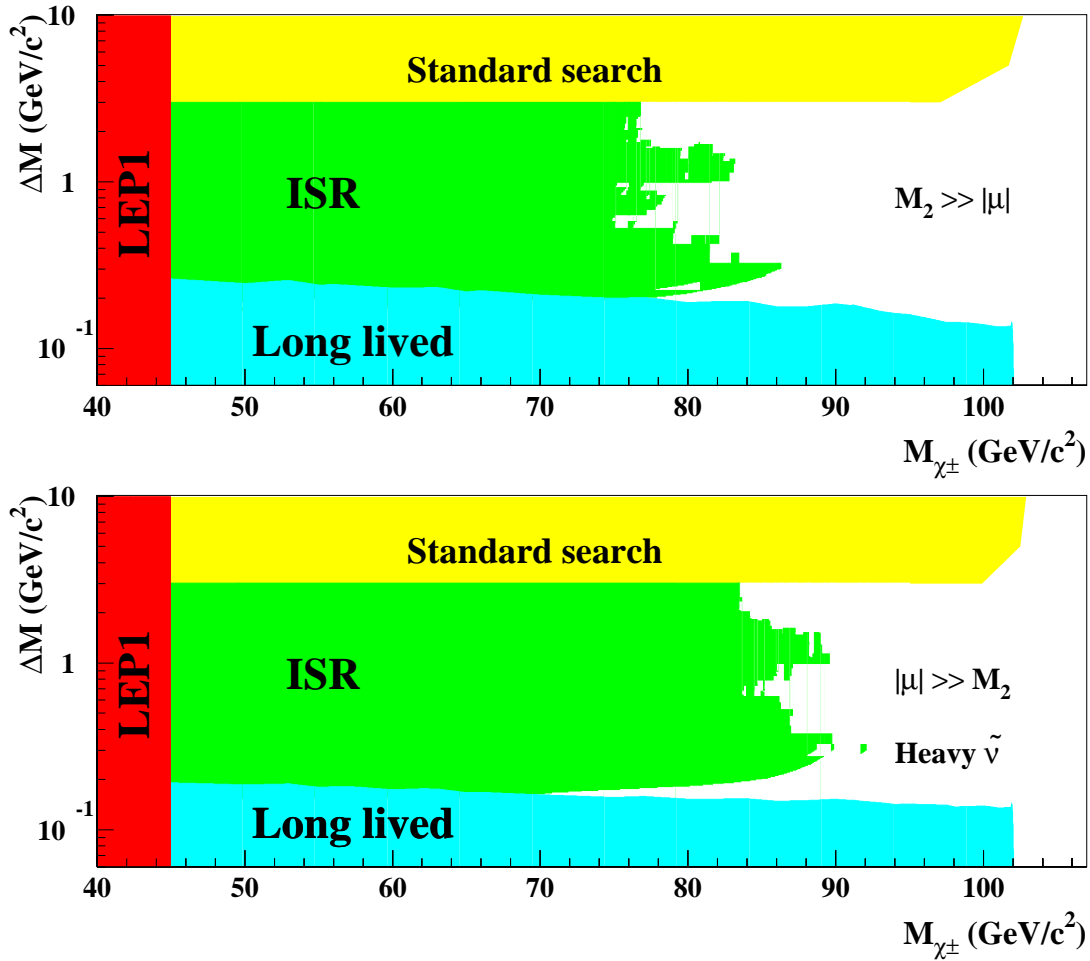
Figure 36: Regions in the plane $(M_{\tilde{\chi}_1^+}, \Delta M)$ excluded by DELPHI at the 95% CL using: the search for high ΔM charginos; the search for soft particles accompanied by ISR; and the search for long-lived charginos. The two scenarios are (a) the one in which the lightest chargino is a higgsino and (b) the one in which the lightest chargino is a gaugino. For the second scenario, the limits are valid in the heavy sfermion approximation, while for the higgsino scenario it is sufficient that $M_{\tilde{f}} > M_{\tilde{\chi}_1^+}$.
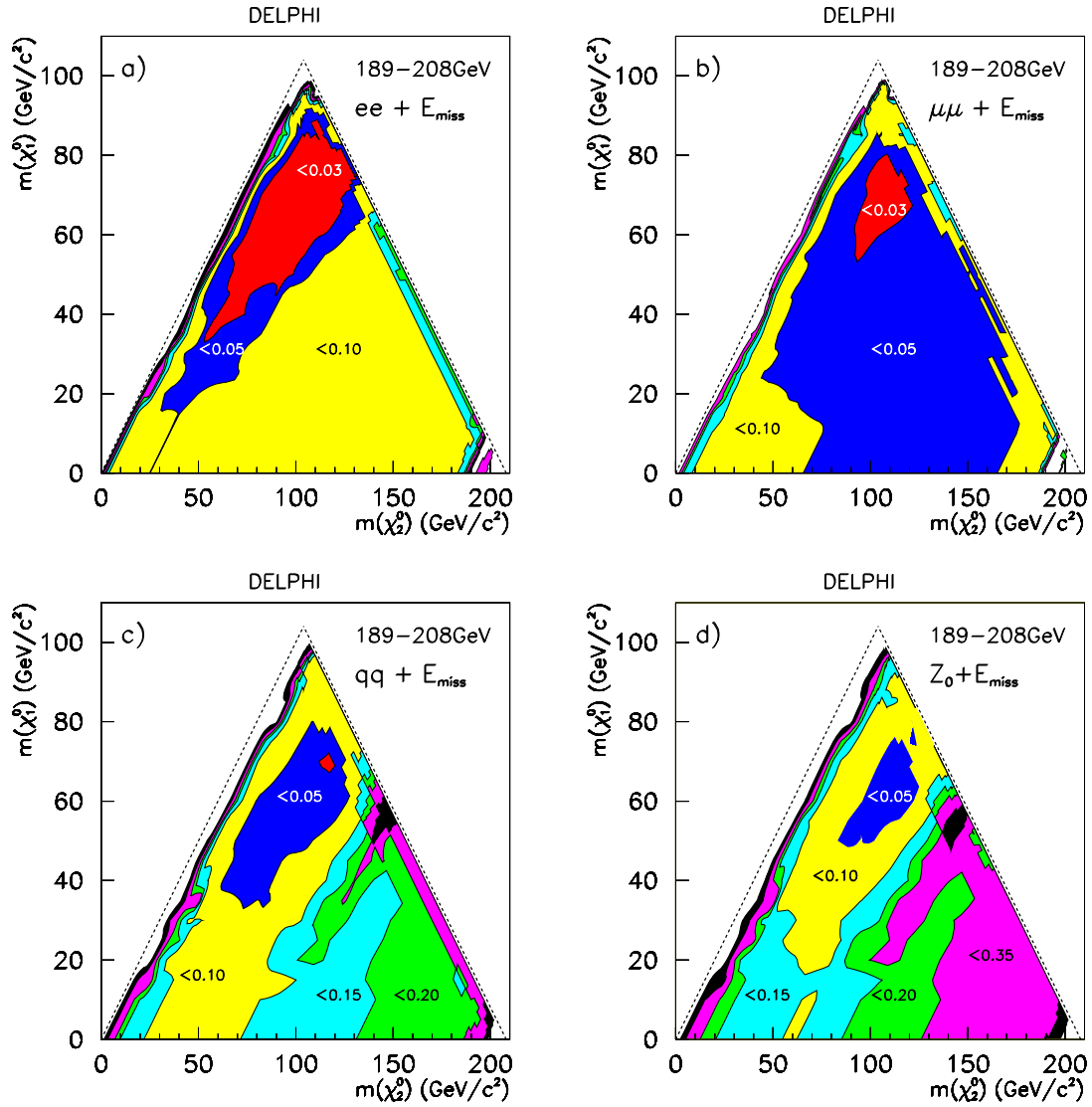
Figure 37: Contour plots of the upper limits obtained on the cross-sections at the 95% confidence level for $\tilde{\chi}_1^0 \tilde{\chi}_2^0$ production at $\sqrt{s} = 206$ GeV. The data at all energies were used, assuming the cross-section energy dependence expected at a chosen high m_0 point in the higgsino region where the neutralino searches play an important role (m_0=1 TeV/c^2, μ=-60 GeV/c^2, M_2=200 GeV/c^2). In each plot, the different shadings correspond to regions where the cross-section limit in picobarns is below the indicated number. For figures a), b), c), $\tilde{\chi}_2^0$ decays into $\tilde{\chi}_1^0$ and a) e^+e^-, b) $\mu^+\mu^-$, and c) $q\bar{q}$, while in d) the branching ratios of the Z were assumed, including invisible states. The dotted lines indicate the kinematic limit and the defining relation $M_{\tilde{\chi}_2^0} > M_{\tilde{\chi}_1^0}$.
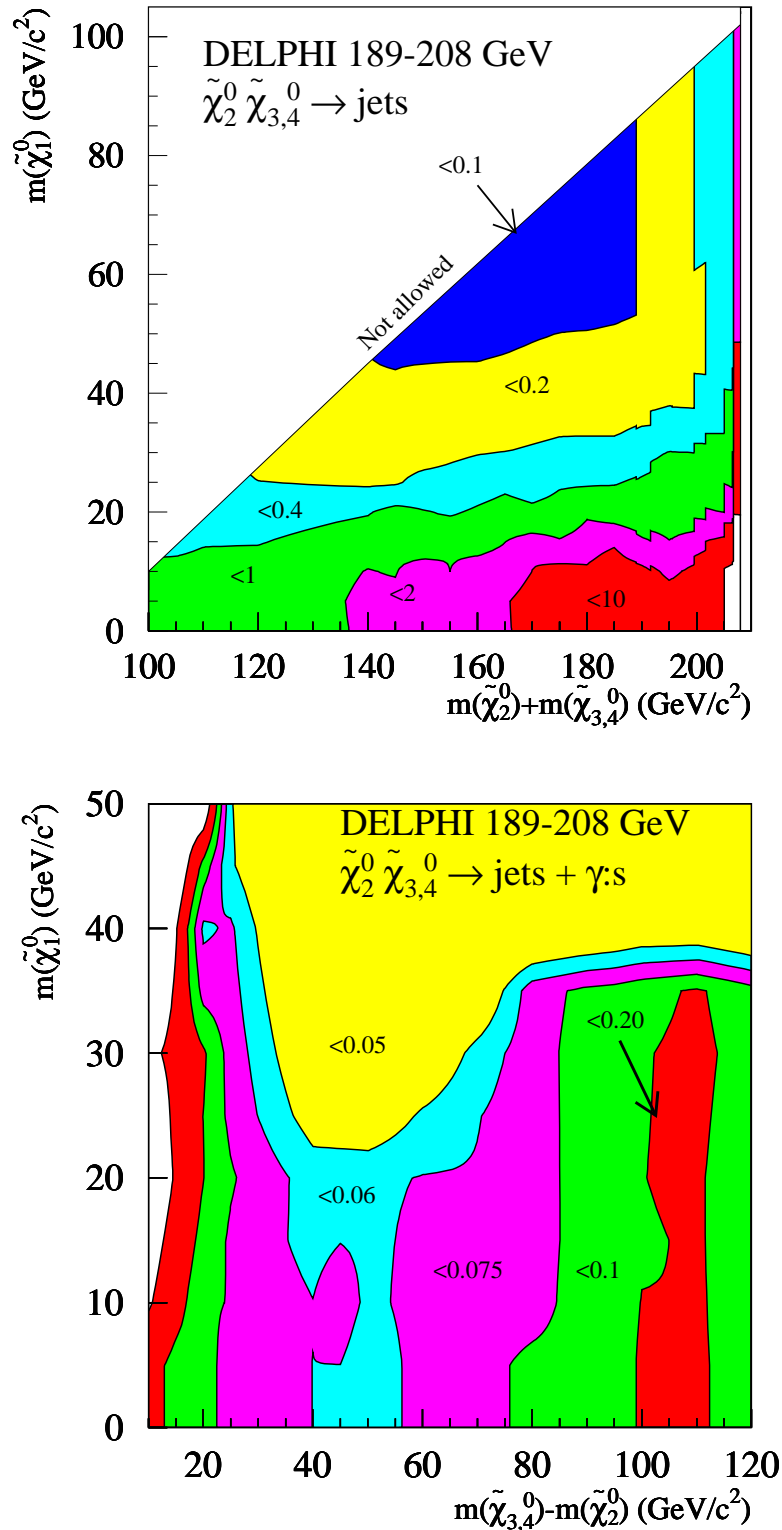
Figure 38: Upper limits on the cross-sections at the 95% confidence level for $\tilde{\chi}_2^0 \tilde{\chi}_i^0$ production with $\tilde{\chi}_i^0 \rightarrow \tilde{\chi}_2^0 q \bar{q}$ (i=3,4) including data up to $\sqrt{s}$ =208 GeV. The different shadings correspond to regions where the cross-section limit in picobarns is below the indicated number. The $\tilde{\chi}_2^0$ was assumed to decay 100% into $\tilde{\chi}_1^0 q \bar{q}$ in a), and into $\tilde{\chi}_1^0 \gamma$ in b). The limits in a) are based on the acoplanar jets and multijets selections, while those in b) derive from the search for multijets with photons.
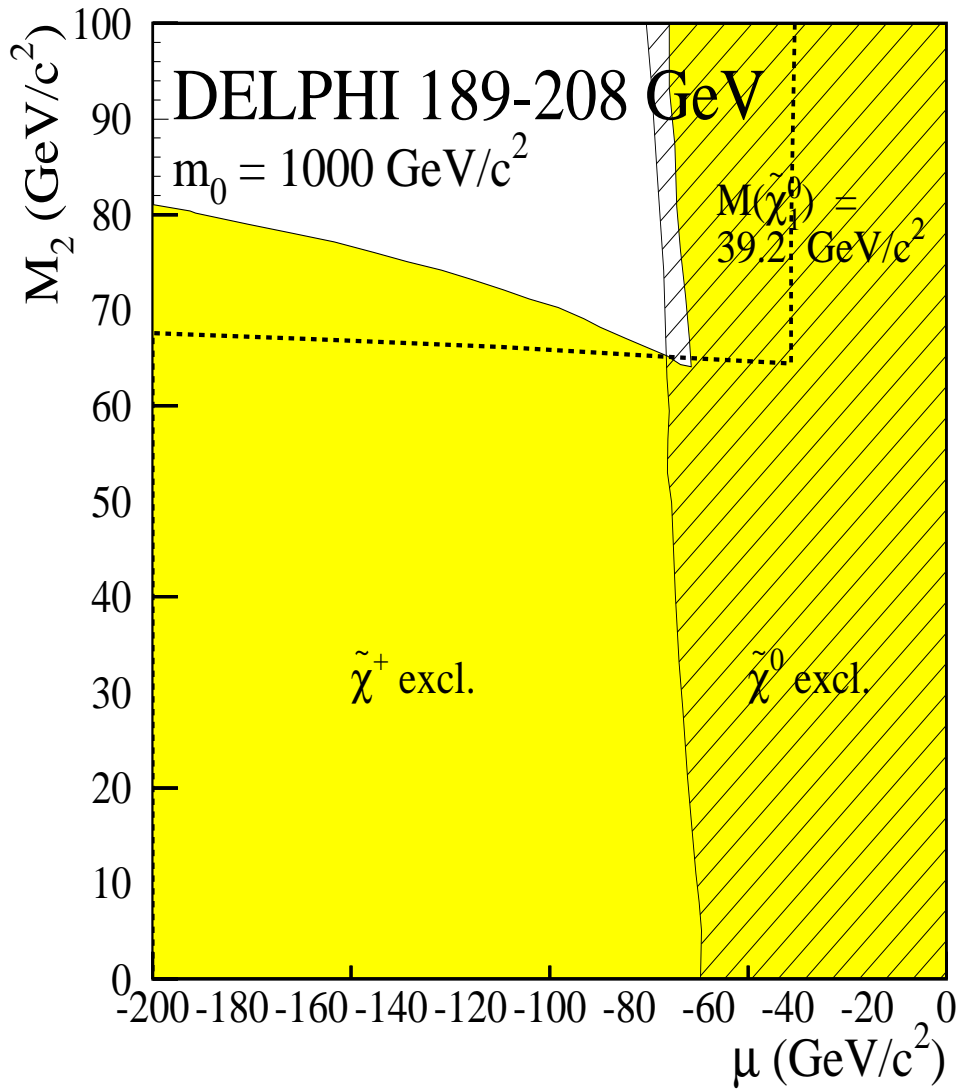
Figure 39: Excluded regions in the (μ, M_2) plane for $\tan\beta = 1$ for $m_0 = 1000$ GeV/c^2. The shaded areas show regions excluded by searches for charginos and the hatched areas show regions excluded by searches for neutralinos. The thick dashed curve shows the isomass contour for $M_{\tilde{\chi}_1^0} = 39.2$ GeV/c^2, the lower limit on the LSP mass obtained at $\tan\beta=1$. The chargino exclusion is close to the isomass contour for $M_{\tilde{\chi}_1^\pm}$ at the kinematic limit. From chargino searches alone the lower limit on $M_{\tilde{\chi}_1^0}$ is $M_{\tilde{\chi}_1^0} = 38.2$ GeV/c^2.
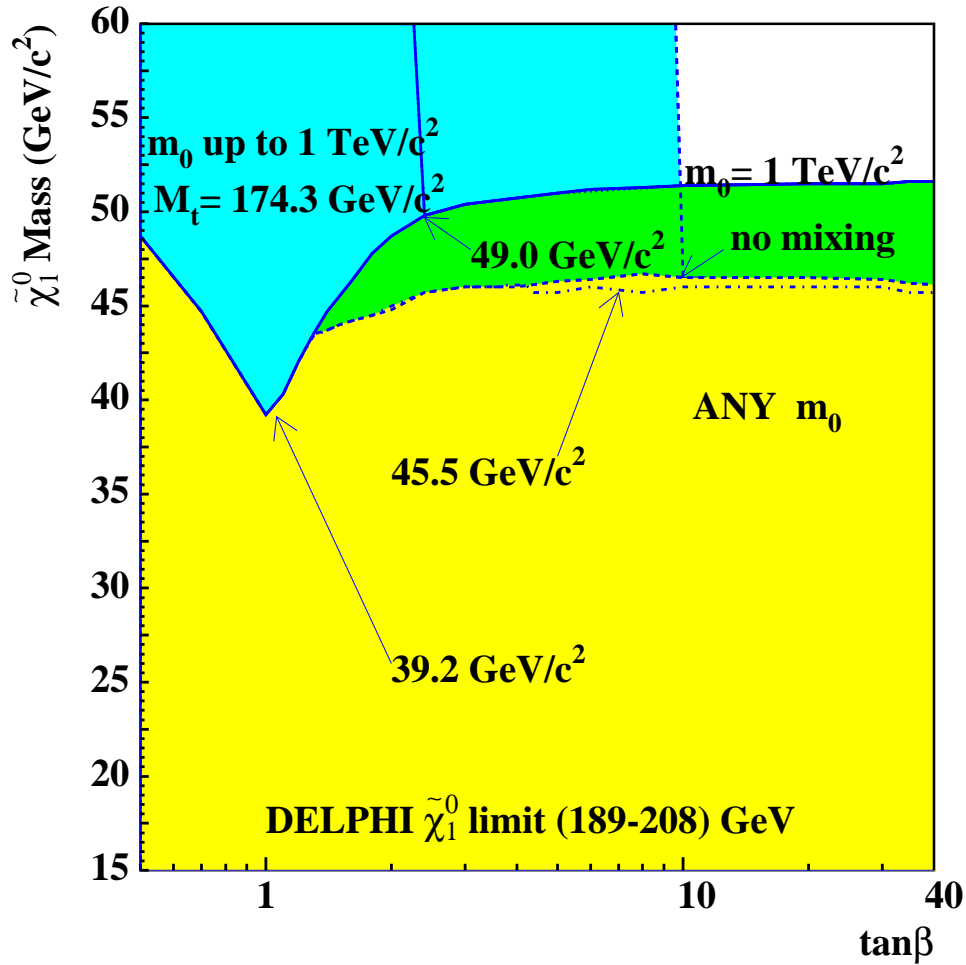
Figure 40: The lower limit at 95% confidence level on the mass of the lightest neutralino, $\tilde{\chi}_1^0$, as a function of $\tan\beta$ assuming a stable $\tilde{\chi}_1^0$. The solid curve shows the limit obtained for $m_0 = 1000$ GeV/c^2, the dashed curve shows the limit obtained allowing for any m_0 assuming that there is no mixing in the third family ($A_\tau = \mu\tan\beta$, $A_b = \mu\tan\beta$, $A_t = \mu/\tan\beta$), and the dash-dotted curve shows the limit obtained for any m_0 allowing for mixing with $A_\tau = A_b = A_t = 0$. The steep solid (dashed) line shows the effect of the searches for the Higgs boson for the maximal M_{h^0} scenario (no mixing scenario), $m_0 \leq 1000$ GeV/c^2 and $M_t = 174.3$ GeV/c^2, which amounts to excluding the region of $\tan\beta < 2.36(9.7)$.
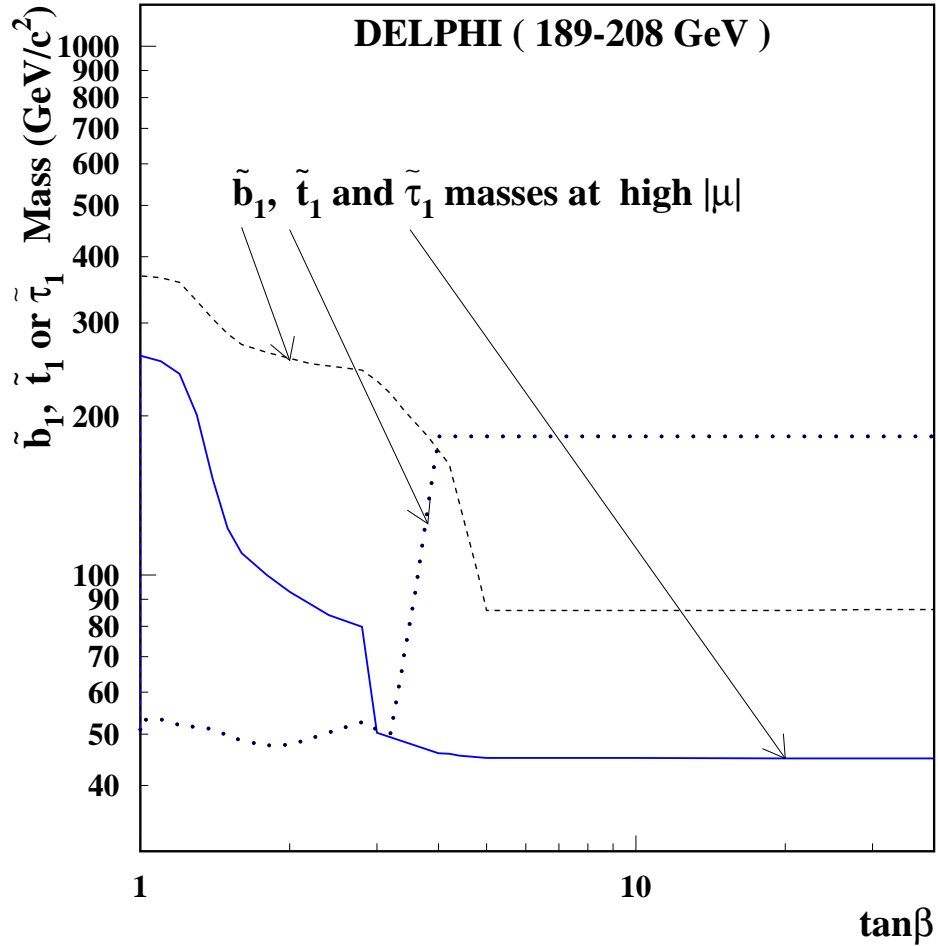
Figure 41: The masses as a function of $\tan\beta$ of the lightest stau (solid curve), stop (dotted curve) and sbottom (dashed curve), at the highest allowed $|\mu|$ for the lowest non-excluded M_2 value. Mass splitting in the stau (sbottom, stop) sector in the form $A_\tau - \mu\tan\beta$ ($A_b - \mu\tan\beta$, $A_t - \mu/\tan\beta$) was assumed, with $A_\tau = 0$ ($A_b = A_t = 0$).
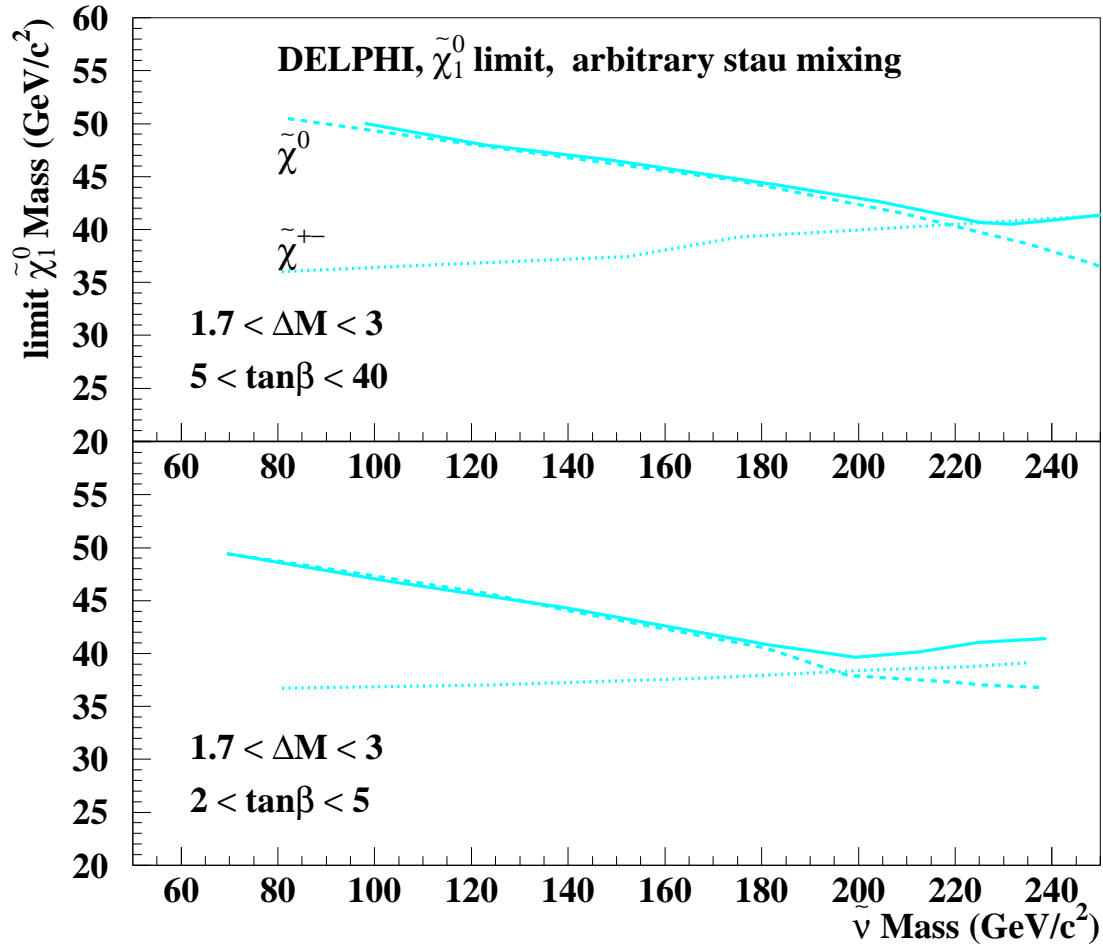
Figure 42: The limit set on the LSP mass by chargino (dotted line) and neutralino searches (dashed line) as a function of the sneutrino mass in the case when the lightest stau is degenerate in mass with the lightest neutralino. The combined limit is shown as solid line. These limits are valid for any model of stau mixing. In any particular model, in which mixing in the stau sector and in the sbottom and stop sector is related a more stringent limit on the LSP mass can be set.
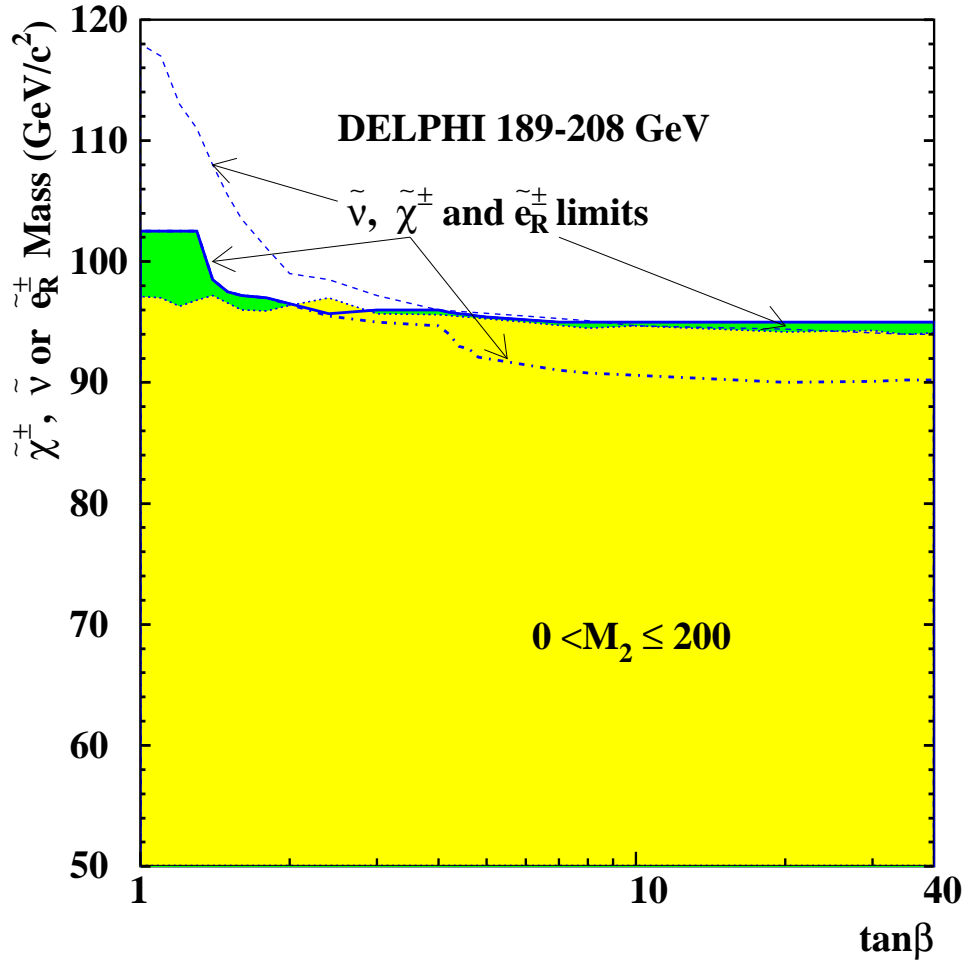
Figure 43: The minimum sneutrino mass (thin dashed curve) and the $\tilde{e}_R$ mass (thin dotted curve and light shading) allowed by the slepton and neutralino searches, as a function of $\tan\beta$, together with the limits on the chargino mass (thick solid curve and dark shading, and thick dash-dotted curve). The chargino mass limit indicated by the solid curve and the sneutrino and selectron mass limits were obtained assuming no mass splitting in the third sfermion family ($A_\tau - \mu\tan\beta = 0$ in particular). The selectron mass limit is valid for $M_{\tilde{e}_R} - M_{\tilde{\chi}_1^0} > 10$ GeV/c^2. The chargino mass limit indicated with the dash-dotted curve was obtained allowing for mass splitting in the third sfermion family, with $A_\tau = A_b = A_t = 0$.
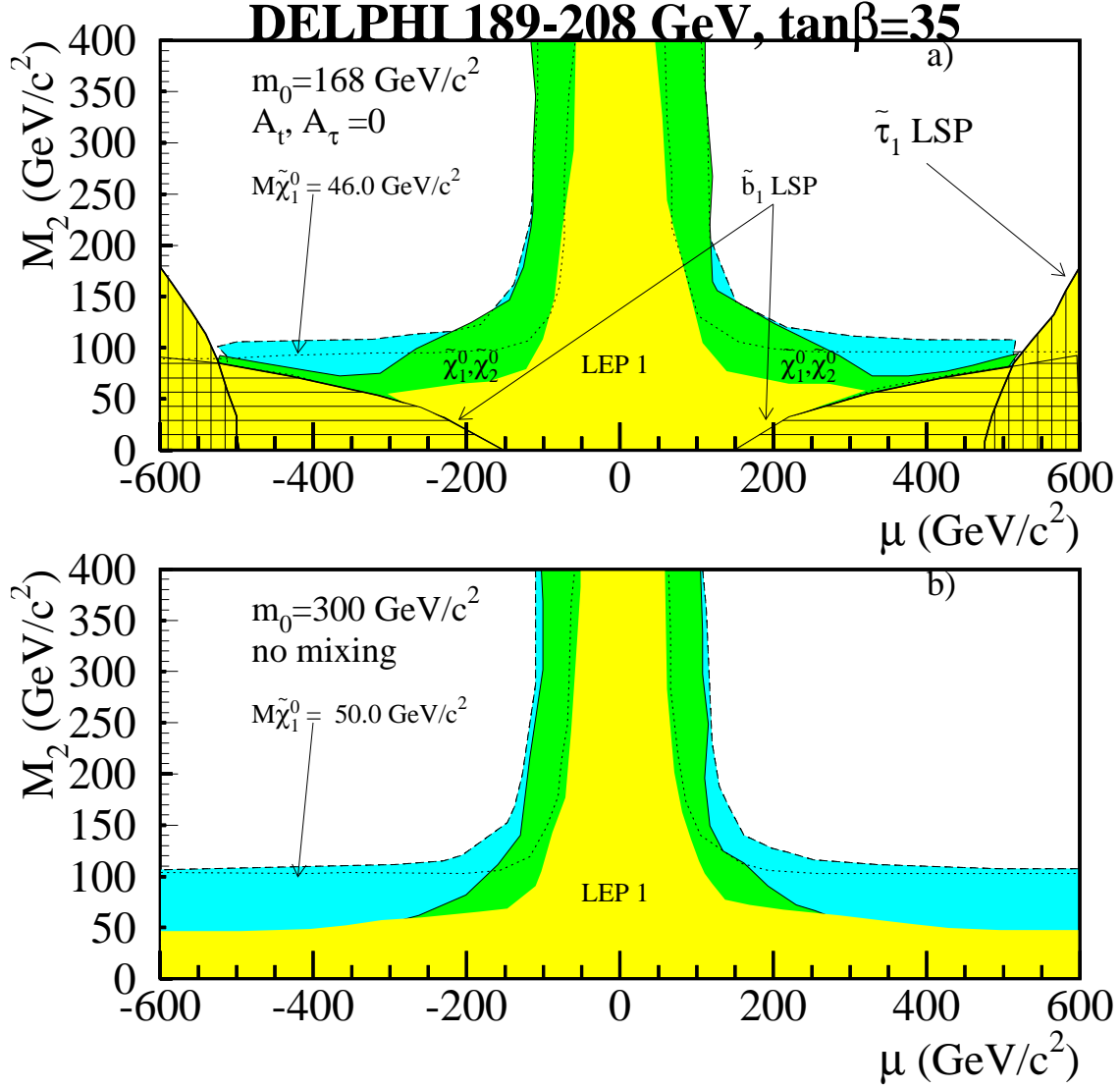
Figure 44: Regions excluded at 95% confidence level in the (μ, M_2) plane for $\tan\beta = 35$ and different assumptions of mixing in the third family. Light shaded regions are excluded by searches at LEP1 energies, darker shading bounded by the solid line marks regions are excluded by neutralino searches, while intermediate shaded regions bounded by the thin dashed line are excluded by chargino searches. Mixing terms in the form $A_\tau - \mu\tan\beta$ ($A_b - \mu\tan\beta$, $A_t - \mu/\tan\beta$) were considered. For plot a) $A_b = A_t = A_\tau = 0$ was assumed. The no-mixing scenario was used in b) ($A_\tau - \mu\tan\beta=0$, $A_b - \mu\tan\beta=0$, $A_t - \mu/\tan\beta=0$). Plot a) is for m_0 values giving the lowest non-excluded LSP mass. In the vertically (horizontally) hatched areas the stau (the sbottom) is the LSP. Relevant isomass contours of the lightest neutralino are also shown ($M_{\tilde{\chi}_1^0}=46$ GeV/c^2 in a) and $M_{\tilde{\chi}_1^0}=50$ GeV/c^2 in b)).